

**INFLUENCE OF AUSTEMPERING AND
QUENCHING AND PARTITIONING (Q&P)
HEAT TREATMENT ON THE
MECHANICAL PROPERTIES AND WEAR
BEHAVIOR OF AISI 9255 STEEL**

Thesis

Submitted in partial fulfillment of the requirements for the degree of

DOCTOR OF PHILOSOPHY

by

PALAKSHA P. A.



DEPARTMENT OF METALLURGICAL AND MATERIALS
ENGINEERING

NATIONAL INSTITUTE OF TECHNOLOGY KARNATAKA,
SURATHKAL, MANGALORE -575025

JULY, 2019

DECLARATION

By the Ph.D. Research scholar

I hereby *declare* that the Research Thesis entitled “**INFLUENCE OF AUSTEMPERING AND QUENCHING AND PARTITIONING (Q&P) HEAT TREATMENT ON THE MECHANICAL PROPERTIES AND WEAR BEHAVIOR OF AISI 9255 STEEL**” Which is being submitted to the **National Institute of Technology Karnataka, Surathkal**, in the partial fulfilment of the requirements for the award of the degree of **Doctor of Philosophy** in the department of Metallurgical and Materials Engineering, is a *bonafide report of the research work carried out by me*. The material contained in this Research thesis has not been submitted to any University or Institution for award of any degree.

Register Number: **145034MT14F03**

Name of the Research Scholar: **PALAKSHA P. A.**

Signature of the Research Scholar:

Department of Metallurgical and Materials Engineering

Place: NITK-SURATHKAL

Date:

CERTIFICATE

This is to *certify* that the Research Thesis entitled “**INFLUENCE OF AUSTEMPERING AND QUENCHING AND PARTITIONING (Q&P) HEAT TREATMENT ON THE MECHANICAL PROPERTIES AND WEAR BEHAVIOR OF AISI 9255 STEEL**” submitted by **Mr. PALAKSHA P. A.** (**Register number: MT14F03**) as the record of the research work carried out by him, is *accepted as the Research Thesis submission* in partial fulfilment of the requirements for the award of degree of **Doctor of Philosophy**.

Research guide

Dr. Ravishankar K. S.

Assistant Professor
Dept. of Metallurgical and
Materials Engineering,
NITK, Surathkal.

Chairman – DRPC

(Signature with Date and Seal)

ACKNOWLEDGEMENTS

First and foremost I thank Lord, the almighty for his grace throughout the research work.

I express my utmost gratitude to my supervisor **Dr. Ravishankar K. S.**, Assistant Professor, Department of Metallurgical and Materials Engineering (MME), National Institute of Technology Karnataka (NITK) Surathkal, for his excellent guidance and support throughout the work. His constant encouragement, help and review of the entire work during the course of the investigation are invaluable.

I am deeply obliged to **Prof. S. Anandhan**, Professor & Head, **Prof. Udaya Bhat K. and Prof. Jagannatha Nayak**, Professors & former heads, Department of MME, NITK Surathkal for providing the necessary facilities and sincere co-operation.

I am grateful to NITK for providing financial assistance and experimental facilities. I also thank all faculty members of the department of MME who taught and helped me.

I am grateful to my RPAC members including **Dr. H. S. Nagaraja**, Associate Professor & Head, Department of Physics and **Dr. K. Rajendra Udupa**, Professor Emeritus, Department of MME, NITK Surathkal for their appreciation and criticism throughout this research work.

I am grateful to **Prof. K. Narayan Prabhu**, Professor, Department of MME, NITK Surathkal for permitting me to use the Shimadzu Micro Vickers Hardness tester.

I am deeply obliged to **Prof. Indradev Samajdhar**, Head of Orientation Imaging Microscopy & Texture laboratory, Department of Metallurgical Engineering and Materials Science, IIT Bombay for providing the Electron Back Scattered Diffraction (EBSD) characterization facility. I also extend my sincere thanks to the research scholars **Mr. Rohith Mathew, Mr. Jayanth Barode & Mr. Arijit** and office staffs **Ms. Shwetali, Ms. Viddulatha & Mr. Parvej Raut** for their co-operation during the EBSD characterization work.

I thank **Mr. Faizy J. K.** Proprietor, Steel Mart Mumbai for providing the materials for the research work. I thank **Mr. Harish Shetty, Mr. Kiran, Mr. Sachin and Mr. Praveen** for their help in carrying out machining work.

I am thankful to **Ms. Sharmila**, Office staff, **Ms. Vinaya Shettigar**, Store keeper, **Ms. Rashmi, Mr. Sundara Shettigar, Mr. Ramachandra, Mr. Yashavantha, Mr. Sathish, Mr. Dinesha, Mr. Ismayil,** and **Mr. Sachin**, Lab staffs in the department of MME for their co-operation during the research work.

I thank my colleagues **Dr. Hemanthkumar V., Dr. Shamanth V, Dr. Sharath P. C., Dr. Bhaskaran, Dr. Vignesh Nayak, Mr. Mohammed Khalifa, Mr. Sangamesh, Mr. Pranesh Rao, Mr. Pavankumar, Dr. Jayalakshmi and Ms. Bindu** for their help and suggestions during the research work.

I also extend my thanks to the P.G. students **Mr. Syamkrishna, Mr. Ajit Kumar and Mr. Dhingaran** for their assistance during my research work.

I also thank my friend **Mr. Mahesh V. P.**, Ph.D. scholar IIT Gandhinagar for his favour during literature review of my research work.

I am grateful to my **parents, sister & brother-in-law** for their affection and constant support during my research work.

Finally I wish to thank all those who have helped me directly or indirectly in completing this research work.

PALAKSHA P. A.

ABSTRACT

The present investigation deals with the influence of two different heat treatments namely: (i) Austempering and (ii) Quenching & Partitioning (Q&P) on the microstructure, mechanical properties and dry sliding wear behavior of AISI 9255 high silicon steel. The as-received steel was checked for microstructure that comprised of pearlite, pro-eutectoid ferrite and undissolved cementite, Mechanical properties mainly tensile strength of 800 MPa, % elongation of 14.1 and hardness of 334 HV. Specific wear rate was found to be $4.076 \times 10^{-5} \text{ mm}^3/\text{N-m}$.

Austempering was carried out on the test samples by initial austenitisation at 900 °C for 45 minutes and thereafter quenching to various temperatures from 280 to 400 °C and holding for varying lengths of time from 15 to 180 minutes, which generates bainite microstructure that mainly comprises of bainitic ferrite and retained austenite (RA). Accordingly, variation in the bainitic morphology from acicular (lower bainite) to lath (upper bainite) was observed with the increasing temperature from 280 to 400 °C. However, increase in austempering time for all temperatures revealed a bit densely packed bainite structure. As a result there was a decrease in the RA; the quantity of decrease was further confirmed by x-ray diffraction (XRD) analysis. When compared to the properties of as-received steel, significant improvement in the tensile properties was observed for all austempered specimens; superior combination of tensile strength and % elongation was attained at austempering time of 15 min, i.e. (1852 MPa & 14%) at 280 °C, (1155 MPa & 33.4%) at 360 °C and (1165 MPa & 34%) at 400 °C. Similarly decrease in hardness from 600 to 342 HV was observed with increase in austempering temperature. During tensile loading, there was transformation of blocky RA to strain induced martensite that resulted in excellent strain hardening response from the samples austempered at higher temperatures 360 and 400 °C. Wear test results showed the slight increase in specific wear rate as the austempering time increases from 15 to 180 minutes. The sample austempered at 280 °C for 15 minutes exhibited the least specific wear rate of $2.063 \times 10^{-5} \text{ mm}^3/\text{N-m}$ implying its superior wear resistance.

In another set of heat treatment experiment i.e. quenching and partitioning was carried on the test samples by initial austenitisation at 900 °C for 45 minutes followed by quenching to 190 °C and finally partitioning at various temperatures from 280 to 400 °C and holding for varying lengths of time from 15 to 90 minutes. This heat treatment

generate multiphase microstructures mainly consisting of martensite of both lath and plate-type, transitional ϵ -carbides in tempered martensite matrix, lower bainite and RA for all the conditions. At higher partitioning temperatures i.e. 360 and 400 °C reveals some bainitic ferrite laths along with martensite and RA. Quantitative analysis shows the decrease in RA content with increasing partitioning time at 280 °C while it remains more or less constant for other partitioning temperatures. RA was non quantifiable for the samples which have undergone prolonged partitioning times at higher temperatures. Electron back scattered diffraction (EBSD) phase distribution maps reveals the RA content quite closer to those measured by XRD. Martensite crystals in inverse pole figure (IPF) maps reveal more of plate like morphology along with some twin orientations. Misorientation profiles indicated that at lower partitioning conditions i.e. 280 °C for 15 & 90 minutes reveals more high-angle grain boundary (HAGB), which signifies the presence of lower bainite in the matrix and similarly at high partitioning condition i.e. 400 °C for 30 minutes shows more low-angle grain boundary (LAGB) indicating the presence of upper bainite along with martensite of various morphologies, transition ϵ -carbides and RA. Compared to the mechanical and wear properties of as-received steel and austempered specimens, the Q&P treated specimens exhibits higher tensile strength and hardness but without much improvement in % elongation for almost all partitioning conditions. An excellent combination of tensile strength and % elongation was attained at partitioning time of 15 minutes i.e. 1859 MPa and 17% at 280 °C, which was also associated with high hardness value of 660 HV. Specific wear rate shows marginal increase with the increasing partitioning time from 15 to 90 minutes for all temperatures from 280 to 400 °C. The least specific wear rate of $1.18 \times 10^{-5} \text{ mm}^3/\text{N-m}$ was obtained at a partitioning condition of 280 °C for 15 minutes which is much less compared with that of austempered condition, which was in turn influenced by presence fine martensite packets (lath and plate morphologies), lower bainite along with stabilized RA.

Keywords: AISI 9255 high silicon steel, microstructure, mechanical properties, dry sliding wear behaviour, austempering, quenching & partitioning, bainitic ferrite, retained austenite, strain-induced martensite, martensite, transitional ϵ -carbides, EBSD phase distribution and inverse pole figure maps, high-angle grain boundary, low-angle grain boundary, tensile strength, % elongation, specific wear rate.

CONTENTS

LIST OF FIGURES	iv
LIST OF TABLES	ix
NOMENCLATURE.....	x
CHAPTER 1: INTRODUCTION.....	1
CHAPTER 2: LITERATURE REVIEW	5
2.1 Austempering Heat Treatment of High Silicon Steel.....	5
2.1.1 Bainitic steel	5
2.1.2 Carbide-free bainitic steels	8
2.1.3 Influence of austempering temperature and time	11
2.1.4 Overview of mechanical behavior of Austempered steels	12
2.1.5 Wear.....	18
2.1.6 Wear behavior of austempered high silicon steels	21
2.2 Quenching and Partitioning (Q&P) Heat Treatment of High Silicon Steels.....	25
2.2.1 Concept of carbon partitioning	25
2.2.2 Design of quenching and partitioning heat treatment.....	26
2.2.3 Overview of microstructure, mechanical and wear behavior of Q&P heat treated high silicon steels.....	28
CHAPTER 3: EXPERIMENTAL WORK.....	36
3.1 Material	36
3.2 Sample Preparation	37
3.3 Heat Treatment.....	37

3.3.1 Austempering.....	37
3.3.2 Quenching and Partitioning (Q&P)	38
3.4 Microstructural Analysis	39
3.4.1 Optical Microscopy	39
3.4.2 Scanning electron microscopy (SEM).....	39
3.4.3 Electron back scattered diffraction (EBSD) studies	39
3.5 X-ray Diffraction (XRD) Studies.....	39
3.6 Mechanical Properties.....	41
3.6.1 Tensile test.....	41
3.6.2 Microhardness	42
3.7 Wear Test	42
3.7.1 Determination of specific wear rate.....	43
3.8 Fractography.....	44
CHAPTER 4: RESULTS AND DISCUSSION	45
<i>PART A: Austempering Heat Treatment</i>	<i>45</i>
4.1 Influence of Austempering Temperature and Time on the Microstructure	45
4.1.1 Optical microscopy.....	45
4.1.2 Scanning electron microscopy.....	48
4.2 X-ray Diffractometry.....	53
4.3 Influence of Austempering Temperature and Time on the Mechanical Properties	57
4.3.1 Tensile properties	57
4.3.2 Microhardness measurement	71

4.4 Influence of Austempering Temperature and Time on the Wear Property	72
4.4.1 Wear mechanism	75
<i>PART B: Quenching and Partitioning (Q&P) Heat Treatment</i>	77
4.5 Influence of Partitioning Temperature and Time on the Microstructure	77
4.5.1 Optical microscopy	77
4.5.2 Scanning electron microscopy	80
4.6 X-ray Diffractometry	83
4.7 Electron Back Scattered Diffraction (EBSD) Analysis	88
4.8 Influence of Partitioning Temperature and Time on the Mechanical Properties	94
4.8.1 Tensile properties	94
4.8.2 Microhardness measurement	102
4.9 Influence of Partitioning Temperature and Time on the Wear Property	103
4.9.1 Wear mechanism	106
CHAPTER 5: CONCLUSIONS AND FUTURE ASPECTS	109
5.1 Conclusions	109
5.2 Summary of conclusions	111
5.3 Scope for Further Research	113
REFERENCES	114
LIST OF PUBLICATIONS	124
BIO-DATA	125

LIST OF FIGURES

Figure No.	Caption	Page No.
2.1	TTT diagram for AISI 9255 steel.	5
2.2	Optical micrographs of high carbon high silicon steel austempered for two hours at temperatures (a) 260 °C (Lower bainite) (b) 399 °C (Upper bainite)	7
2.3	Schematic representation of the microstructural differences obtained by austempering of plain carbon steel and high silicon steel	8
2.4	Schematic representation of crack nucleation and growth during tensile testing of CFB steel	9
2.5	Fe-0.39C-4.09Ni-2.05Si wt. % alloy austempered at 380 °C. (a) Scanning electron micrograph indicating the blocky austenite (γ). (b) Transmission electron micrograph indicating bainitic ferrite (α) & retained austenite (γ) films	10
2.6	Scanning electron micrograph of nano-structured CFB steel	11
2.7	Schematic portrayal of Q&P heat treatment to generate carbon-lean martensite and carbon rich RA mixture	27
2.8	Predicted quantity of retained austenite for various carbon contents	28
2.9	Steel subjected to various heat treatment (a) HT1- To create the necessary quenching rate; (b) HT2- Austempering; (c) HT3- Effect of partitioning conditions; (d) HT4- Effect of varying quenching temperature.	30
3.1	Microstructure of as-received AISI 9255 high silicon steel	36
3.2	Schematic representation of Austempering heat treatment schedule	37

3.3	Schematic representation of Q&P heat treatment schedule	38
3.4	Schematic diagram of tensile specimen	41
3.5	Schematic representation of wear pin sample.	43
3.6	Schematic representation of pin-on-disc set up	43
4.1	Optical micrographs of samples austempered at 280 °C for (a) 15 min. (b) 30 min. (c) 90 min. (d) 180 min.	45
4.2	Optical micrographs of samples austempered at 320 °C for (a) 15 min. (b) 180 min.	46
4.3	Optical micrographs of samples austempered at 360 °C for (a) 15 min. (b) 180 min.	46
4.4	Optical micrographs of samples austempered at 400 °C for (a) 15 min. (b) 180 min.	46
4.5	Scanning electron micrographs of samples austempered at 280 °C for (a) 15 min. (b) 60 min. (c) 90 min. (d) 180 min.	48
4.6	Scanning electron micrographs of samples austempered at 320 °C for (a) 15 min. (b) 60 min. (c) 90 min. (d) 180 min.	49
4.7	Scanning electron micrographs of samples austempered at 360 °C for (a) 15 min. (b) 60 min. (c) 90 min. (d) 180 min.	50
4.8	Scanning electron micrographs of samples austempered at 400 °C for (a) 15 min. (b) 60 min. (c) 90 min. (d) 180 min.	51
4.9	XRD patterns fitted to the line profiles by Gaussian function for the samples austempered at (a) 280 °C (b) 320 °C (c) 360 °C (d) 400 °C.	53-55
4.10	Variation in the amount of retained austenite for different austempering conditions.	56
4.11	Engineering stress-strain curves for various austempering conditions (a) 280 °C (b) 320 °C (c) 360 °C (d) 400 °C.	57-59
4.12	Influence of austempering temperature and time on the tensile properties of the specimens (a) Yield strength (b) Ultimate	60-61

	tensile strength (c) % Elongation (d) Modulus of toughness.	
4.13	Fractographs of the austempered samples (a) 280 °C–15 min. (b) 280 °C–180 min. (c) 320 °C–15 min. (d) 320 °C–180 min. (e) 360 °C–15 min. (f) 360 °C–180 min. (g) 400 °C–15 min. and (h) 400 °C–180 min.	63-64
4.14	True stress-strain curves for austempering at 400 °C for various durations	65
4.15	Strain-hardening behavior of the specimens austempered at (a) 280 °C–15 min. (b) 280 °C–60 min. (c) 280 °C–180 min. (d) 320 °C–15 min. (e) 320 °C–60 min. (f) 320 °C–180 min. (g) 360 °C–15 min. (h) 360 °C–60 min. (i) 360 °C–180 min. (j) 400 °C–15 min. (k) 400 °C–60 min. and (l) 400 °C–180 min.	66
4.16	Microstructures of fracture surfaces of the specimens austempered at (a) 360 °C–15 min. (b) 360 °C–60 min. (c) 360 °C–180 min. (d) 400 °C–15 min. (e) 400 °C–60 min. (f) 400 °C–180 min.	69
4.17	XRD profiles of the specimens austempered at 360 °C for 60 min.	70
4.18	Variation of micro-Vickers hardness with austempering conditions.	71
4.19	Cumulative weight loss against wear time plot for as-received and samples austempered at 280 °C for various durations.	72
4.20	Variation in specific wear rate for different austempering conditions.	74
4.21	SEM of worn out samples austempered at (a) 280 °C- 15 min. (b) 280 °C- 120 min. (c) 320 °C- 60 min. (d) 360 °C- 120 min. (e) 400 °C- 180 min.	75
4.22	Optical micrographs of samples quenched at 190 °C and partitioned at 280 °C for (a) 15 min. (b) 30 min. (c) 60 min.	77

	(d) 90 min.	
4.23	Optical micrographs of samples quenched at 190 °C and partitioned at (a) 320 °C for 15 min. (b) 320 °C for 90 min. (c) 360 °C for 15 min. (d) 360 °C for 90 min. (e) 400 °C for 15 min. (f) 400 °C for 90 min.	78
4.24	Scanning electron micrographs of samples quenched at 190 °C and partitioned at 280 °C for (a) 15 min. (b) 30 min. (c) 60 min. (d) 90 min.	80
4.25	Scanning electron micrographs of samples quenched at 190 °C and partitioned at (a) 320 °C for 15 min. (b) 320 °C for 90 min. (c) 360 °C for 15 min. (d) 360 °C for 90 min. (e) 400 °C for 15 min. (f) 400 °C for 90 min.	81
4.26	XRD patterns fitted to the line profiles by Gaussian function for samples quenched at 190 °C and partitioned at (a) 280 °C (b) 320 °C (c) 360 °C (d) 400 °C.	83-85
4.27	Effect of varying partitioning temperature and time on (a) Retained austenite content (b) Carbon content in retained austenite.	86
4.28	EBSD maps of the steel samples quenched at 190 °C and partitioned at 280 °C- 15 minutes (a) PD map (b) IPF map (c) Misorientation distribution profile	88
4.29	EBSD maps of the steel samples quenched at 190 °C and partitioned at 280 °C- 90 minutes (a) PD map (b) IPF map (c) Misorientation distribution profile	89
4.30	EBSD maps of the steel samples quenched at 190 °C and partitioned at 320 °C- 15 minutes (a) PD map (b) IPF map (c) Misorientation distribution profile	90
4.31	EBSD maps of the steel samples quenched at 190 °C and partitioned at 360 °C- 15 minutes (a) PD map (b) IPF map	91

4.32	EBSD maps of the steel samples quenched at 190 °C and partitioned at 360 °C- 60 minutes (a) PD map (b) IPF map	91
4.33	EBSD maps of the steel samples quenched at 190 °C and partitioned at 400 °C- 30 minutes (a) PD map (b) IPF map (c) Misorientation distribution profile.	92
4.34	Engineering stress-strain curves for samples quenched at 190 °C and partitioned at (a) 280 °C (b) 320 °C (c) 360 °C (d) 400 °C.	94-95
4.35	Influence of partitioning temperature and time on the tensile properties of the specimens (a) Yield strength (b) Ultimate tensile strength (c) % Elongation (d) Modulus of toughness.	96-98
4.36	Fractographs of the Q&P samples (a) 280 °C- 15 min. (b) 280 °C- 90 min. (c) 320 °C- 15 min. (d) 320 °C- 90min. (e) 400 °C- 15 min. (f) 400 °C- 90 min.	100
4.37	Variation of micro-Vickers hardness with partitioning times and temperatures	102
4.38	Cumulative weight loss against wear time plot for as-received and samples partitioned at 280 °C for various durations	103
4.39	Variation in specific wear rate with partitioning times and temperatures	105
4.40	SEM of worn out samples partitioned at (a) 280 °C- 15 min. (b) 280 °C- 90 min. (c) 320 °C- 15 min. (d) 320 °C- 90 min. (e) 360 °C- 15 min. (f) 360 °C- 90 min. (g) 400 °C- 15 min. (h) 400 °C- 90 min.	106-107

LIST OF TABLES

Table No.	Caption	Page No.
2.1	Parameters and variables influencing the wear	19
3.1	Chemical composition of the steel used in this investigation	36
3.2	Specifications of rotating disc	42
3.3	Wear testing parameters	42
4.1	Variation of strain hardening exponent values with respect to varying austempering conditions	67
4.2	Wear property of the as-received steel	72
4.3	Wear property of the austempered samples	73
4.4	Wear property of the Q&P heat treated samples	104
5.1	Summary of the “exceptional” mechanical properties and specific wear rate obtained with their processing conditions	112

NOMENCLATURE

AISI American Iron and Steel Institute	HV Vickers Hardness
ASTM American Society for Testing & Materials	YS Yield Strength
AHSS Advanced High Strength Steel	UTS Ultimate Tensile Strength
TRIP Transformation Induced Plasticity	% EL Percentage Elongation
TWIP Twinning-Induced Plasticity	MT Modulus of Toughness
Q&P Quenching and Partitioning	SWR Specific Wear Rate
Q&T Quenching and Tempering	
TTT Time Temperature Transformation	
CCT Continuous Cooling Transformation	
LVDT Linear Variable Differential Transformer	
XRD X-Ray Diffraction	
FEI Field Electron and Ion	
FEG Field Emission Gun	
SEM Scanning Electron Microscope	
EDX Energy Dispersive X-Ray Spectroscopy	
EBSD Electron Back Scattered Diffraction	
OIM Orientation Image Microscopy	
IPF Inverse Pole Figure	
ADI Austempered Ductile Iron	
DP Dual Phase	
CFB Carbide Free Bainite	
LB Lower Bainite	
UB Upper Bainite	
M_L Martensite lath	
M_P Martensite plate	
TM Tempered Martensite	

CHAPTER 1

INTRODUCTION

Over the years, considerable evolution has been made in the field of complex or multi phase steels as a venture to accomplish the industrial necessities, especially for automotive and machinery applications. Improvements in the properties of steel have been attained by tailoring the chemical composition during the processing stage. The key objective in the advancement of these grades are to attain superior mechanical properties i.e. tensile strength of 1500 MPa and a total elongation of 20-25% at comparatively low processing cost (Da Silva et al. 2015), (Liu et al. 2017), which were achieved by the steel containing high silicon (1.5 to 2.2 wt.%) after subjecting it to austempering heat treatment, which exhibits a carbide free bainitic structure (Garcia-Mateo and Caballero 2005). The mechanical properties of this austempered high silicon steel were found to be superior to those of hardened and tempered steel of same hardness, basically as a result of its microstructure that comprises of fine bainite laths and retained austenite, which was achieved by isothermal holding technique. Fine bainite laths results in high strength of this steel and retained austenite in film morphology was most beneficial in order to attain excellent combination of strength and ductility (Sharma et al. 2011), (Bhadeshia and Edmonds 1983).

The presence of silicon in steel stabilizes ferrite due to its high solubility in ferrite, additionally silicon content of minimum 1.5 wt. % leads to the hindrance of cementite precipitation in the matrix due to its poor solubility in cementite (Chang and Bhadeshia 1994), (Acharya et al. 2018). Addition of manganese in steel stabilizes austenite. Further quantity of manganese less than 2 wt. % has a favorable effect on hardenability and solid solution strengthening (Mandal et al. 2009) and also reduces the M_s temperature resulting in increased retained austenite content at room temperature (Tariq and Baloch 2014). Steel with chemical composition (weight %) in the range: 0.55-0.6 carbon, 1.8-2.2 silicon and 0.7-0.95 manganese is designated as AISI 9255 steel. Properly heat treated steels of this category have high yield strength and fatigue strength. As an outcome, these high

silicon steels find extensive applications like leaf springs, bearings and gears in automobiles, cutting tools and dies (Avner 1997 and Lindstrom 2006). Moreover, the excellent strain hardening ability and formability of this austempered high silicon steels finds applications in the area of metal forming (Varshney et al. 2017).

Another characteristic group of steels, whose progress was predominantly obsessed by the automotive industry, is the advanced high strength steels (AHSS). The *First Generation* AHSS grades exhibited multiphase microstructures mainly ferrite and martensite mixture i. e. dual phase (DP) steels, TRIP steels that includes ferrite and bainite with retained austenite (RA) or CP steels with an intricate blend of martensite, bainite and RA. The *Second Generation* AHSS included high alloyed TWIP steels, which revealed austenitic structure due to the high manganese content, but made it expensive (Da Silva et al. 2015). As of late there has been increased attention in the advancement of the *Third Generation* of AHSS, i.e. steels with superior blend of strength and ductility than those of first generation AHSS but economical than those of second generation AHSS (Sun et al. 2014). One such encouraging and pioneering heat treatment for the formation of *Third Generation* AHSS i.e. Quenching and Partitioning (Q&P) process intended by Speer et al. (2003) which is a novel idea for the heat treatment of martensite, dissimilar to conventional quenching and tempering.

Q&P process can be adopted to create blended microstructures of martensite and controlled proportions of retained austenite exhibiting remarkable properties (Edmonds et al. 2006). Here, the carbon supersaturation of martensite is utilized to stabilize the untransformed austenite. This is done in a partitioning step, where carbon partitions from the carbon supersaturated martensite to the retained austenite (Gerdemann et al. 2004). While partitioning the carbon supersaturation of martensite is wiped out via carbon enrichment of the austenite, until the point when the carbon potential is uniform all through the microstructure. In the subsequent Q&P microstructure, martensite contributes for high strength whereas stabilized retained austenite results in superior ductility due to event of TRIP effect (Nishikawa et al. 2018).

Extensive experimental works has been carried out by the researchers regarding austempering heat treatment and Q&P heat treatment alternatively based on its influence on microstructure, mechanical and wear behavior of various grades of steels comprising of expensive alloying elements like nickel, chromium, molybdenum, cobalt and so forth alongside high silicon and manganese, however limited research works have been dedicated towards the transformation and its consequence on the microstructural, mechanical properties of AISI 9255 steel which comprises of basic alloying elements like silicon and manganese. Moreover from the literature it is not completely clear about the exceptional austempering and quenching & partitioning (Q&P) heat treatment condition for AISI 9255 steel, as far as mechanical and wear behavior are concerned. In addition, with respect to quenching and partitioning heat treatment, limited work was carried out based on the utilization of benefits of stabilizing retained austenite towards development of high strength steel. Considering above aspects it is proposed to study the influence of two different heat treatments namely, austempering and Q&P on mechanical properties and wear behavior of AISI 9255 steel. Accordingly, the following objectives are made.

1.1 Objectives

1. To carry out two different heat treatments for AISI 9255 steel specimens i.e. austempering and quenching & partitioning, thereafter to study the effect of these two heat treatments on microstructure, dry sliding wear behavior and mechanical properties viz. tensile properties and hardness.
2. To study the mechanism of crack initiation and propagation of the heat treated specimens during tensile loading.
3. To establish structure-property relationship for understanding the possibility of improvement in mechanical and wear behavior, which would help in component design.
4. To arrive at an optimum combination of heat treatment parameters in such a way that the above said properties are maximized.

Thesis outline

The thesis is divided into five chapters. Chapter 1 incorporates the introduction along with research gaps and objectives. Chapter 2 presents the literature review based on the Austempering and Quenching & Partitioning (Q&P) heat treatment, the respective microstructural and property (mechanical & wear) variations after these heat treatments. Chapter 3 provides the description regarding the material used and experimental methods employed. Chapter 4 presents the results obtained and are discussed based on the results obtained by other worldwide research groups. Chapter 5 presents the conclusions and scope for future work.

CHAPTER 2

LITERATURE REVIEW

2.1 Austempering Heat Treatment of High Silicon Steel

2.1.1 Bainitic steel

Bain and Davenport were the first to recognize bainitic microstructure which was acquired when steel was permitted to transform at a steady temperature alluded to as austempering (Leiro 2014). Austempering includes austenitising the steel thereafter quenching to a temperature anywhere between bainite start ' B_s ', and martensite start ' M_s ' temperature, where isothermal transformation occurs until the point that all austenite gets transformed to bainite, according to the TTT plot for AISI 9255 steel shown in figure 2.1, which was constructed using an *online CCT/TTT diagram calculation link that was originally developed by Oak Ridge National laboratory*.

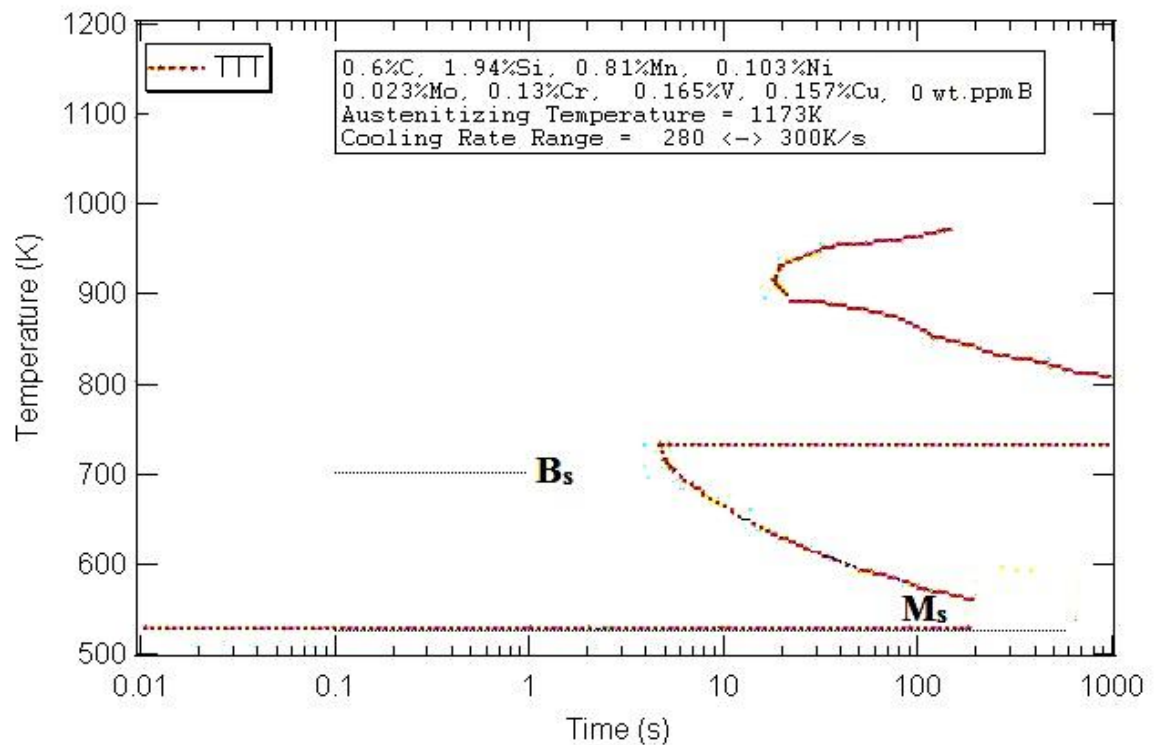


Figure 2.1 TTT diagram for AISI 9255 steel.

According to this plot, the B_s and M_s temperatures were found to be **432 and 255 °C** respectively.

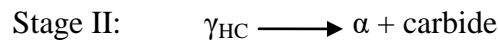
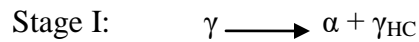
The B_s and M_s temperatures were also determined using the following equations: [compositions are in wt.%] (Monia et al. 2015)

$$B_s (^{\circ}C) = 656 - 57.7C - 35Mn - 75Si - 5.3Ni - 34Cr - 41.2Mo \dots \dots \dots (1)$$

$$M_s (^{\circ}C) = 539 - 423C - 30.4Mn - 17.7Ni - 12.1Cr - 7.5(Mo, W, Si) \dots \dots \dots (2)$$

From the above equations B_s and M_s temperatures were calculated to be **442 and 237 °C**, respectively, accordingly the isothermal transformation temperatures were selected within this temperature range in the present investigation.

The aim of austempering involves bainite formation, which is comparable in frame and has a practically identical hardness to martensite tempered at a similar temperature; nevertheless it has a higher toughness and comparatively lower residual stress than the corresponding martensite. In plain carbon steel, bainite is formed in two stages. In the initial stage, ferrite (α) laths nucleate and then grow in carbon rich retained austenite (γ_{HC}), second stage involves carbide precipitation (either within the ferrite or at the boundaries of ferrite/austenite) after the austenite has turned out to be saturated with carbon.



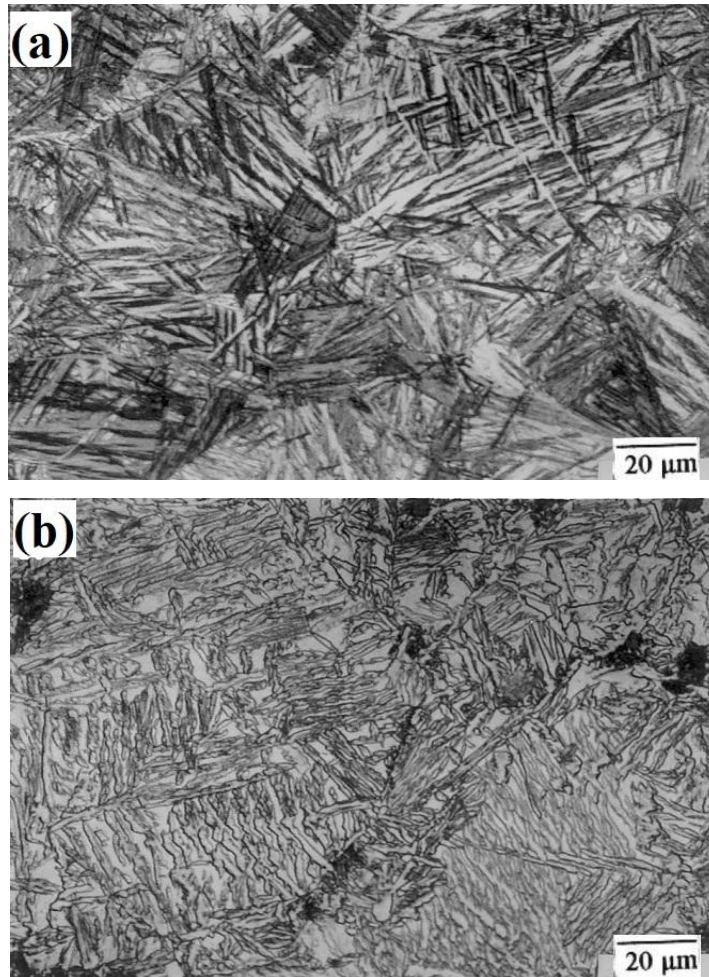


Figure 2.2 Optical micrographs of high carbon high silicon steel austempered for two hours at temperatures (a) 260 °C (Lower bainite) (b) 399 °C (Upper bainite) (Putatunda 2001).

The terms upper and lower bainite are utilized to recognize these two sorts (figure 2.2). Upper bainite is formed at higher austempering temperatures where the diffusion rates are sufficiently high for carbon to diffuse to the lath boundaries. Lower bainite is formed at lower temperatures where the carbon is trapped inside the growing ferrite lath bringing about carbide precipitation inside the ferrite (Bhadeshia 2001). Lower bainite structure in steel provides high strength and fracture toughness. Austempered steel offered the benefits of high ductility, minimum distortion, and a reduced interval for overall hardening of steel (Putatunda 2001).

2.1.2 Carbide-free bainitic steels

One fundamental class of steels in the third era of AHSS depends on fine grained bainite which can be CFB steels if the chemical composition is retained in the range 1.5-3 wt.% Si and/or Al addition to the steel (Vuorinen 2012).

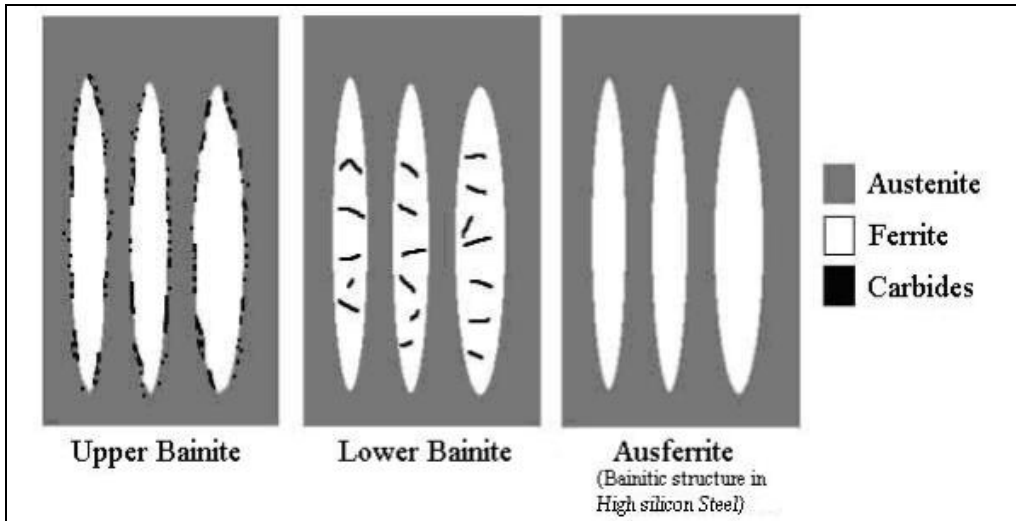


Figure 2.3 Schematic representation of the microstructural differences obtained by austempering of plain carbon steel and high silicon steel (Lindstrom 2006).

Silicon is nearly insoluble in iron carbide. Henceforth, it is essential for silicon to diffuse out of the forming carbides (Diffusion coefficient of Si= in γ -Fe at 900 °C = 2.57×10^{-17} m²/s), which is a slower process by many orders of magnitude than the interstitial diffusion of carbon atoms (Diffusion coefficient of C in γ -Fe at 900 °C = 1×10^{-11} m²/s) (Fridberg et al. 1969). This difference in diffusion coefficients amongst carbon and silicon in iron is the purpose behind silicon's impeding effect on the second stage of bainitic transformation. The difference increased with decreasing temperature, as the activation energy (Q) [Activation energy for carbon diffusion (Q_{γ} =135.7 kJ/mol) & for Si (Q =286 kJ/mol)] of the substitutional diffusion surpassed that of interstitial diffusion. Since the second stage in bainite formation (carbide precipitation) is smothered in high silicon steel. Thus the structure that comprises of carbide free blend of acicular ferrite and austenite is portrayed by the term ausferrite (figure 2.3).

The mechanical properties of CFB steels were observed to superior compared to those of hardened and tempered steels of a similar hardness in view of their exciting microstructure comprising of thin bainite plates in retained austenite matrix.

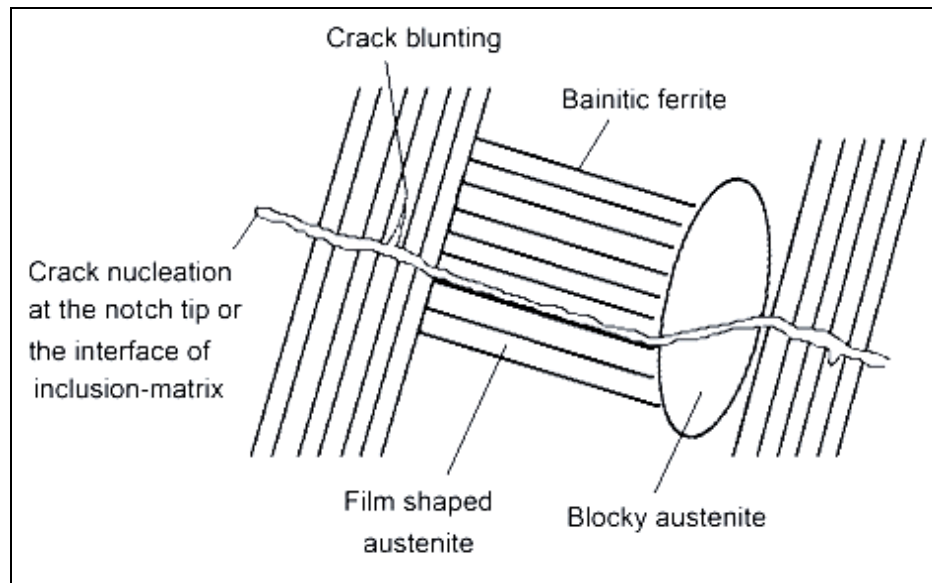


Figure 2.4 Schematic representation of crack nucleation and growth during tensile testing of CFB steel (Xiang et al. 2009).

The fine structured bainite laths and high dislocation densities contributed to high strength, while the film shaped retained austenite (figure 2.4) within these bainite laths provided a cushioning effect for any crack propagation resulting in increased ductility. The retained austenite content transforming to martensite was reduced by carbon rich austenite due to its increased stability (Sharma et al. 2011).

Caballero and Bhadeshia (2004) worked on designing advanced high-strength steels and effectively created a multiphase microstructure comprising of bainitic ferrite laths (light regions) and retained austenite films (dark regions) between the laths shown in figure 2.5. A superior blend of fracture toughness of $30-40 \text{ MPa}\sqrt{m}$ and strength of 2.5 GPa at a temperature of 125 °C were accomplished. With cautious plan, Caballero et al. (2001) attained a excellent blend of a strength of 1.6 to 1.7 GPa and fracture toughness of $130 \text{ MPa}\sqrt{m}$.

Bhadeshia and Edmonds (1983) reported that the impact toughness of bainitic steels diminished significantly due to the presence of carbides in the microstructure. Other than the carbide, the presence of certain amount of mechanically or thermally unstable austenite also caused diminishment in the toughness of bainitic steels. The presence of vast "blocky" regions of austenite (figure 2.5) in the microstructures caused hindrance to the mechanical properties of CFB steel.

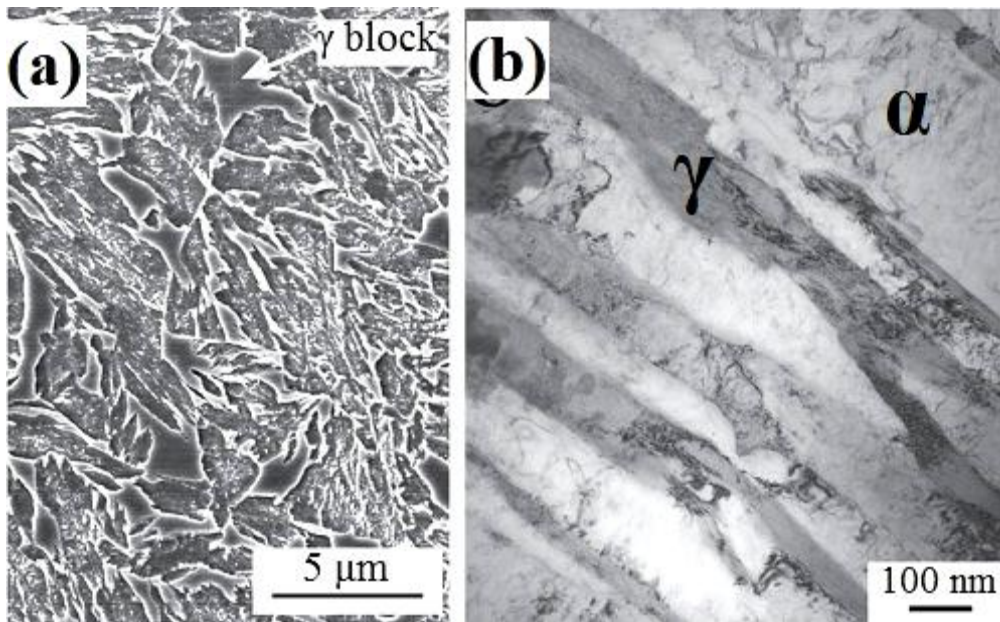


Figure 2.5 Fe-0.39C-4.09Ni-2.05Si (wt. %) alloy austempered at 380 °C.
(a) Scanning electron micrograph indicating the blocky austenite (γ).
(b) Transmission electron micrograph indicating bainitic ferrite (α) & retained austenite (γ) films (Podder et al. 2011).

This austenite is mechanically unstable and undergoes transformation to martensite under moderate stress condition. The high hardness and brittleness of martensite will lead to reduction in the toughness of the alloy. Nevertheless, if austenite shows up as a film covering the bainitic ferrite, it requires considerably higher strains so as to change to martensite. For this situation the austenite is mechanically stable and acts as dislocation trap, prompting further strengthening of the material without conciliating its toughness (Bhadeshia 2001). A comparable nature is seen with respect to the carbon content in retained austenite. Increased quantity of carbon in retained austenite keeps it more stable

and thus the strength and toughness of the material are increased. The most recent advancements have facilitated the design of alloys that can be isothermally transformed at temperatures as low as 200 °C (Leiro 2014).

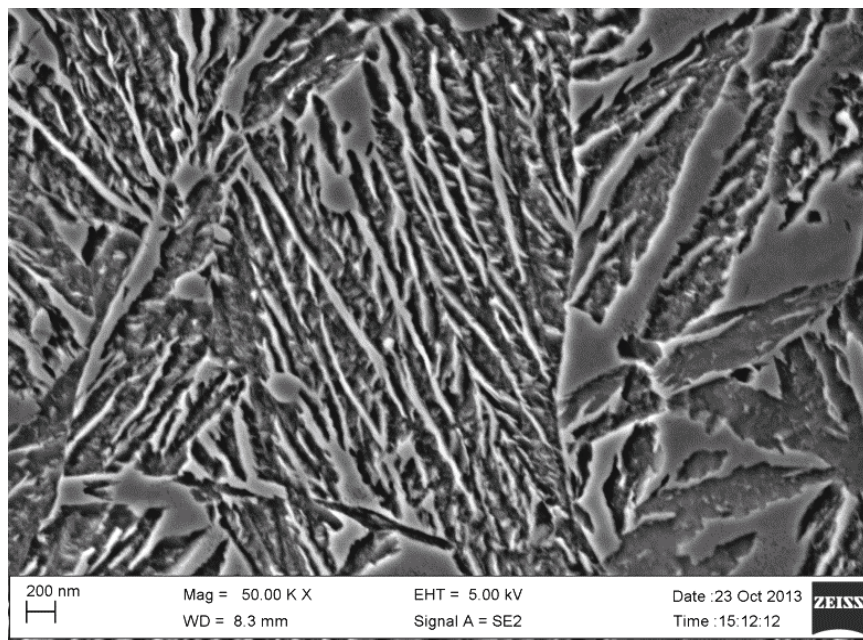


Figure 2.6 Scanning electron micrograph of nano-structured CFB steel (Leiro 2014).

The low transformation temperatures restrict the diffusion of carbon atoms and offers large degree of supercooling at that point resulting in high nucleation that generates structure of bainitic ferrite laths and retained austenite with nanometer level thickness (figure 2.6). The combination of the aforementioned microstructural characteristics results in steel which has yield and ultimate tensile strength that could match those of quenched and tempered steels along with improved toughness.

2.1.3 Influence of austempering temperature and time

The microstructure of these CFB steels attained by austempering process firmly relies upon the transformation temperature. At lower austempering temperature around 250 °C just above martensite start temperature (M_s) the carbon diffusion rates are low. Thus the retained austenite contains low carbon concentration at this temperature and also ferrite nucleated here appears finer and have random orientation. It has been confirmed that the

length of the ferrite laths remain equal with the varying austempering temperature however the width of the same increases. On the other hand austempering at higher temperature possess lower degree of supercooling and results in lower ferrite content and large quantity of RA (Putatunda 2003). At high temperatures, basically the austenite contains almost all the carbon and the quantity of the same in austenite attains a maximum value (solubility limit 2.10%). Further increase in temperature, the carbon diffusion rates are very high and subsequently the carbon content in austenite begins to diminish once more. Ultimately the carbon diffusion rates at high temperature i.e. 390 °C makes the austenite incapable of holding the carbon (Putatunda 2001).

Once the austempering temperature has been chosen, the austempering time must be selected in order to optimize properties through the creation of a stable structure of ausferrite. Shorter austempering intervals generates a microstructure comprising of bainitic ferrite and RA; for extended intervals, austenite turns out to be more stable and further increase in time brings about decomposition of RA to ferrite and carbide. Prolonged austempering did not bring about additional improvement in hardness and strength (Kankanala 2010).

2.1.4 Overview of mechanical behavior of Austempered steels

Several research works have been carried out so far based on the microstructure and mechanical properties of austempered steels, the same are reviewed in this section.

Bhadeshia and Edmonds (1979) explored the bainite transformation in a 0.43C-3Mn-2.12Si (wt. %) steel. Austenitization was carried out at 1200 °C for 5 minutes, successive austempering heat treatments were performed in temperature range 250-450 °C for definite intervals. Results revealed distinct C-curves and transformation mechanisms for upper and lower bainite. TEM studies showed the growth of both upper and lower bainite. Confirmation for carbon super saturation was acquired for the lower bainitic ferrite. Carbide precipitation occurrences were likewise described and the confirmation proposed that precipitation came about because of the aging of a supersaturated lattice in lower bainite.

Tomita and Okawa (1993) examined the microstructure and mechanical properties of 0.41C-1.7Si-0.8Mn-0.8Cr-1.76Ni (wt. %) steel. Results demonstrated the change in fracture toughness (K_{1C}) and Charpy impact toughness of isothermally transformed steel when contrasted with regular hardened and tempered steel. Austempering beyond 370 °C possessed extensive retained austenite content (22-25 vol.%), in conjunction with carbon free upper bainite; however deleterious effect was viewed on strength and toughness, which is because of some blocky sort of retained austenite transformed to untempered martensite during plastic deformation.

Erik Navara (1995) carried out work on austempering of EN45 spring steel (0.5-0.6C, 1.5-2.0Si, and 0.7-1.0Mn) that generated ausferrite structure. Results demonstrated that mechanical properties of ausferrite structure depended on austempering temperature (300-350 °C). Its blend of strength and impact toughness surpassed that of tempered martensite (tempered at 400-500 °C) in a low alloy hardened and tempered steels and has also achieved the values close to that of maraging steels.

Li and Chen (2001) who evaluated the effect of austempering heat treatment on the microstructure and mechanical properties of high Si cast steel. Results demonstrated the ausferrite microstructure that comprised of bainitic ferrite and RA. The outcome of experiment showed that ausferrite structure had superior properties. Austempering at a temperature range i.e. 320 to 360 °C yielded the optimum structure that exhibited high strength, toughness and hardness.

Caballero and Garcia-Mateo (2005) examined the function of retained austenite on tensile properties of two types of high carbon silicon rich steels with bainitic microstructures. The outcomes revealed that the isothermally heat treated microstructure (200 to 300 °C) comprises of thin ferrite plates (nm), in a retained austenite matrix. The fine sized ferrite plates contributed to the strength and retained austenite on the other hand contributed for ductility. Improvement in ductility was accomplished by strain induced martensitic transformation from austenite (TRIP effect).

Liu et al. (2006) evaluated the mechanical properties of lathlike upper bainite formed isothermally at 400 °C for various holding times in 0.64C-1.83Si-0.74Mn steel. Results showed that there was no proof of carbide precipitation in the microstructure. The retained austenite content increased with holding intervals from 300 to 600 seconds and declined with times from 600 to 3600 seconds. Excellent blend of strength and ductility was ascribed to the existence of bainitic ferrite laths and plenty of carbon rich retained austenite films. The blocky sort of retained austenite was noticed for holding times beyond 600 seconds, bringing about the most noticeably deleterious blend of strength and ductility.

Sajjadi and Zebarjad (2007) studied the bainitic transformation in high carbon steels. Results indicated that austenite in the high carbon steel, changed to bainite over the temperature range 250-475 °C, as per separate C-curves on the TTT plot. It was demonstrated that over 325 °C, austenite transformation begins with formation of upper bainite and beneath that temperature lower bainite formation occurs. Additionally, in a few areas in the temperature range 250-375 °C both upper and lower bainite could be seen, at the same time.

Putatunda et al. (2009) investigated the influence of austempering temperature on the microstructure and physical properties of 0.4C-2Si-1Cr-0.6Mn-0.2Mo-0.5Cu (wt. %) steel. Results revealed an assorted microstructure consisting of bainitic ferrite and RA like ausferritic structure in ADI in the austempering temperature range of 316– 400 °C. However existence of some martensite was likewise examined. Blend of exceptionally superior yield strength of 1336 MPa and fracture toughness of 116 MPa \sqrt{m} (a value practically identical to maraging steel) were acquired in this steel at austempering condition of 316 °C for 2 hours.

Santos et al. (2009) examined the mechanical behavior and microstructure of 0.56C-1.43Si-0.58Mn-0.47Cr (wt. %) steel with transformation induced plasticity effect (TRIP). The heat treatment cycle included annealing at 900 °C, austempering at 400 °C and water quenching. Results showed the most excellent blend of tensile strength (1350 MPa) and

ductility (25%) because of the high amount of retained austenite in the microstructure at room temperature, moreover the transformation of austenite to martensite during plastic deformation (TRIP) is liable of this blend of high tensile strength and ductility. The samples transformed at 600°C generally comprises of ferrite and pearlite microstructure. This is related with the diminishment in strength and ductility when contrasted with the samples transformed at 400 °C.

Son et al. (2010) examined the effect of austempering parameters on the microstructures and mechanical properties in Fe-0.9C-2.3Si-0.3Mn (wt. %) steel. This austempered steel exhibited superior tensile strength ranging from 1300 to 2200 MPa and ductility about 25% when compared to austempered ductile iron that offered tensile strength (850 to 1600 MPa) and ductility (13%). At austempering temperatures of 260 °C and 380 °C, lower ausferrite and upper ausferrite microstructure was formed respectively. As the isothermal transformation temperature increased from 260 to 380 °C, the hardness and tensile strength diminished, however the elongation and retained austenite content increased. Furthermore, the microstructures were coarser.

Sharma et al. (2011) carried out their examination on advancement of two grades (S1 and S2) of carbide free bainitic steels for high strength applications: S1:0.3C-1.76Si-1.57Mn-0.7Cr-0.04Ni-0.01(Mo, Al, S, P) and S2:0.47C-1.22Si-1.07Mn-0.144Cr-0.045Ni-0.025-Mo-0.04Al-0.016S-0.022P (wt. %). The samples were hardened and tempered to accomplish high hardness and strength levels. Results showed that the mechanical properties of these two steels were additionally a function of the microstructure consisting of bainite, retained austenite, martensite and finer bainite laths. Notable outcomes were obtained i.e. strength of 1557 MPa and fracture toughness $236 \text{ MPa}\sqrt{m}$ for intermediate transformation temperature because of the improvement in the quantity of bainite and retained austenite. The isothermal temperature of 350 °C with time of 30 minutes was the optimum treatment condition for high Si steel of grade S2.

Yang et al. (2012) evaluated the effect of low-temperature austempering on the microstructure-mechanical properties of high-carbon steel enriched with Si-Al alloy.

Results revealed the nanostructured bainite and superior blend of mechanical properties were accomplished in this steel by austempering in the range 220-260 °C. The bainite structure consisting of bainitic ferrite and RA had a lath thickness in the range 38-57 nm. The yield and tensile strengths attained up to the range 1534-1955 MPa and 2080-2375 MPa respectively along with % EL of 6.7-7.8% and Charpy impact toughness of 7.8-22.2 J. The fractured surface of impact tested specimens revealed quasi cleavage mode.

Junior da Cruz et al. (2014) studied the role of retained austenite on impact toughness of bainitic-martensitic dual phase steel. Results demonstrated the isothermally heat treated and tempered samples indicated higher mechanical properties than that of just isothermally treated samples. A more notable effect of RA occurred on the Charpy impact and microhardness tests. It was observed that higher the RA content, more prominent was the impact toughness which is independent of RA morphology (film/block).

Wang et al. (2014) examined the influence of multi-stage bainitic transformation in Fe-0.30C-1.46Si-1.97Mn-1.50Ni (wt. %) steel. Results revealed the increase in quantity of nanoscale bainitic ferrite plates and film-like austenite when contrasted with regular bainitic transformation, which prompts a refinement in the normal thickness of the bainite plates. Excellent mechanical properties were revealed by the samples with refined microstructure.

Caballero et al. (2014) discussed the effect of transformation temperature on carbide precipitation series during the formation of lower bainite for three steels with differing contents of carbon and silicon. Results affirmed that dislocations in lower bainite that are more unique at the lower the transformation temperature, snare a considerable amount of carbon and consequently can affect the carbide precipitation arrangement and specifically can figure out where ϵ -carbide forms before the cementite growth.

Mandal et al. (2014) examined the advancement of microstructure and mechanical properties under numerous austempering intervals of cast Fe-1.5Si-1.5Mn-V (wt. %) steels. Results revealed the bainite and retained austenite microstructure. It was also observed that tensile strength increased however % EL diminished with increasing

austempering duration. Morphological variation of bainite from fine to coarse laths was observed with increment in holding time. There was evidence of carbide precipitation as the austempering interval increased from 30 to 60 minutes that resulted in reduction in ductility yet increment in strength. Superior blend of strength and ductility was observed for holding interval within 10-30 minutes at isothermal temperature of 400 °C.

Long et al. (2014) investigated the carbide-free bainite in medium carbon steel. Outcomes demonstrated that the kinetics of bainitic transformation generally experiences 3 stages: short incubation, explosive nucleation and sluggish growth. Mechanical testing results revealed that the low temperature bainite exhibited high UTS and impact toughness all the while the lower bainite exhibited less UTS and superior impact toughness and vice versa for upper bainite.

Monia et al. (2015) investigated the advancement of highly ductile spheroidized steel containing 0.6% C-1.71% Si. Structure-property relationship was examined in this steel with increasing strain and the longer holding interval in the intercritical area. Carbides of spherical shape turned finer with the increasing holding time and strain. Thus possessed best blend of high UTS around 800 MPa and % EL up to 29%.

Avishan et al. (2015) studied the microstructural characterization and mechanical properties in two diverse nanostructured bainitic steels. Results showed that diverse nanostructured bainitic ferrite and carbon rich RA were attained at lower isothermal temperatures (200–300 °C) are obtainable in two grades of high carbon high alloy steels. High strength with moderate ductility and impact toughness was acquired. It was demonstrated that the YS and UTS depend upon thickness and quantity of bainitic ferrite.

Baradari and Boutorabi (2015) studied the effect of austempering conditions on the microstructure and hardness evaluation of high-carbon steel alloyed with Al–Si. Microstructural studies revealed that the samples austempered in the temperature range 300-360 °C for the duration of 1 to 8 hours predominantly comprised of bainitic ferrite and retained austenite. YS of 1170 MPa, UTS of 1370 MPa, and an aggregate % EL of

9.1% were acquired after austempering at 360 °C for 4 hours. Increase in hardness was observed with decrease in transformation temperature i.e. from 500-660 HV₃₀.

Hofer et al. (2016) studied the morphological variation of retained austenite during austempering of CFB steel. Results demonstrated that the RA content remained unaffected for longer partitioning times. However the morphology of RA changes from film to blocky structure because of which the carbon diffusion is extensive and in turn brought about TRIP effect prompting high ductility.

Wang et al. (2016) investigated the effect of austempering on microstructure-property relationship in bainitic steel. This investigation revealed the bainite/martensite multiphase microstructure on post austempering in the vicinity of 325 and 400 °C. Austempering at higher temperature offered lower strength and toughness, due to the existence of bainitic ferrite lath of large width and blocky martensite/austenite constituents. Austempering below M_s temperature displayed superior impact toughness, because of the lower bainite containing superfine sub-plates of ferrite. In the meantime, toughness of air-cooled material at low temperature was better than the steel austempered at 325 °C, on account of successful grain refinement.

Varshney et al. (2017) investigated the exceptional strain hardening behavior of medium carbon high silicon steel (0.6C-1.71Si-0.86Mn wt. %). The samples after austenitization were continuously cooled from 0 to 40 seconds, subsequently austempering at 300, 350 and 400 °C. Results showed superior strain hardening reaction with three strain hardening steps during tensile loading. The samples with hard bainite and soft ferrite in various amount revealed a poor strain hardening response. The presence of small quantity of pearlite increased strain hardening reaction. The strain-hardening exponent constantly increases with strain in the samples where retained austenite had considerably experienced strain-induced transformation.

2.1.5 Wear

Wear is defined as the damage caused to the solid surface, resulting in gradual loss of material from the operating solid surface, which is in turn due to the relative motion

between two surfaces (Teer and Arnell 1975). Wear, identical to friction, is not a property of material; it is a response of system. It can be reduced by appropriate choice of materials, lubricants and operating conditions (Kankanala 2010). Wear is linked with interactions amongst surfaces and particularly the removal and deformation of material on a surface because of mechanical action of the contrary surface. In most industrial situations, wear is generally caused by adhesive and abrasive mechanisms. When compared to other wear mechanisms, the fatigue mechanism involves slow material removal. Wear is infrequently catastrophic yet it lessens operating efficiency by escalating the power losses, oil consumption and the rate of component substitution (Eyres 1979).

2.1.5.1 Parameters influencing Wear

There are several parameters that influence the wear. Wear essentially depends on the material, design and environment. Some of the parameters that influence the wear are given in the Table 2.1.

Table 2.1: Parameters and variables influencing the wear

Parameters	Variables
Material	Composition, grain size, thermal conductivity and hardness
Design	Shape, loading, type of motion, toughness, vibration cycle and time
Environmental	Temperature, humidity, atmosphere and contamination
Lubrication	Type of lubricant and lubrication stability

2.1.5.2 Methods of wear measurement

- Weighing method: This method includes measurement of wear specimen before and after wear test.
- Mechanical gauging method: In this method, wear is measured by specimen displacement using LVDT.
- Optical method: In this, wear is noted by the reduction in size of a micro hardness indentation taken on the surface.

2.1.5.3 Types of Wear

A primary system to categorize wear was first proposed by Burwell and Strang (1952). Later Burwell (1957) tailored the classification to comprise the subsequent different types of wear, namely:

- i. **Adhesive wear:** This occurs when two ostensibly flat solid objects are in sliding contact, irrespective of lubrication. Adhesion/bonding arises at the asperity contacts at the interface and gets sheared by sliding, leading to the separation of a fragment from one surface and addition to the other surface (Radziszewski and Tarasiewicz 1993).
- ii. **Abrasive Wear:** This occurs by material removal from a surface by another harder object, resulting in the formation of debris of hard particles between the two surfaces usually referred to as scratching, gouging or scoring on the basis of wear severity. The rate at which the surface abrades depends on the characteristics of material surface, presence of abrasive particles, the speed and other environmental conditions. Abrasive wear is typically classified based on the types of contact and environment. Types of contacts include two-body and three-body wear.
- iii. **Fretting Wear:** This occurs between two mating surfaces; initially being adhesive in nature and quivering or oscillation with low amplitude is an essential contributing aspect. Fretting is frequently accompanied by corrosion. Normally, fretting arises among two tight-fitting surfaces under cyclic condition, relative movement of least amplitude.
- iv. **Surface Fatigue Wear:** This is seen during frequent descending rolling over a track. The materials exposed to recurring cycles of loading and unloading type may persuade the development of cracks on the surface or subsurface, which ultimately damages the exterior with the formation of large fragments and also forms craters in the exterior. An analogous form of wear is shown by brittle materials, which break up in the form of large fragments.

- v. **Corrosive Wear:** Generally metals are thermodynamically insecure in air and get oxidized when reacted with oxygen i.e. layer/scale formation on the exterior of metal or alloys due to their inadequate interfacial bonds. Corrosive wear is caused by deterioration of exposed surfaces of metal by the impacts of the air, gases, acids, antacids, and so forth. This kind of wear generates pits and might ultimately lead to break down of metal parts.
- vi. **Erosive Wear:** Erosion of materials and components are generally caused due to the impingement of solid particles or droplets of liquid or gas. Cavitation erosion arises during the relative motion of solid and a fluid, thereafter the fluid becomes unsteady and bubbles up and burst on the hard surface, especially in fluid handling machines as marine propellers, hydro foils and all other hydraulic turbines cavitation erosion abrades a surface similar to that of an etchant.
- vii. **Oxidative Wear:** Under non aqueous conditions due to the presence of air, an oxide will form on the metal surface. The surface changes chemically by environmental factors. This results in the formation of surface layer with properties that differ from those of the parent material. Consequently this layer may wear differently. This induces fracture at the interface of the surface layer and parent material resulting in removal of the entire surface layer when wear occurs and its debris assist the wear process. Increasing the oxidation rate enhances the wear rate.

2.1.6 Wear behavior of austempered high silicon steels

AISI 9255 steel finds application in manufacturing the main components of cultivator, especially reversible shovel which is normally fitted on cultivator as soil working tool for many purposes such as loosening the soil, destroying weeds and to mixing soil particles. The low quality of the shovel material influences the efficiency of work and prompts the loss of time particularly in urgency. Abrasive wear of the soil-engaging components like cultivator shovel is a reason for worry as it causes damage to the material and increases

the cost and time lost in supplanting worn parts of agriculture machinery (Jagtar et al. 2013).

The generation of wood pellets incorporates several processing steps in which the wear on the tool components is extensive. The knives utilized for cutting sawmill dust and the ring die made of EN 1.5026 grade steel (comparable to AISI 9255) which is utilized for pelletizing the fragmented saw dust, are two illustrations where this extensive wear happens. The essential material property necessities of the knives are high wear resistance and toughness (Lindstrom 2006).

Shah et al. (1986) investigated the erosion resistance of two distinctive high-silicon steels austempered at two diverse holding times. They reported that a completely CFB microstructure brought about great resistance from erosive wear. Presence of both untempered martensite (inadequate transformation) and carbides (longer austempering times) brought about a decrease of both erosion resistance and mechanical properties. In this investigation, a significant strain hardening of the CFB microstructure was seen and was regarded as the reason for the enhanced wear resistance.

Liu Ping and Bahadur (1990) investigated the sliding wear behavior of high-silicon steels and contrasted it and that of ADI. These samples were austempered in the upper bainite zone (370 °C), and high silicon steel austempered at 420 °C at various lengths. The aim of this examination was to check whether graphite would affect friction and wear of an austempered steel microstructure. The outcomes indicated no effect of graphite on friction. Moreover, the nodules caused considerable weakening of the surface when contrasted with austempered steel. Under the test conditions utilized, the graphite nodules in the iron prompted subsurface cracking, while no cracks were seen in the austempered steels.

Clayton and Jin (1996) while investigating about bainitic steels found that increasing amount of CFB in the microstructure can be useful towards rolling/sliding wear. The contemplated steel contained a blend of CFB, retained austenite and martensite. Results demonstrated that this steel had a wear rate in the same order of magnitude from

Hadfield's manganese steel i.e. commonly used for railway track work and also for junction pieces at the highest loads and slip ratios.

Lee and Polycarpou (2005) taken after this examination and analyzed a similar steel alloy utilized by Clayton and Jin in 1996 (named J6). Field and laboratory tests were carried out on the "J6" material and contrasted and Hadfield's manganese steel. Their basic finding was that Hadfield's steel had a lower wear rate than the test alloy both in lab and field tests. Nevertheless, it was additionally seen that the bainitic steel had a higher resistance to rolling contact fatigue than the regular rail steel. This was credited to a nonappearance of surface hardening in the exploratory alloy rails.

Shipway et al. (1997) published their first studies on the effect of the austempering temperature on the sliding wear execution of CFB steels. It was observed that in 0.45C-2.08Si-2.69Mn steel, the least sliding wear rate was attained when an austempering treatment was applied. The hardness of the steel diminished with increasing austempering temperature up to ~ 370 °C. The best wear property was observed at lower austempering temperature, while the poor wear property was seen at intermediate austempering temperatures. The high wear resistance of the structure was ascribed to the grade of refinement of the bainite and the absence of cementite and martensite in the microstructure.

Chang (2005) compared the rolling/sliding wear resistance of different high silicon austempered steels through research laboratory tests. One of his fundamental discoveries was that steel with completely CFB microstructure yielded extremely low wear rate. Allotriomorphic ferrite was unfavourable to the wear resistance. In this examination the surface change of austenite into martensite was contemplated by XRD estimations. It was observed that all the retained austenite in the contact surface transformed to martensite that further caused surface hardening and in turn increased the wear resistance.

Leiro et al. (2011) investigated the tribological behavior of CFB steel under dry rolling/sliding conditions at various temperatures and sliding distance. The point was to contemplate the wear behavior of the 60SiCr7 spring steel with a microstructure that is free from carbide containing diverse amount of RA. The outcomes revealed that the

increased wear resistance of the specimen austempered at 250 °C was ascribed to its predominant mechanical properties also due to its finer microstructure. The absence of RA peak after XRD of worn samples confirmed that the steel during wear had experienced TRIP effect.

Leiro et al. (2013) studied the wear behavior of nano-structured CFB steels subjected to dry rolling-sliding conditions; steels having carbon content in the range 0.6-1.0 wt. % were isothermally transformed at low temperatures, in the range 220-270 °C, so as to attain a bainite structure with a lath thickness in the range 32-60 nm. Overall, the nano-structured CFB steels exhibited superior wear resistance when compared to those of upper bainite structured steel of similar hardness.

Yang et al. (2012) studied the sliding wear behavior of nanostructured bainitic steel subjected to various austempering temperatures and contrasted it with the Q&T condition of similar steel. Results demonstrated that sliding wear resistance of this steel increases as the austempering temperature decreased from 260 to 220 °C. At the point when contrasted with Q&T condition wear resistance of this austempered steel was observed to be 21-51% more prominent, however the hardness of austempered steel was lower when contrasted with Q&T. The mean size of the nano grains in the worn surface of the AT samples at 240 °C is not as much as that of Q&T samples.

Bakshi et al. (2014) studied the dry rolling/sliding wear of nanostructured bainite. Results revealed that the nanostructure, produced by isothermal transformation at 200 °C, and had wear resistance that surpassed that of other CFB steels mainly due to the fine scale nanostructured bainite associated with high strength, hardness and retained austenite morphology and also by work-hardening effect i.e. deformation induced martensite.

2.2 Quenching and Partitioning (Q&P) Heat Treatment of High Silicon Steels

The Q&P treatment differs from austempering (CFB microstructure) in which it separates the carbon-advancement of austenite, and subsequently its stabilization, from the underlying decomposition of austenite however Q&P treatment includes quenching to martensite (Between M_s & M_f temperature). This proposes a element of control over the carbon content of the RA, which separated from regulating its mechanical and thermal stability, may likewise prompt superior properties (Edmonds et al. 2011).

2.2.1 Concept of carbon partitioning

Partitioning of carbon from martensite to RA is generally disregarded in hardened steels, since the temperature is excessively small for significant amount of carbon diffusion to occur past quenching, supersaturation of carbon in martensite is conventionally abolished by a diverse mechanism i.e. precipitation of carbide during hardening. A model was generated, which portrays the end of carbon partitioning among quenched martensite and RA without carbide precipitation. This model expected a stationary interface between ferrite (α) and austenite (γ), and a consistent chemical potential for carbon, however not iron, in the 2 stages, prompting a condition of metastable equilibrium referred to as "constrained paraequilibrium" [CPE]. Post consultations with Hillert and Agren (2004) the model was renamed as "Constrained-Carbon paraequilibrium" (CCE) condition. The model was clarified with case computations demonstrating the qualities of CCE and connected to another Q&P process, to make blends of carbon lean martensite and carbon-rich RA. The element for the carbon enrichment of austenite during partitioning was contemplated by Clarke et al. (2008), theoretical calculations demonstrated that carbon partitioning from martensite gave a more attractive clarification to tentatively estimated austenite fractions, in spite of the fact that the formation of bainite during partitioning couldn't be totally rejected. Alloying additions like Si, Al, and P were utilized to stifle the carbide precipitation and generate martensite and controlled quantity of retained austenite in the final microstructure.

2.2.2 Design of quenching and partitioning heat treatment

The Q&P heat treatment process is schematically shown in figure 2.7 and can be separated into three main stages. The principal heat treatment step is austenitizing, where the carbon is homogeneously distributed, and the initial carbon content (C_i) is equivalent to the overall carbon concentration of the steel.

The second step involves cooling to a quench temperature (QT) between martensite-start (M_s) and martensite-finish (M_f), in order to form a controlled quantity of martensite. After quenching, the carbon content of austenite (C_γ) and martensite (C_m) are the same, and are indistinguishable to the initial carbon content (C_i).

The third treatment step is heating to the partitioning temperature (PT) at, or over, the underlying quench temperature, and holding for a particular time. This enriches the austenite with carbon, by partitioning of carbon from carbon-supersaturated martensite. During this step, the carbon partitions from the martensite to the austenite (where its chemical potential is lower) so the martensite carbon content reduces, while the carbon content of the austenite increases. Computations demonstrated that at the CCE condition, almost the greater part of the carbon in the martensite would have partitioned to the austenite.

Consequently, a clear method to assess the austenite composition is to assume complete partitioning (Gerdemann et al. 2004). Higher carbon increases the chemical stability of the austenite with the goal that much or the greater part of the carbon rich austenite stays stable at room temperature.

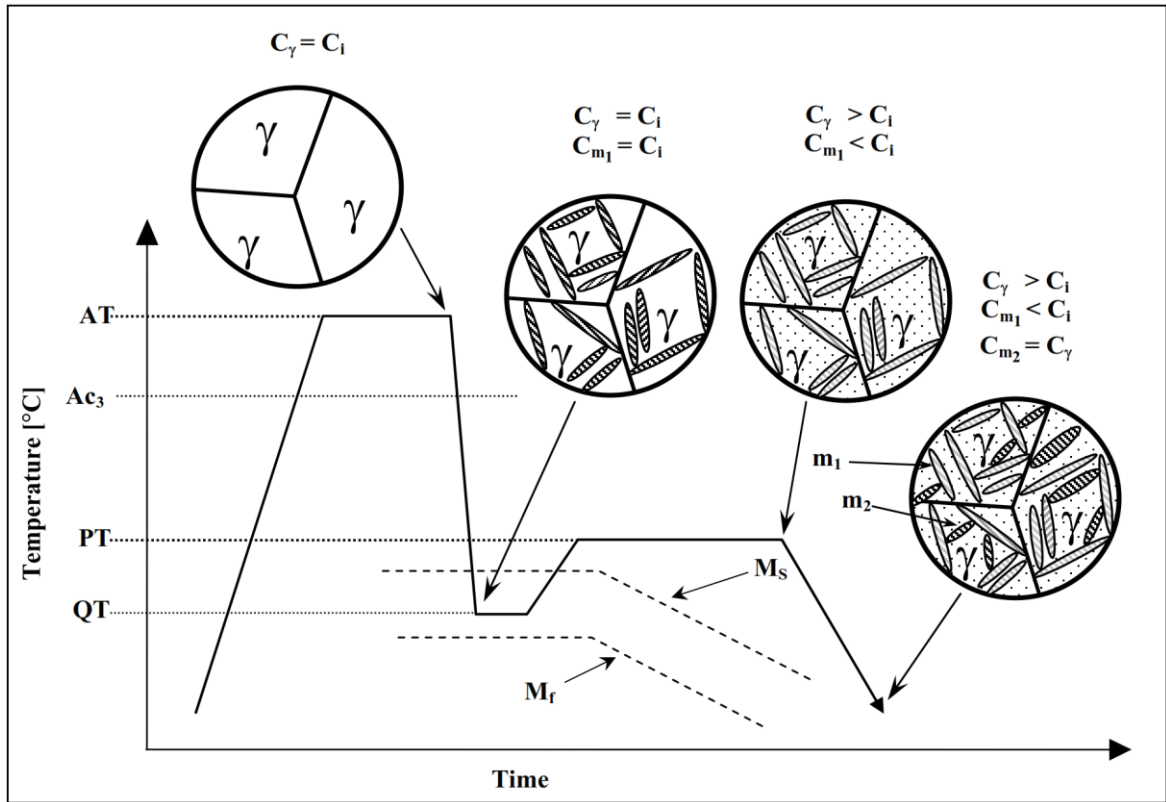


Figure 2.7 Schematic portrayal of Q&P heat treatment to generate carbon-lean martensite and carbon rich RA mixture: (Gerdemann et al. 2004) [C_i , C_γ and C_m are the carbon contents of the initial alloy, austenite and martensite respectively, and AT, QT and PT are the respective austenitising, quenching and partitioning temperatures.]

The effect of carbon enrichment on phase stability is appeared through the effect on the M_s and M_f temperatures, envisioned in figure 2.7 by the descending slope of the dashed lines. The last step is quenching to room temperature. During this step, a portion of the austenite may transform to martensite. This martensite (m_2) has higher carbon content and consequently unexpected properties in comparison to the martensite that was available before partitioning.

Figure 2.8 represents how this model foresees the increase in final RA content as a function of the initial carbon content of the steel (Edmonds et al. 2006).

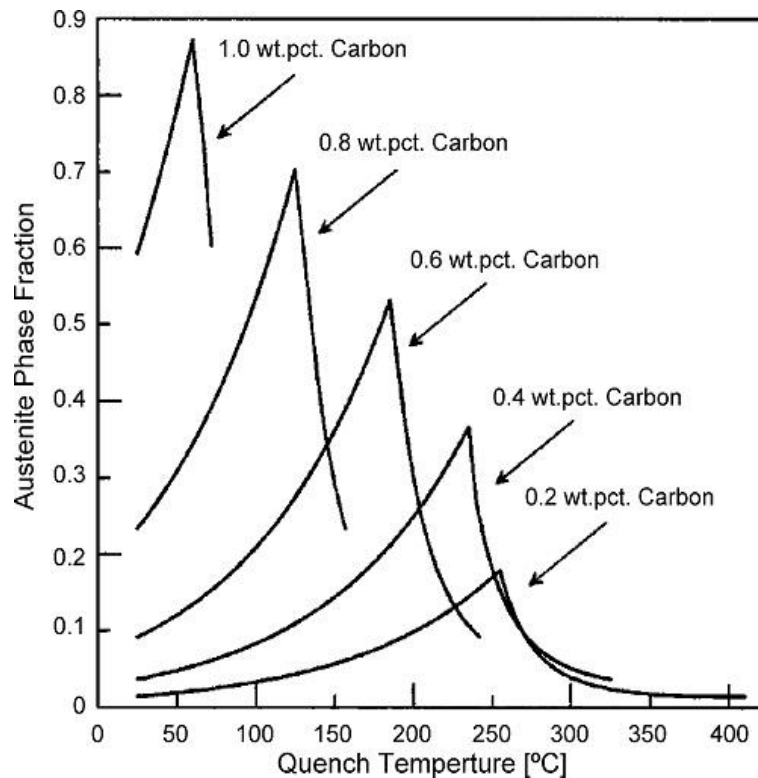


Figure 2.8 Predicted quantity of retained austenite for various carbon contents

This plot was formerly created to think about the reaction of a carburized part throughout Q&P treatment, and demonstrates the significance of austenite stabilization by carbon and inducing important processing temperatures.

2.2.3 Overview of microstructure, mechanical and wear behavior of Q&P heat treated high silicon steels

Gerdemann et al. (2004) studied the microstructure and hardness of 9260 steel by Q&P heat treatment. The outcomes demonstrated that considerable retained austenite content may perhaps be accomplished by this process, moving toward 30% by volume for 10 seconds partitioning at 500 °C. Lower temperature i.e. 250 °C prompted partitioning times to facilitate for manufacturing of bulk samples (e.g. 45-60 minutes), though substantially shorter intervals were related with the maximum RA content. At partitioning condition of 400 °C for 10 sec, some favourable properties were recorded in this investigation, for example, hardness in overabundance of HRC58 in mix with RA content approach 10%.

Nayak et al. (2008) investigated microstructure-hardness correlation of medium and high carbon steels containing silicon subjected to Q&P heat treatment. The investigation proposed that in medium-carbon steels, increased carbon partitioning from supersaturated martensite to RA and austenite stabilization ensues. Another essential feature that arises from this examination is that the precipitation of transition (ϵ) carbide at lower temperature i.e. 250 °C due to high Si content. The reduction in hardness in this steel during partitioning is an aggregate effect of RA stabilization, martensite softening and decline in supersaturation of carbon in martensite.

Li et al. (2010) investigated the bainitic transformation during the two step Q&P process in medium carbon steel with silicon as alloy. The outcomes demonstrated the variation of strength in Q&P steels was an aggregate effect of increment of RA content, diminishing of carbon supersaturation of fresh martensite, and especially quite a bit of lower-bainite arrangement. The UTS continuously diminished while the YS in 2-step Q&P treated steels diminished initially and therefore prolonged partitioning are ascribed to the combined effect of increased quantity of RA, diminished carbon supersaturation in martensite and arrangement of lower bainite from RA at the conclusive stage.

Santofimia et al. (2011) investigated microstructural improvement during the quenching and partitioning process in recently designed low-carbon steel.

Four diverse heat treatment arrangement (Fig 2.9) beginning from austenitization at 900 °C for 600 seconds.

The outcomes demonstrated that during the stage of partitioning the thermal stabilization of austenite isn't really conveyed by a considerable growth of the material.

This infers the process of carbon partitioning from martensite to austenite happens across martensite–austenite interfaces of low-mobility. The amount of martensite formed during the primary quench was estimated. Dissimilar to martensite formed in the last quench, there was also indication of tempered martensite on partitioning.

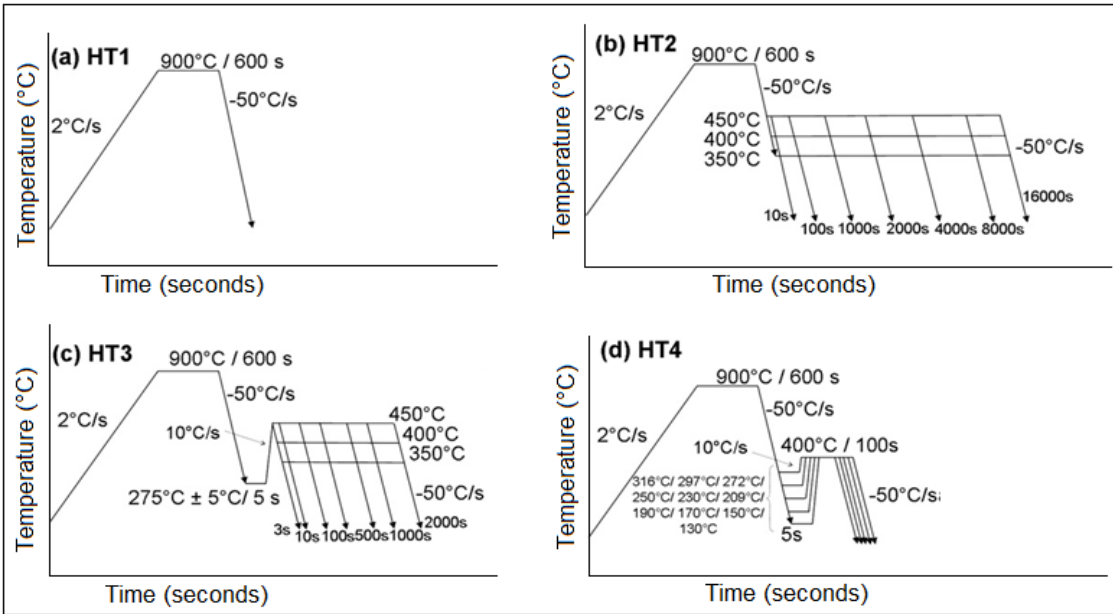


Figure 2.9 Steel subjected to various heat treatment (a) HT1- To create the necessary quenching rate; (b) HT2- Austempering; (c) HT3- Effect of partitioning conditions; (d) HT4- Effect of varying quenching temperature.

Estimated quantities of RA after various heat treatments (Fig. 2.9(a-d)) were contrasted and simulations utilizing model depictions for partitioning of carbon from martensite to austenite. Simulation outcomes affirmed that the carbon partitions at low-mobility interfaces of martensite & austenite.

Paravicini Bagliani et al. (2013) investigated the effect of Q&P heat treatment on microstructure, the tensile and toughness properties of medium-carbon steel. Results showed that the best blend of yield strength and toughness was attained at quenching temperature of 250 °C. This outcome can be ascribed to a blend of effects of: higher RA stabilization, the carbon diminution of martensite and the diminishment of untempered martensite content. The same steel after Q&T treatment revealed poor combination of strength and toughness when compared to Q&P treated condition.

Sun et al. (2014) studied the structure-property correlation and mutual deformation of Q&P steel. Results showed that the bainite transformation occurred at the primary stage of partitioning and the quantity is comparative to quenching temperature. Martensite

softening, kinetics of bainite transformation, quantity of stabilized RA jointly had effect on the mechanical properties. The EBSD examination provided better understanding of mutual deformation-transformation behavior. Plastic deformation particularly happened in the interface region of ferrite–martensite and extends to the core of ferrite grain with increasing strain. Superior combination of strength (990-1100 MPa) and ductility (25.9-29.3%) was observed for this Q&P steel.

Tan et al. (2014) studied the mechanical properties of 40Mn2Si2Cr steel treated by Quenching-Partitioning-Tempering (Q-P-T). The outcomes demonstrated that the partitioning time of Q-P-T treatment can be extended incredibly to 90 minutes or on the other hand even longer. The tensile strength, elongation and product of strength and elongation (PSE) of the test steel achieved were 1650 MPa, around 20% and beyond 33 GPa%, respectively.

De Knijf et al. (2015) studied the heat treatment parameters and kinetics of Q&P cycles of 0.25C-1.5Si-3Mn (wt. %) steel. Results demonstrated the stabilization of the some amount of RA occurred more rapidly with a larger amount of austenite formed at a higher quench temperature. Partitioning at 300 °C brought about the arrangement of ϵ -carbides draining the accessible carbon for partitioning. Partitioning in the temperature range 370-400 °C was found to be optimum, which improved carbon diffusivity without contending reactions. Over 400 °C, austenite decomposition and tempered martensite along with cementite thereby diminishing the RA content and total elongation.

Wu et al. (2016) studied the improvement of mechanical properties for Q&P steels by means of intragranular austenite. The chemical composition of the steel was Fe–0.2C–1.4Si–1.8Mn (wt. %). Q&P route was adopted to generate a multiphase microstructure comprising of large quantity of RA. Results demonstrated that the mechanical properties of Q&P steels (partitioning at 350 °C for 10 seconds) were drastically improved by two sorts of austenite, incorporating intragranular austenite in ferrite grains and allotriomorphic austenite.

Pierce et al. (2016) carried out quantitative examination concerning the effect of temperature on carbide and austenite advancement during partitioning of 0.38C-1.54Mn-1.48Si (wt. %) steel. Results revealed the arrangement of η -carbide while quenching, holding and partitioning stages. Partitioning of carbon from martensite to austenite was found to be more effective at 450 than 400 °C leading to lower carbon content in martensite, less carbide formation, and higher RA content for small partitioning intervals.

Seo et al. (2016) investigated the microstructure-mechanical properties relationships for Q&P heat treated steel. Results showed the microstructure of a Q&P treated medium Mn steels involved carbon rich retained austenite and carbon depleted tempered primary martensite when the quench temperature, T_Q, was low. The tensile behavior of Q&P treated steel was interpreted by utilizing a microstructure-based dislocation evaluation model. It demonstrated that the retained austenite showed a high work hardening rate, predominantly because of the TRIP effect.

Wang et al. (2016) carried out comparison investigations of three body affect abrasive wear behavior for quenching-partitioning-tempering (Q-P-T) and quenching-tempering (Q-T) of 20Si2Ni3 steels. The outcomes demonstrated that weight loss during wear increased and after that diminished with the escalating impact energy and the maximum occurred under 2.5 J. Less weight loss during wear was possessed by Q-P-T steel compared to Q-T steel because of the increasing quantity of RA which favored to acquire thicker hardened layer on account of its high phase transformation strengthening and strain hardening.

Arlazarov et al. (2016) studied the influence of partitioning on mechanical behavior of Q&P treated 0.2C-2.22Mn-1.44Si-0.21Cr (wt. %) steel. Results demonstrated that partitioning temperature had a vital effect on the strength and ductility of Q&P steels. Tensile studies revealed that the YS increase with tempering conditions had a few similarities with the YS advancement of Q&P steels with partitioning conditions.

Luo et al. (2016) studied the influence of Q&P heat treatment on the structure-property relationship of high carbon steel alloyed with Mn-Si-Cr. Results revealed the multiphase

microstructure containing martensite/austenite and nanostructured bainite that displayed UTS of 1923 MPa and aggregate % EL of 18.3%. The superior mechanical properties are ascribed to the improved refinement of blocky RA islands acquired by the Q&P treatment.

Li et al. (2017) studied the microstructure and mechanical properties of quenching and dynamic partitioning (Q-DP) heat treated medium-carbon bainitic steel. Results revealed that the Q-DP treated microstructure comprised of bainite, martensite and RA. The specimen treated by Q-DP process at 250 °C showed the superior blend of UTS (1519 MPa), % EL (21.3%) and the product of strength & elongation (PSE, 32.4 GPa%) and most extreme impact toughness of 108 J contrasted with the Q&P process and other Q-DP forms.

Wang et al. (2017) studied the martensite size effects for harm in quenching and partitioning Fe-0.3C-2.5Mn-1.5Si-0.8Cr (wt. %) steels. These examinations revealed that the existence of coarse martensite prompts early strain localization, particularly when they are in the region of untempered martensite islands.

Gui et al. (2017) studied the mechanical properties of ultrahigh strength 0.40C-2.1Mn-1.7Si-0.4Cr (wt. %) subjected to bainite Q&P process. Results demonstrated the multiphase microstructures containing CFB, bainitic ferrite lath in addition to filmy RA). An ideal blend of strength and ductility was accomplished at a partitioning temperature of 360 °C which lies bainitic transformation range (UTS of 1495 MPa; uniform % EL and total % EL of 26.2% and 31.8% respectively and area reduction of 47.9%).

Huyghe et al. (2017) investigated the effect of Q&P treatment on the structure-property relationship of 0.2C-1.405Si-2.308Mn (wt. %) steel. Results showed that the Q&P brought about faster stabilization of austenite and subsequently for a specified holding time at 400 °C, lesser amount of fresh martensite was available in the microstructure of Q&P when contrasted with the Q&T microstructure. Best correlation amongst the initial martensite fraction and the yield strength was acquired.

Haiko et al. (2018) carried out comparison studies of impact-abrasive wear features and execution of two evaluations of medium-carbon (0.3%) steels with varying contents of silicon, aluminum and chromium at that point subjected to coordinate direct quenching (DQ) and direct quenching and partitioning (DQ&P). Contrasted with the DQ treatment, DQ&P treated specimens displayed high strengths and ductility i.e. the DQ&P 225 °C treatment showed superior UTS of 1600 MPa with low respect tensile ratio (0.58) and sensible elongation to fracture while holding a surface hardness over 500 HV₁₀.

Liu et al. (2018) carried out an investigation to optimize the properties of Q&P steels by balancing volume fraction of RA and its stability. Results revealed the microstructure that comprised of fine lath martensite and RA alternately dispersed as films, which provided most favorable balance between quantity of RA and its stability and in turn resulted in the superior combination of strength and ductility.

Lu et al. (2018) carried out a comparative study of Q&P heat treated medium carbon steel and Hadfield steel with respect to microstructure, mechanical and erosive wear behavior. Results showed the multiphase microstructure for the Q&P heat treated steel that comprised of martensite and RA offered superior mechanical properties i.e. UTS of 1921 MPa, % EL of 11.5 and hardness around 56 HRC. On the other hand superior wear resistance was observed which was due to the deformation induced martensite (twin morphology) that was formed over RA regions which in turn made the surface hard and reduced the erosive wear rate.

From the literature review it can be concluded that several research works were carried out so far on austempering heat treatment and Q&P heat treatment alternatively based on its influence on microstructure, mechanical and wear behavior of various grades of steels comprising of expensive alloying elements like nickel, chromium, molybdenum, cobalt and so forth alongside high silicon and manganese, however limited research works have been dedicated towards the transformation and its consequence on the microstructural, mechanical properties of AISI 9255 steel which comprises of basic alloying elements like silicon and manganese.

Moreover from the literature it is not completely clear about the exceptional austempering heat treatment condition for AISI 9255 steel, as far as mechanical and wear behavior are concerned. In addition, with respect to quenching and partitioning heat treatment, limited work was carried out based on the utilization of benefits of stabilizing retained austenite towards development of high strength steel. Considering above aspects it is proposed to study the influence of two different heat treatments namely, austempering and Q&P on mechanical properties and wear behavior of AISI 9255 steel.

CHAPTER 3

EXPERIMENTAL WORK

This chapter describes the experimental techniques used in the present investigation.

3.1 Material

The material used for this investigation is AISI 9255 steel, was procured from Steel Mart, Mumbai. The as-received material was hot rolled in the form of cylindrical bars of diameter 14 mm and 1000 mm long. The as-received material was checked for its chemical composition by using a 21 channel ARL 3460 Optical Emission Spectrometer (Switzerland made), which was carried out at Gwasf quality castings, Bikampady, Mangaluru. Chemical composition shown in the table 3.1. are the average of 2 runs.

Table 3.1 Chemical composition of the material used in this investigation.

Element	C	Si	Mn	Cr	Ni	Mo	Cu	V	S	P
Weight %	0.6	1.94	0.81	0.13	0.103	0.024	0.157	0.166	0.006	0.017

The scanning electron micrograph of the as-received AISI 9255 steel presented in figure 3.1. reveals pearlite (P) and some pro-eutectoid ferrite (PEF) in the deformed and

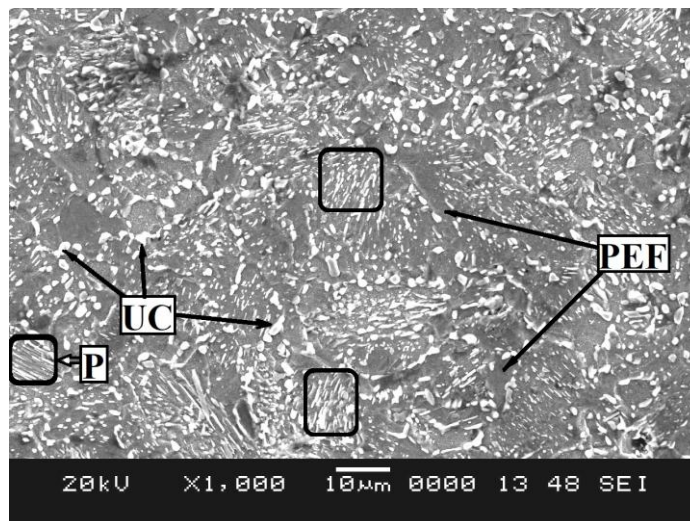


Figure 3.1 Microstructure of as-received AISI 9255 high silicon steel.

randomly oriented manner, additionally the white regions represents different morphology of undissolved cementite (UC).

3.2 Sample Preparation

The present investigation was focused to carry out tensile and wear testing for which the samples were machined from the as-received AISI 9255 steel bars. A dummy sample (14mm diameter and 25mm length) was also used along with the machined samples during heat treatment, which was helpful to carry out microstructural characterization before testing.

3.3 Heat Treatment

3.3.1 Austempering

Austempering heat treatment was performed as per the schematic diagram shown in figure 3.2, the test samples were first austenitized at 900 °C for 45 minutes in a high temperature muffle furnace fabricated by Indfurr Superheat furnaces, Chennai. The furnace temperature was controlled to ± 5 degrees of the set temperature value.

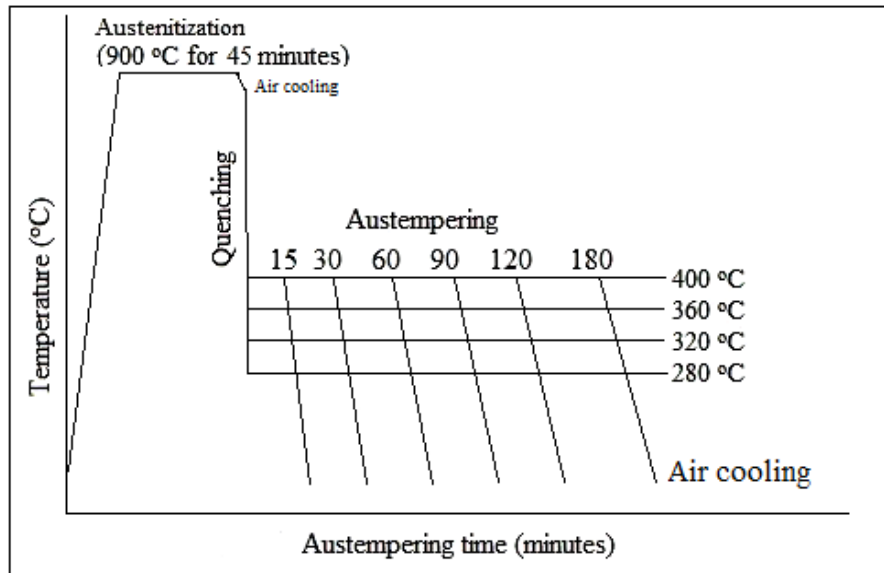


Figure 3.2 Schematic representation of Austempering heat treatment schedule.

Next step is austempering heat treatment, which was carried out in a resistance heated salt bath furnace fabricated by Indfurr Superheat furnaces, Chennai. This furnace was controlled to ± 5 degrees of the set temperature value. The salt mixture consists of 55 wt.% KNO_3 and 45 wt.% NaNO_3 , procured from SRK chemicals, Mangaluru. This composition has a wide working temperature range varying from 222 to 540 °C.

3.3.2 Quenching and Partitioning (Q&P)

The Q&P heat treatment process for test steel (figure 3.3) started with initial austenitisation at 900 °C for 45 minutes, in a high temperature muffle furnace, with an accuracy of ± 5 °C of the set temperature value, next step is quenching to a temperature of 190 °C (between M_s and M_f temperatures), in a resistance heated salt bath furnace, with an accuracy of ± 5 °C, this ternary salt mixture consists of 53 wt.% KNO_3 , 7 wt.% $NaNO_3$ and 40 wt.% $NaNO_2$, procured from SRK chemicals Mangaluru. This composition has a wide working temperature range varying from 142 °C to 538 °C.

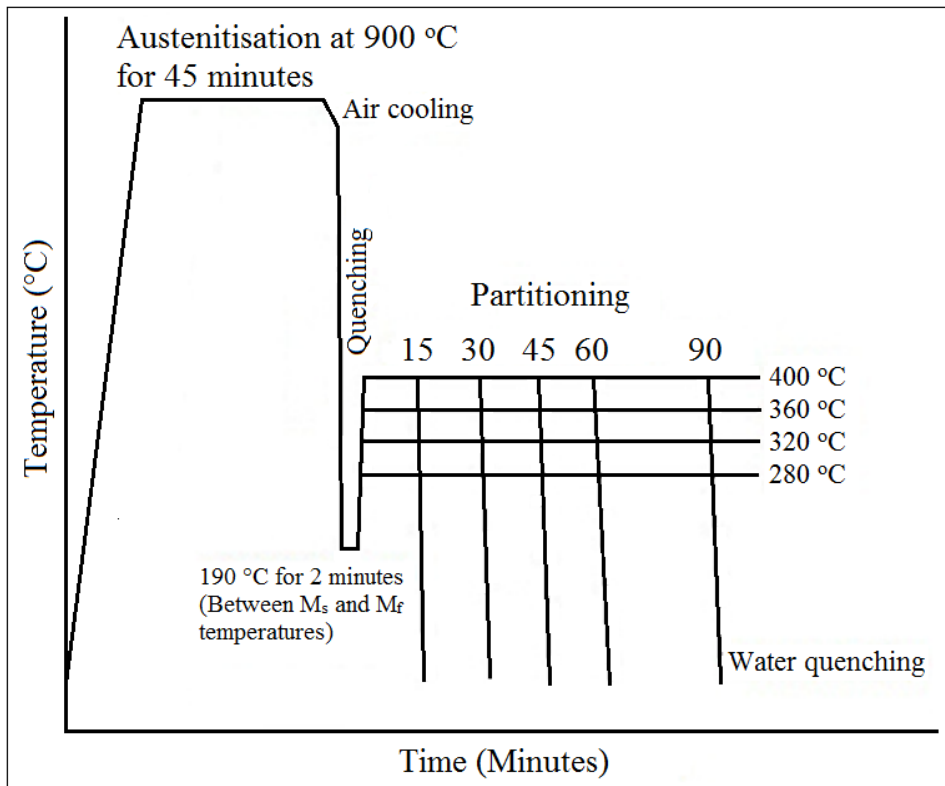


Figure 3.3 Schematic representation of Q&P heat treatment schedule.

The last step is partitioning at various temperatures and durations, which was again carried out in a resistance heated salt bath furnace, with an accuracy of ± 5 °C, this salt mixture consists of 55% KNO_3 and 45% $NaNO_3$ by weight. Finally the specimens were water quenched to room temperature.

3.4 Microstructural Analysis

3.4.1 Optical Microscopy

The microstructural characterization was carried out using Zeiss AXIO Lab.A1TM optical microscope (Germany made) for all the samples under each heat treated condition to investigate the grains and the phase distribution. Standard metallographic techniques were used to prepare the samples for microstructural studies. Finally the polished samples will be etched using 2 % nital (2 ml of concentrated nitric acid & 98 ml ethanol) solution to reveal the microstructure.

3.4.2 Scanning electron microscopy (SEM)

The microstructures of the specimens under each heat treated condition were analyzed at higher magnifications in a JEOL JSM-6380LA scanning electron microscope (Japan made) using the secondary electron mode. SEM was also used for fracture surface analysis of tensile and wear samples.

3.4.3 Electron back scattered diffraction (EBSD) studies

EBSD analysis was carried out by means of FEI Quanta TM 450-FEG-SEM (Oregon, USA made) with a Hikari detector controlled by the TSL-EDX-OIM system. Prior to EBSD analysis, the Q&P treated specimens were electro-polished with acetic acid and perchloric acid in the rationale 90:10. The EBSD data was acquired on a hexagonal scan grid with an accelerating potential of 20 kV, working distance of 16 mm, tilt angle of 70° and step size of 100 nm.

3.5 X-ray Diffraction (XRD) Studies

The test material after heat treatment was quantitatively analysed using a JEOL-JDX-8P X-ray diffractometer (Japan made) with $\text{CuK}\alpha$ radiation. A tube voltage of 30 kV and tube current of 20 mA was selected during scanning. The quantitative analysis was done to estimate the volume fractions of retained austenite and ferrite. The samples were scanned in the angular 2θ range of 40-50 degrees at a scan speed of 1 °/min. The XRD profile revealed two peaks within this angular range namely the (111) peak of austenite and the (110) peak of ferrite. Direct comparison method suggested by (Cullity 1974) was

used to determine the volume fraction of austenite and ferrite for austempered specimens. Integrated intensities of the peaks were obtained by measuring the area under the peaks using the Peak analyzer operation in OriginPro™ 9.0. Then the volume fraction of austenite and ferrite were estimated using the following relationship:

$$\frac{I_{\gamma}}{I_{\alpha}} = \frac{R_{\gamma}}{R_{\alpha}} \times \frac{X_{\gamma}}{X_{\alpha}} \text{----- (3.1)}$$

where I_{γ} and I_{α} are the integrated intensities of the (111) peak of austenite and the (110) peak of ferrite respectively, X_{α} is the volume fraction of ferrite and X_{γ} is the volume fraction of austenite, R_{α} and R_{γ} are constants given by the following expression for each peak:

$$R = \frac{1}{V^2} [|F|^2 \times P \times LPF] e^{-2m} \text{----- (3.2)}$$

where V is the atomic volume of the unit cell, F is the structure factor, P is the multiplicity factor, LPF is the Lorentz Polarization factor and e^{-2m} is the temperature factor.

For quenching and partitioning heat treated specimens, the volume fraction of retained austenite (X_{γ}) was determined using equation 3.3 (Miller 1964).

$$X_{\gamma} = \frac{1.4}{\left(\frac{I_{\alpha}}{I_{\gamma}} \right) + 1.4} \text{----- (3.3)}$$

The carbon concentration of the retained austenite (C_{γ} , weight %) i.e. carbon partitioning from martensite to austenite was determined using equation 3.4 (Dyson and Holmes 1970).

$$C_{\gamma} = \frac{(a_{\gamma} - 0.3547)}{0.00467} \text{----- (3.4)}$$

The lattice parameter a_{γ} (Å) can be calculated by the equation;

$$a_{\gamma} = d_{(hkl)} \sqrt{h^2 + k^2 + l^2} \text{----- (3.5)}$$

$$d_{(hkl)} = \frac{\lambda}{2 \sin \theta_{\gamma}} \text{----- (3.6)}$$

Where, λ (Å) is the wavelength of Cu K α radiation and θ_{γ} is Bragg angle for austenite.

3.6 Mechanical Properties

3.6.1 Tensile test

The tensile samples were machined from the rolled bars in accordance with ASTM A370-14 standard for mechanical testing of steel products. The gauge length and gauge diameter of the tensile specimen are 30 mm and 6 mm respectively which is as per ASTM E8-M standard as shown in figure 3.4.

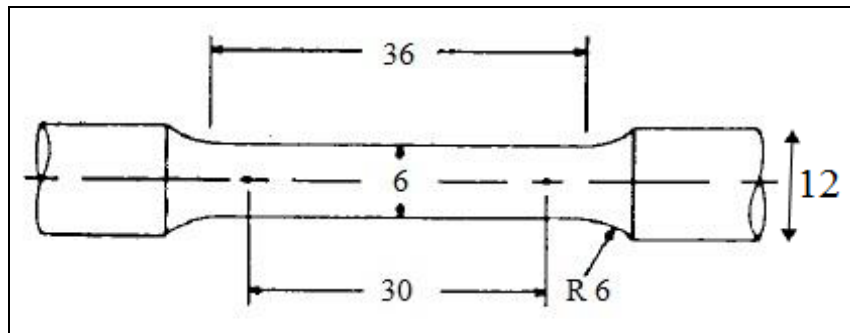


Figure 3.4 Schematic diagram of tensile specimen (All dimensions in mm)

The tensile testing was carried out using a Shimadzu AG-X plus™ 100kN universal testing machine (Japan made) with a crosshead speed of 1 mm/min. The stress-strain curves obtained during each test was used to estimate tensile properties such as yield strength, ultimate tensile strength, percentage elongation and modulus of toughness.

3.6.1.1 Strain hardening behavior

The stress-strain plots obtained during the tensile tests were further used to study the strain hardening behavior of austempering heat treated specimens. For this purpose it was assumed that the flow curve could be expressed by the Holloman relationship (Holloman 1945) given below:

$$\sigma = K\varepsilon^n$$

Where ' σ ' is the true stress, ' ε ' is the true strain, ' K ' is the strength coefficient, According to this a double natural logarithmic plot of true stress against true strain must result in a straight line with a slope ' n ' which is the strain hardening exponent, in the present investigation n values for various austempering conditions were determined by considering the corresponding stress-strain diagram. The points from stress-strain curve

from yield stress up to ultimate tensile stress were considered for plotting the true stress-strain diagram on the logarithmic scale.

3.6.2 Microhardness

The microhardness of the specimens under each heat treated condition was measured using a Shimadzu HMV-G 20ST micro-Vickers hardness tester (Japan made) with a 1kg load. The samples were polished to a mirror finish level and etched so that the phases could be distinguished. Load was selected so as to get indentations that are large enough to give accurate results and at the same time, small enough not to be influenced by the adjacent softer or harder phase. The reported values were an average of at least seven readings.

3.7 Wear Test

Dry sliding wear test was performed using pin-on-disc equipment and specimens were machined as per ASTM G99 standard (Fig. 3.5 & 3.6) using counter face of steel disk EN-31 grade, which was heat treated to achieve the hardness of 65 HRC.

The specific wear rate of the heat treated specimens was evaluated as per the procedure shown in section 3.7.1., using the wear test parameters shown in table 3.3.

Table 3.2 Specifications of rotating disc.

Disc size	Dimension
Outer diameter	215 mm
Inner diameter	45mm
Thickness	20mm

Table 3.3 Wear testing parameters.

Parameters	Values
Load	2 kg
Wear track diameter	120 mm
RPM	1000
Sliding speed	377 m/min
Sliding distance in 180 minutes	67.86 km

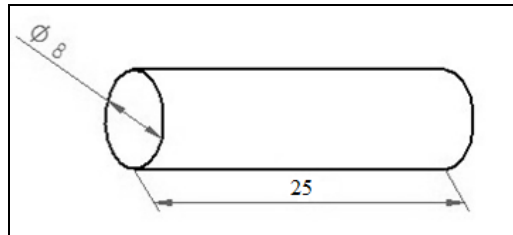


Figure 3.5 Schematic representation of wear pin sample. (All dimensions in mm).

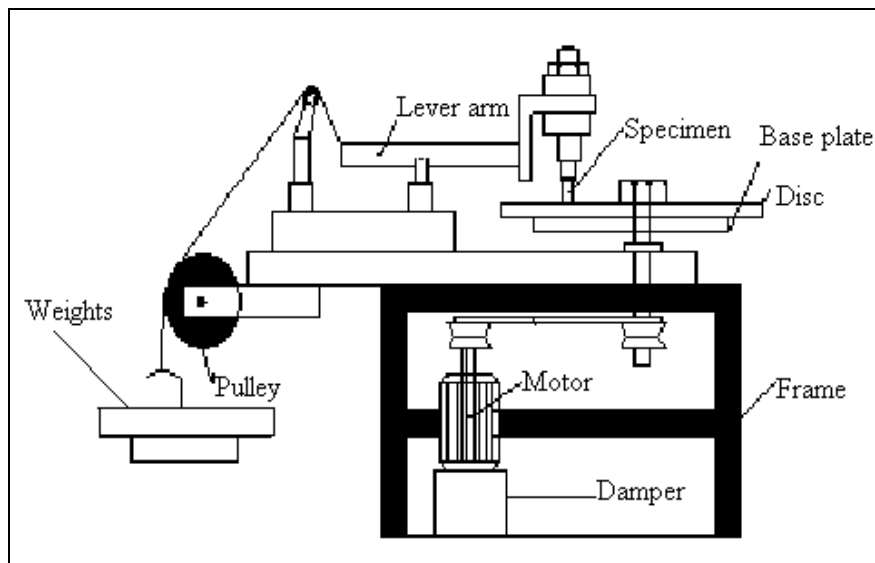


Figure 3.6 Schematic representation of pin-on-disc set up

3.7.1 Determination of specific wear rate

- Weight loss in grams, $\Delta w = \text{Initial weight } (w_i) - \text{Final weight } (w_f)$
- Volume loss (mm^3), $\Delta V = \Delta w / \rho$
 $\rho = \text{Density of the material } (\text{g} / \text{mm}^3)$
- Sliding speed (m / min), $v = (\pi \times D \times N) / 1000$
 $D = \text{Wear track diameter in mm, } N = \text{Disc speed in rpm}$
- Sliding Distance in 'meters', $d = v \times t$
 $v = \text{Sliding speed in m/min, } t = \text{Time in minutes}$
- Specific wear rate ($\text{mm}^3 / \text{N-m}$), $\text{SWR} = \Delta V / (L \times d)$
 $\Delta V = \text{Volume loss } (\text{mm}^3), L = \text{Load in Newton, } d = \text{Sliding distance in meters.}$

3.8 Fractography

After the completion of tensile test of both Austempered and Quenched & Partitoned specimens, the broken specimens within the gage length were cut to the desired length and the fractured surfaces were characterized using Scanning electron microscopy to study the mode of fracture like ductile, brittle and mixed mode.

Similarly the heat treated specimens after completion of wear test were also cut to desired length and characterized under SEM to observe the wear tracks and understand various damage mechanisms.

CHAPTER 4

RESULTS AND DISCUSSION

PART A: Austempering Heat Treatment

Experiments have been carried out to assess the microstructural characterization, mechanical properties and wear behavior of austempered AISI 9255 high silicon steel. Their results and discussions are presented in this chapter.

4.1 Influence of Austempering Temperature and Time on the Microstructure

4.1.1 Optical microscopy

Figure 4.1 to 4.4 shows the microstructure of AISI 9255 high silicon steel samples austempered at various austempering temperatures such as 280, 320, 360 and 400°C for various austempering durations.

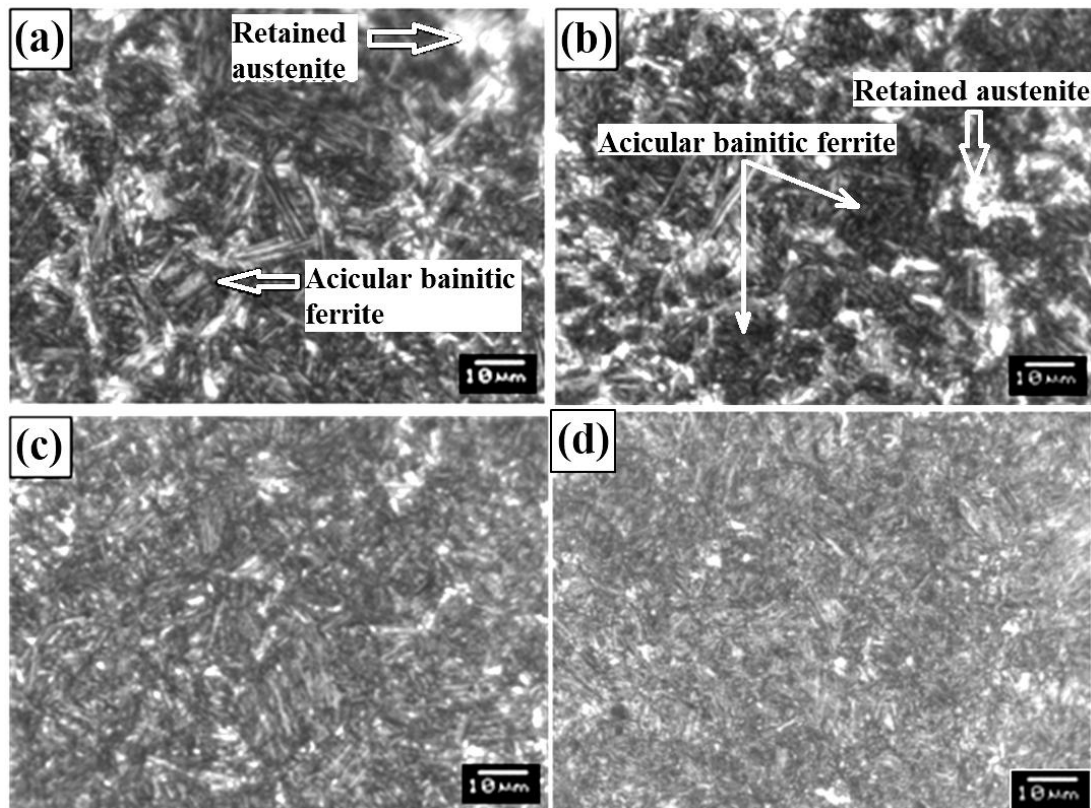


Figure 4.1 Optical micrographs of samples austempered at 280 °C for (a) 15 min. (b) 30 min. (c) 90 min. (d) 180 min.

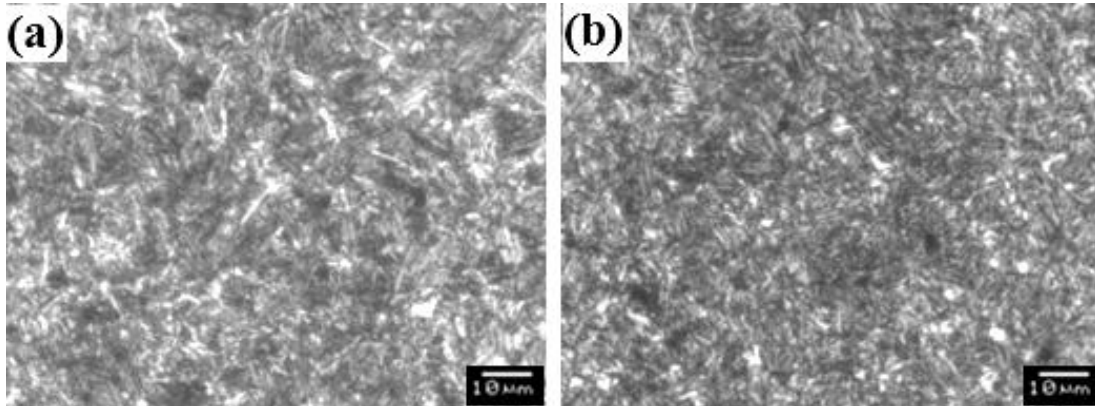


Figure 4.2 Optical micrographs of samples austempered at 320 °C for (a) 15 min. (b) 180 min.

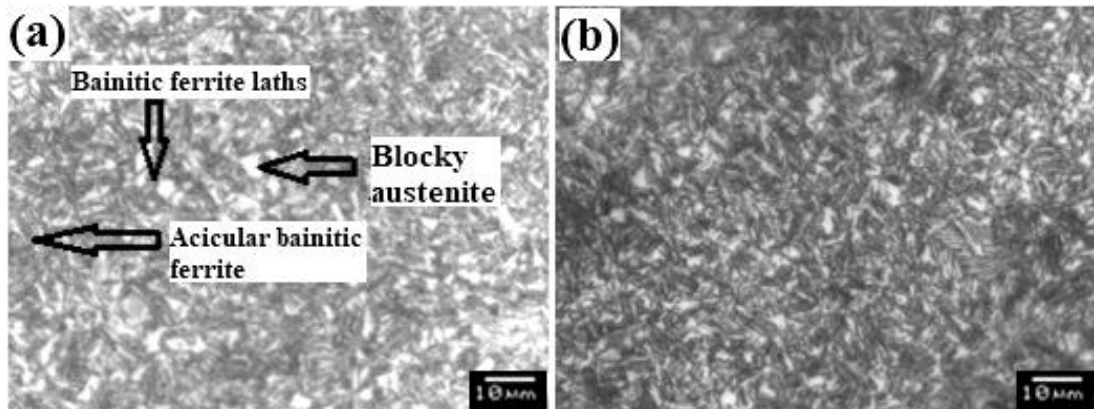


Figure 4.3 Optical micrographs of samples austempered at 360 °C for (a) 15 min. (b) 180 min.

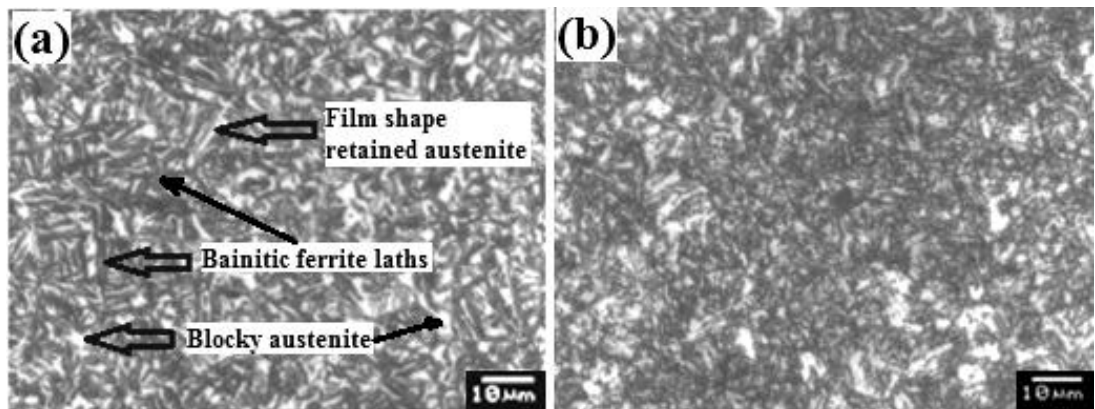


Figure 4.4 Optical micrographs of samples austempered at 400 °C for (a) 15 min. (b) 180 min.

Microstructural studies indicate the bainite structure (dark etched bainitic ferrite and retained austenite as white regions) formed at lower austempering temperatures i.e. 280 and 320 °C (Fig. 4.1 and 4.2) is fine acicular structure while those at higher austempering temperatures 360 and 400 °C (Fig. 4.3 and 4.4) has feathery morphology. The bainitic structure obtained at lower temperatures of austempering is known as “lower bainite” while those at higher is known as “upper bainite”.

It is also observed that the bainitic transformation is enhanced with increasing austempering time, which is due to the kinetics of nucleation and growth. As the austempering time increases the formation of bainite is more and hence results in a densely packed bainitic ferrite microstructure (Fig. 4.1(a-d)). At lower austempering time, the amount of retained austenite is more and bainitic ferrite is less. As the austempering time is increased, more time is available for the growth of ferritic needles, which in turn results in reduction of retained austenite content in the matrix, which implies that bainitic transformation had taken place to a great extent (Fig. 4.1 to 4.4).

4.1.2 Scanning electron microscopy

The microstructural features of the specimens at various austempering temperatures from 280 to 400 °C at various time intervals, prior to tensile testing are presented in figures 4.5 to 4.8.

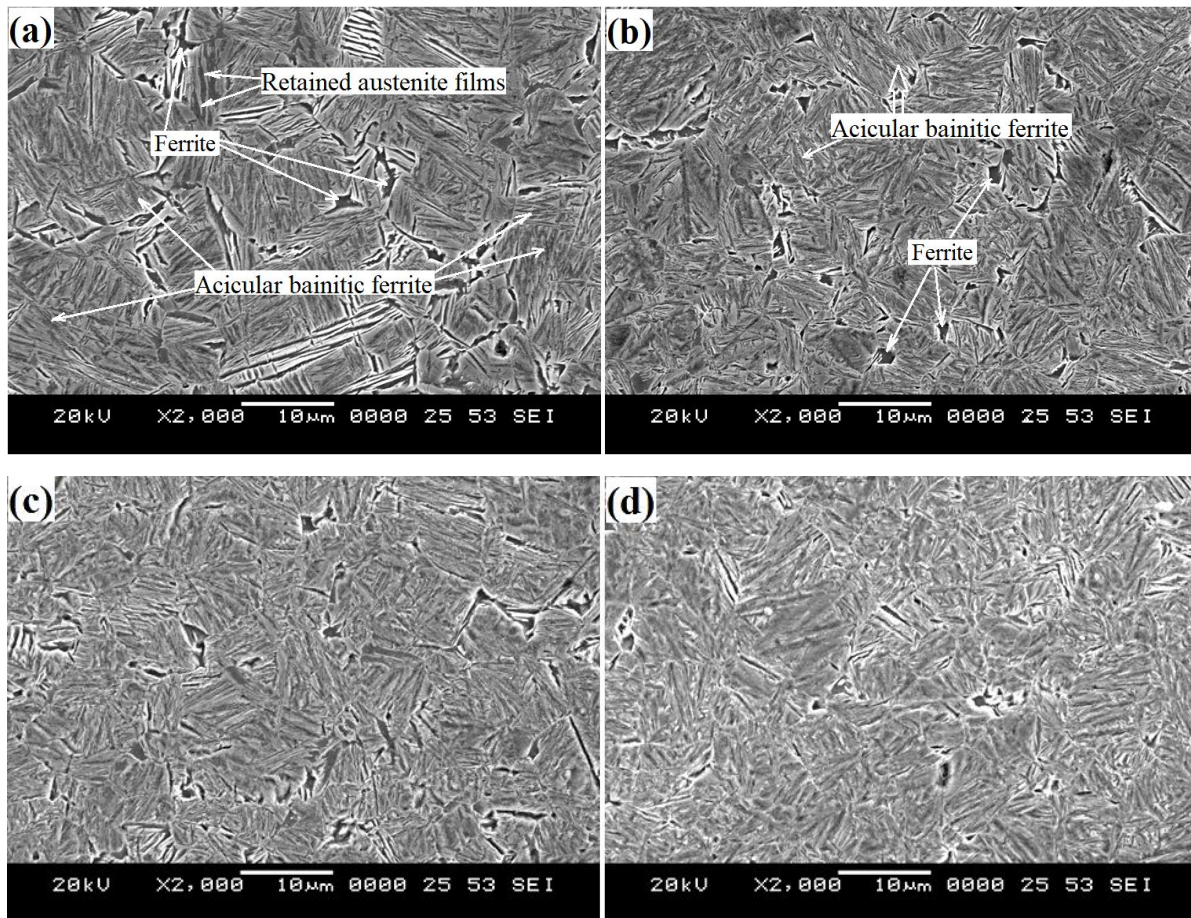


Figure 4.5 Scanning electron micrographs of samples austempered at 280 °C for (a) 15 min. (b) 60 min. (c) 90 min. (d) 180 min.

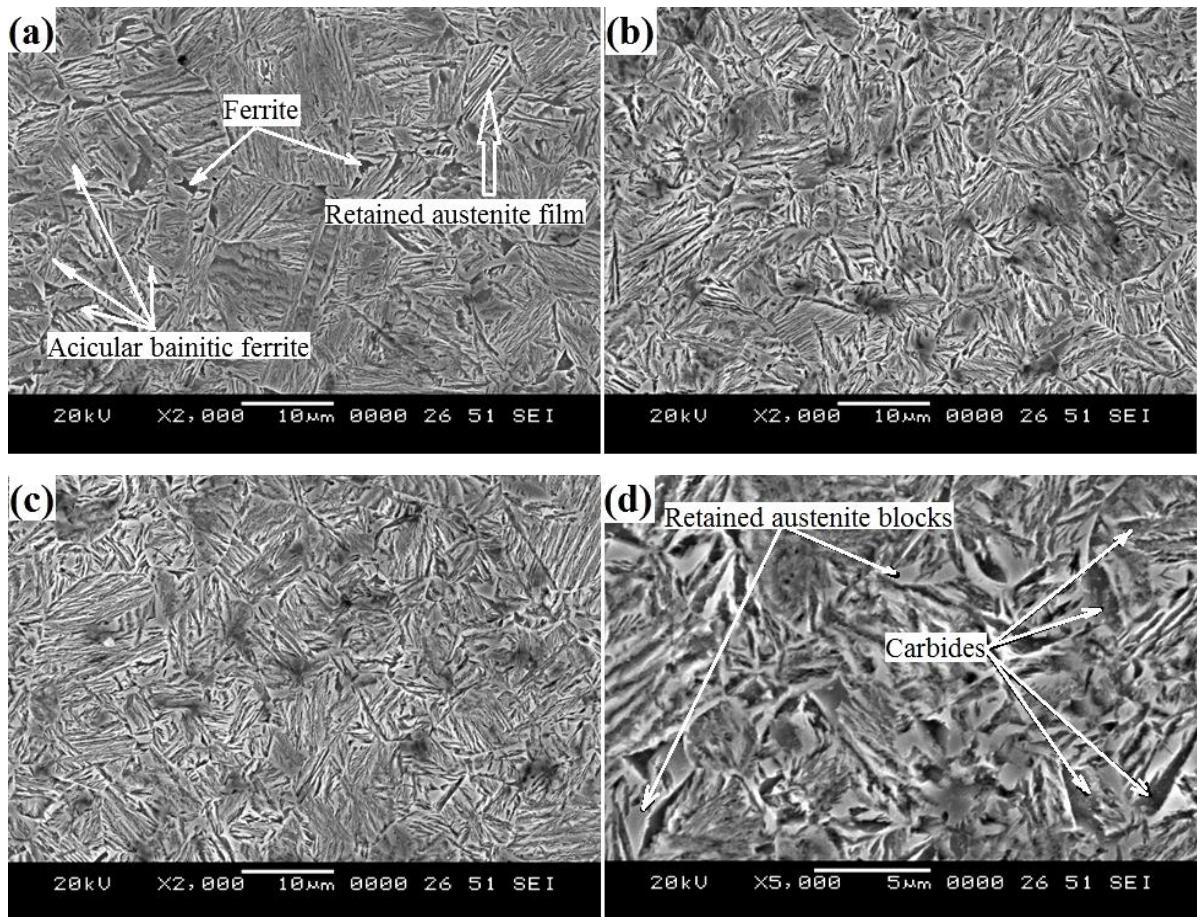


Figure 4.6 Scanning electron micrographs of samples austempered at 320 °C for (a) 15 min. (b) 60 min. (c) 90 min. (d) 180 min.

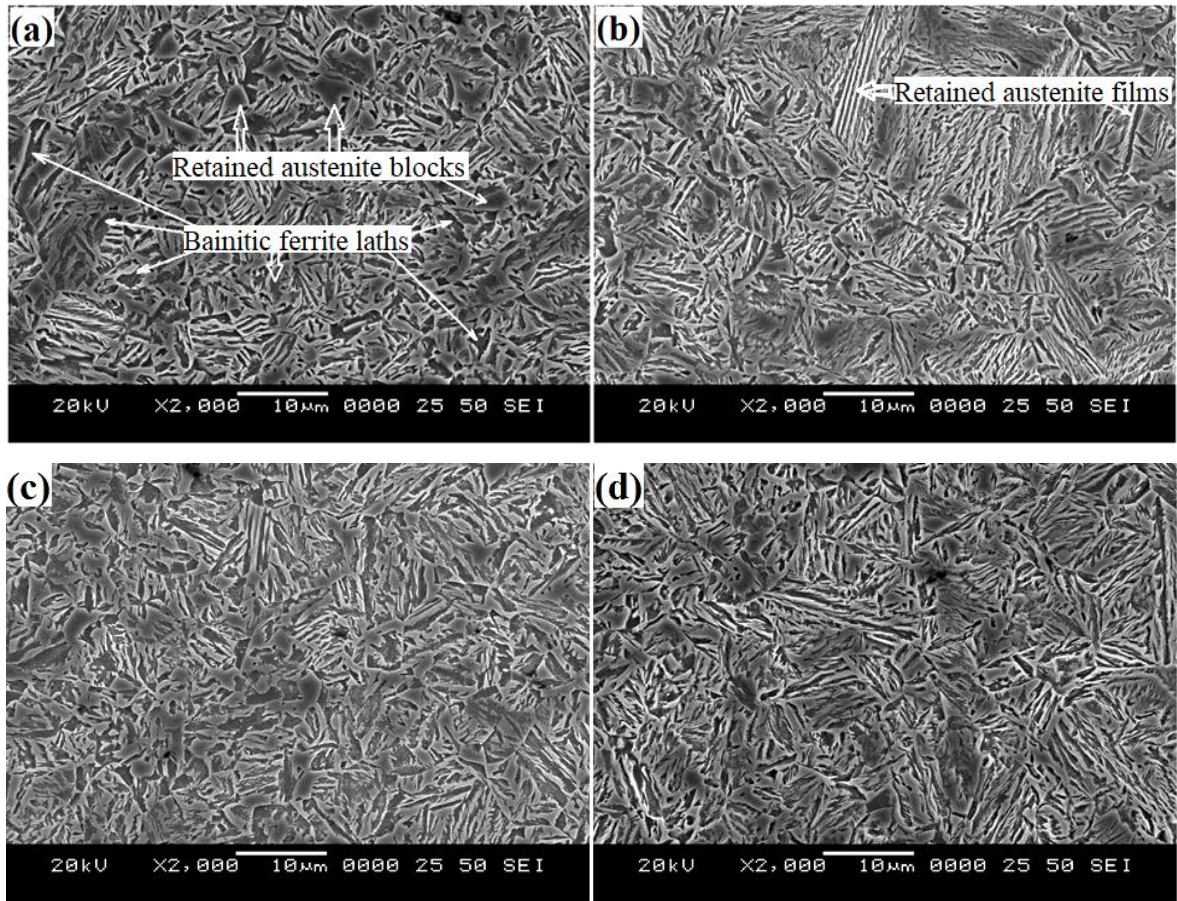


Figure 4.7 Scanning electron micrographs of samples austempered at 360 °C for (a) 15 min. (b) 60 min. (c) 90 min. (d) 180 min.

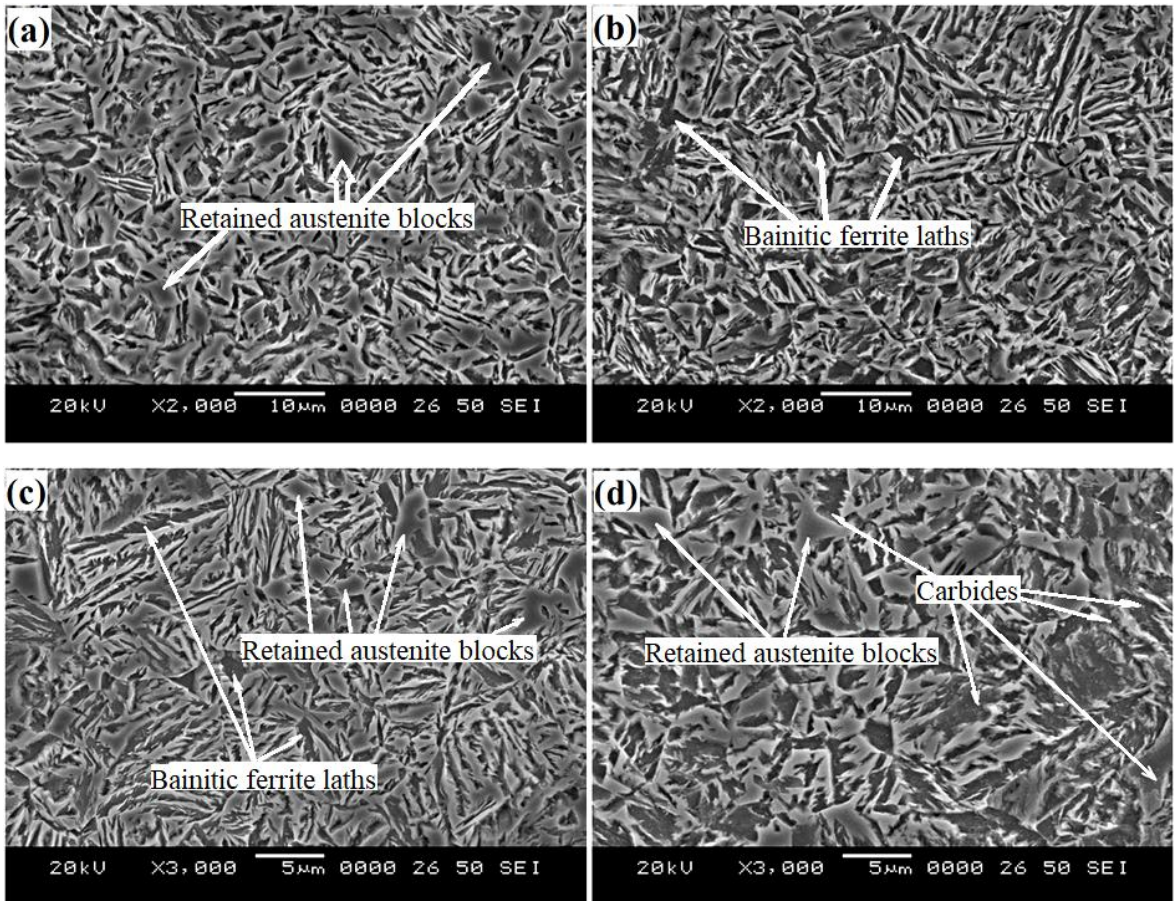


Figure 4.8 Scanning electron micrographs of samples austempered at 400 °C for (a) 15 min. (b) 60 min. (c) 90 min. (d) 180 min.

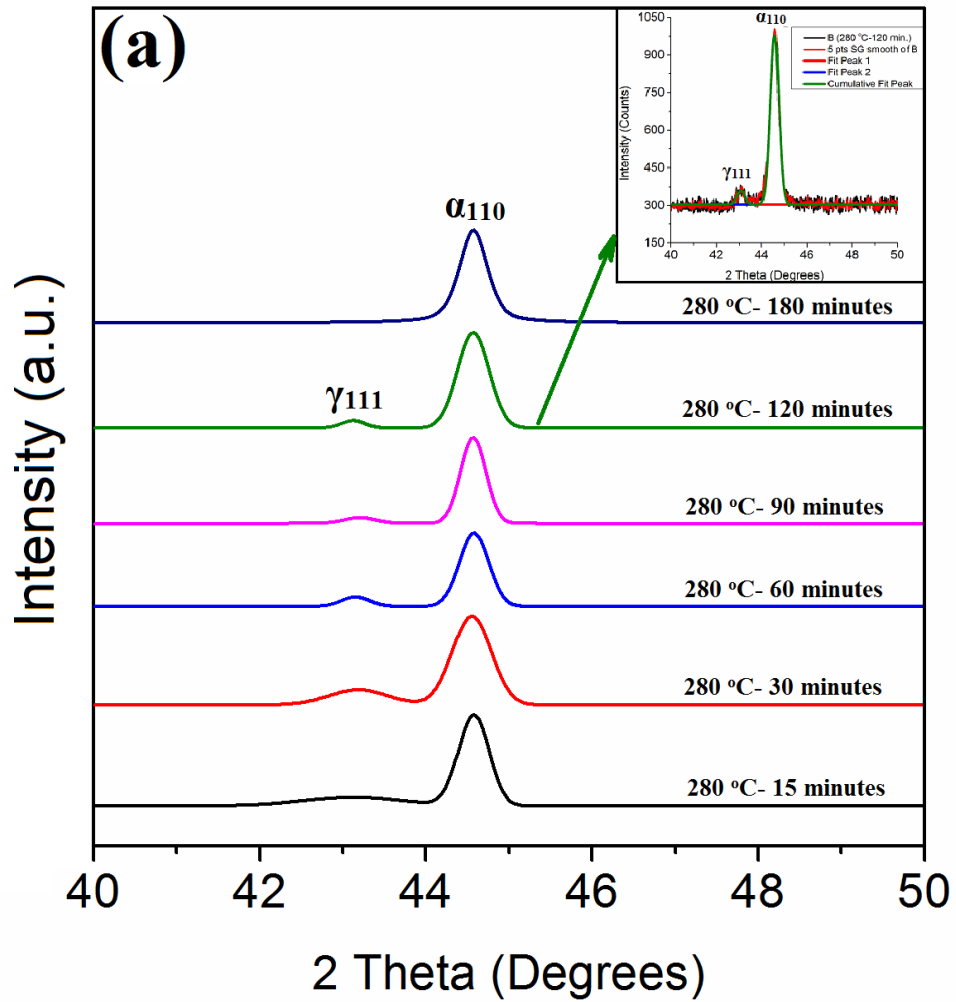
As observed in case of optical microscopy, the scanning electron micrographs also reveal the same bainite structure that consists of bainitic ferrite and retained austenite. Further, bainite formed at lower austempering temperatures i.e. 280 and 320 °C (Figure 4.5 and 4.6) exhibit a fine acicular structure (lower bainite), however few regions in this lower bainite structure reveals a slightly coarse structured ferrite which is a soft phase (Varshney et al. 2017), which was formed during continuous cooling for a short time around 5 seconds i.e. while transferring samples from austenitising temperature to salt bath furnace. At higher austempering temperatures i.e. 360 and 400 °C (Figure 4.7 and 4.8) shows wide feathery structure (upper bainite). However the presence of ferrite (soft phase) was difficult to indicate in the upper bainite structured specimens due to their identical morphologies.

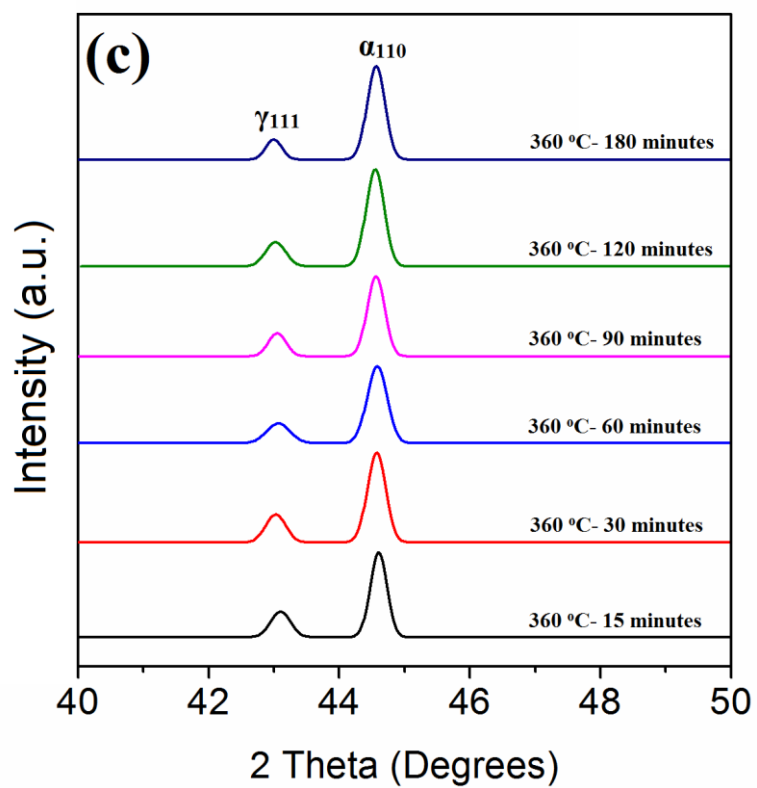
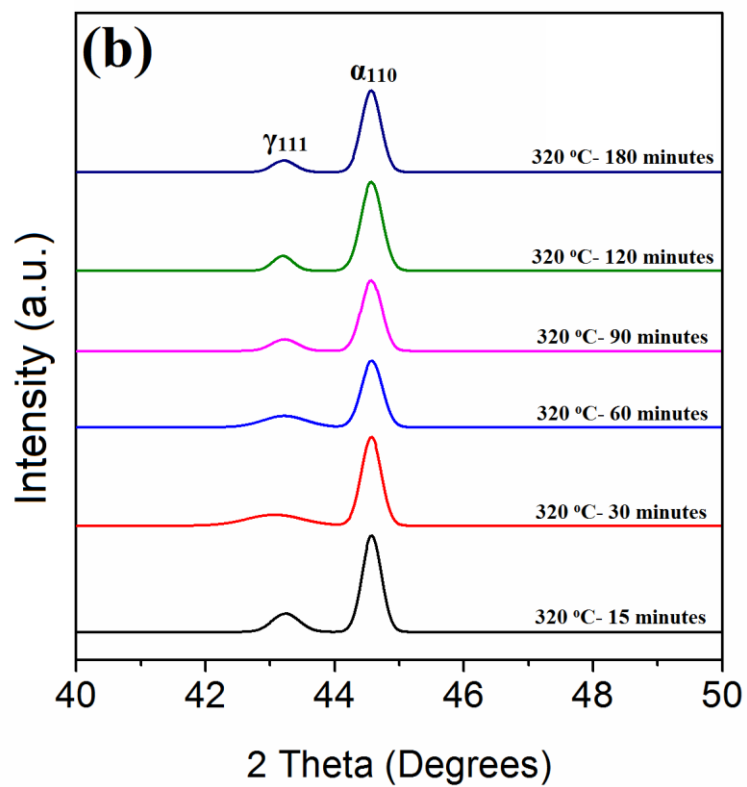
It is discussed by Putatunda (2001) that austempering at lowest temperature around 280 °C leads to high nucleation rates of ferritic phase, due to larger supercooling effect and moreover the carbon diffusion rate is low. As meager carbon is rejected from the bainitic ferrite into retained austenite, transformation has to continue at a slower rate resulting in the presence of small amount of retained austenite at the end of austempering. As the austempering temperature increments from 360 to 400 °C, the degree of supercooling is lower and therefore the nucleation rate is likewise low however the carbon diffusion rates are superior, As a result bainitic ferrite growth takes place by rejecting more and more carbon atoms to surrounding austenite, which in turn results in coarseness of both bainitic ferrite i.e. in the form of laths and retained austenite as blocks (Figure 4.7 and 4.8). Moreover the retained austenite content additionally increments, when austempered in this upper bainitic temperature range.

The role of austempering time is found to be highly influential in evolving the microstructure of austempered materials. The present microstructural studies reveal that as the austempering time was increased from 15 to 180 minutes (Figure 4.7 to 4.8), scope for formation of bainite improves and resulting in excess densely packed bainitic ferrite in the material. For the similar reason, at the shorter austempering duration, the material is found to be consisting of higher amount of retained austenite and smaller amount of bainitic ferrite. Conversely, if austempering is carried out for longer duration there will be more and more nucleation of bainitic ferrite needles in case of lower transformation temperatures i.e. 280 °C and 320 °C (Figure 4.5 and 4.6(a-d)) and similarly at higher transformation temperatures i.e. 360 °C and 400 °C (Figure 4.7 and 4.8(a-d)) growth of bainitic ferrite laths are predominant, which in turn results in the reduction of retained austenite content in the material. These observations are further confirmed by x-ray diffractometer studies, in which constituent phases are quantified and recorded in fig. 4.9.

4.2 X-ray Diffractometry

X-ray diffraction analysis was performed to determine the retained austenite content and the quantity of bainitic ferrite. Figure 4.9 (a to d) illustrates the XRD patterns fitted to the line profiles by Gaussian function for the specimens austempered at various temperatures i.e. 280, 320, 360 and 400 °C for different austempering times i.e. 15 to 180 minutes.





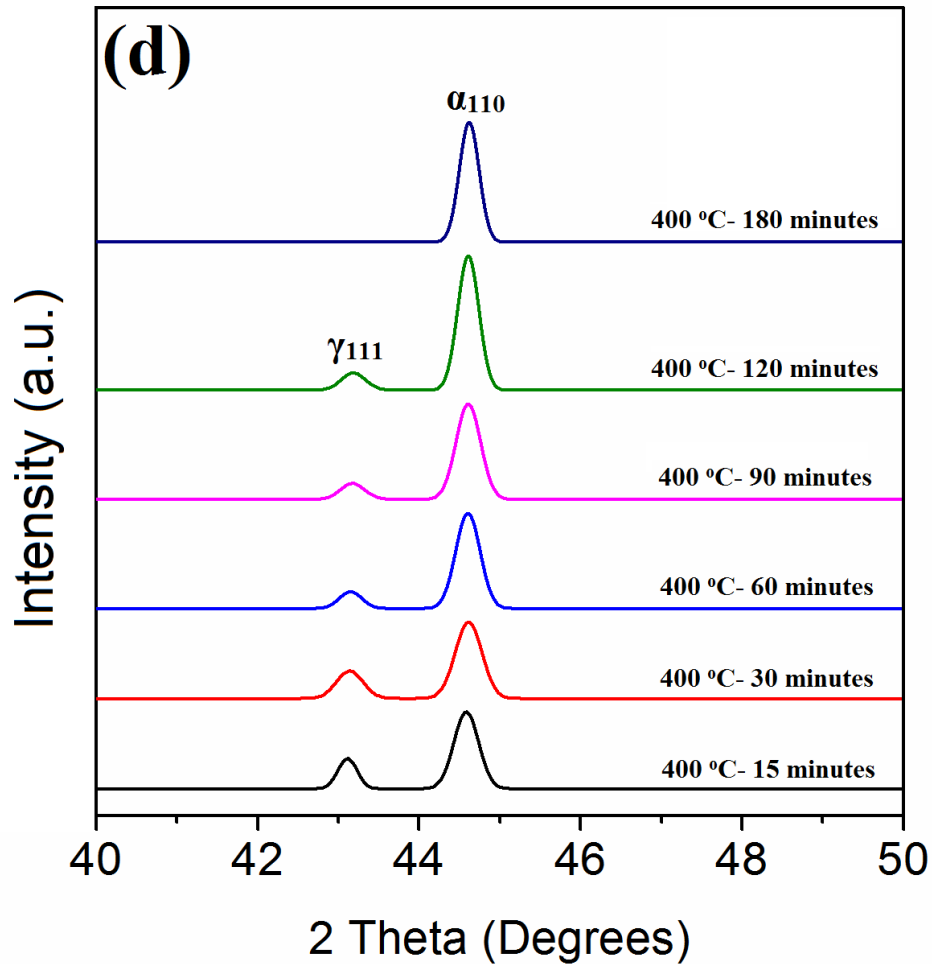


Figure 4.9 XRD patterns fitted to the line profiles by Gaussian function for the samples austempered at (a) 280 °C (b) 320 °C (c) 360 °C (d) 400 °C.

The XRD technique was useful in determining the quantity of bainitic ferrite and retained austenite. The XRD line profiles show two peaks in the range (40 to 50°) of 2θ angle. The first peak from (111) planes of austenite gives the information about the amount of retained austenite. The second peak from (110) planes of ferrite gives the information about the amount of bainitic ferrite present in the matrix.

For a particular austempering temperature the intensity of bainite peak increases with increase in austempering time, which implies that with increase in the austempering time, the amount of bainitic ferrite increases and retained austenite decreases.

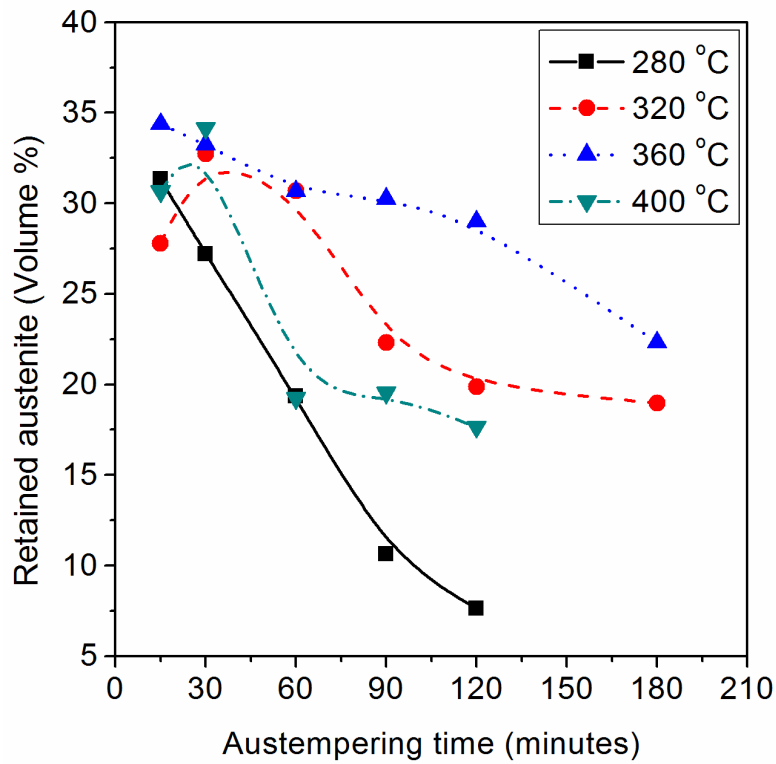


Figure 4.10 Variation in the amount of retained austenite for different austempering conditions.

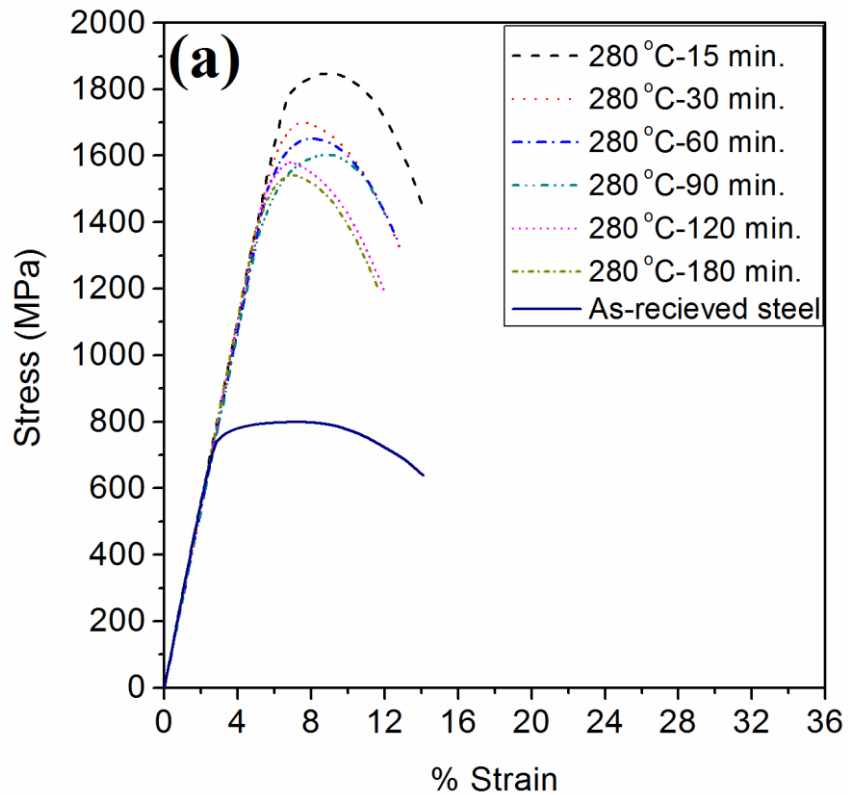
Figure 4.10 shows the profiles depicting the variation of retained austenite content with austempering time for different austempering temperatures. It is observed that the retained austenite content decreases with increasing austempering time for all austempering temperatures, although the quality of change is different for different austempering temperatures. The profiles reveal that the rate of change of the amount of retained austenite with austempering time is highest when austempering is carried out at 280 °C. Though the rate of transformation is controlled by the rate of diffusion of carbon atoms, which happens to be poor at a lower temperature, the completion of transformation is achieved faster because the distance required to diffuse is smaller due to closely placed nuclei. The carbon diffusion rates are sufficiently high to take care of the phase transformation if specimens are austempered at temperatures of 320 and 360 °C even for a shorter holding time. Consequently, these materials register a large proportion of retained austenite; such a comparable mechanism of two-stage reactions is seen to be

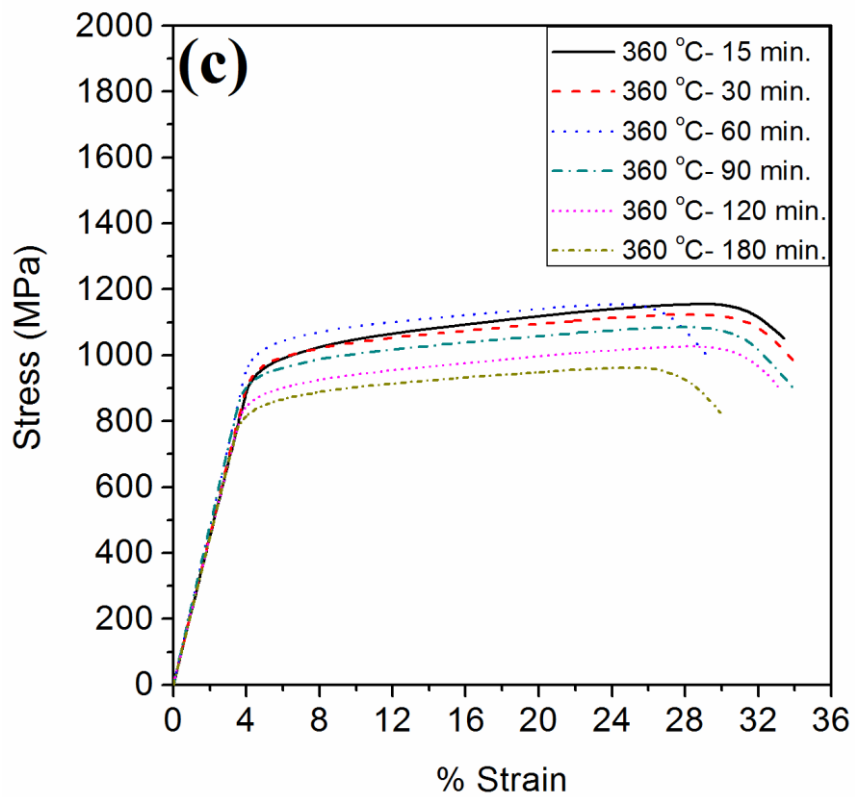
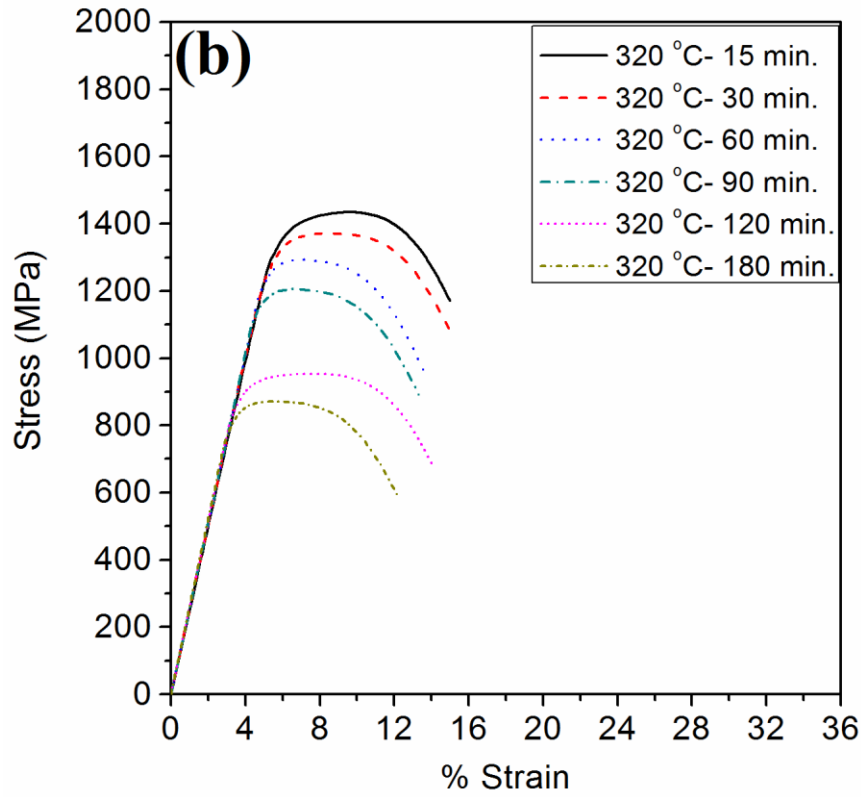
happening in case of austempered ductile iron (ADI) as well, where the upper bainite contains a large portion of blocky untransformed austenite, apart from an inter-lath sliver of retained austenite under similar heat treatment conditions (Putatunda 2003), (Son et al. 2010). The case of austempering at 400 °C is worth noting. It shows that the rate of transformation sharply decreases after 60 minutes of austempering; it could be conceived to be happening due to carbide precipitation at this stage triggered by the onset of the second stage of austempering reaction. This fact is evidenced in SEM images (Figure 4.15(d)) under section 4.31. (b), which reveal the presence of carbide precipitates.

4.3 Influence of Austempering Temperature and Time on the Mechanical Properties

4.3.1 Tensile properties

Tensile tests were carried out for as-received steel and the austempered specimens to study the variations in their properties, accordingly figure 4.11 (a-d) shows the engineering stress-strain plots for the same.





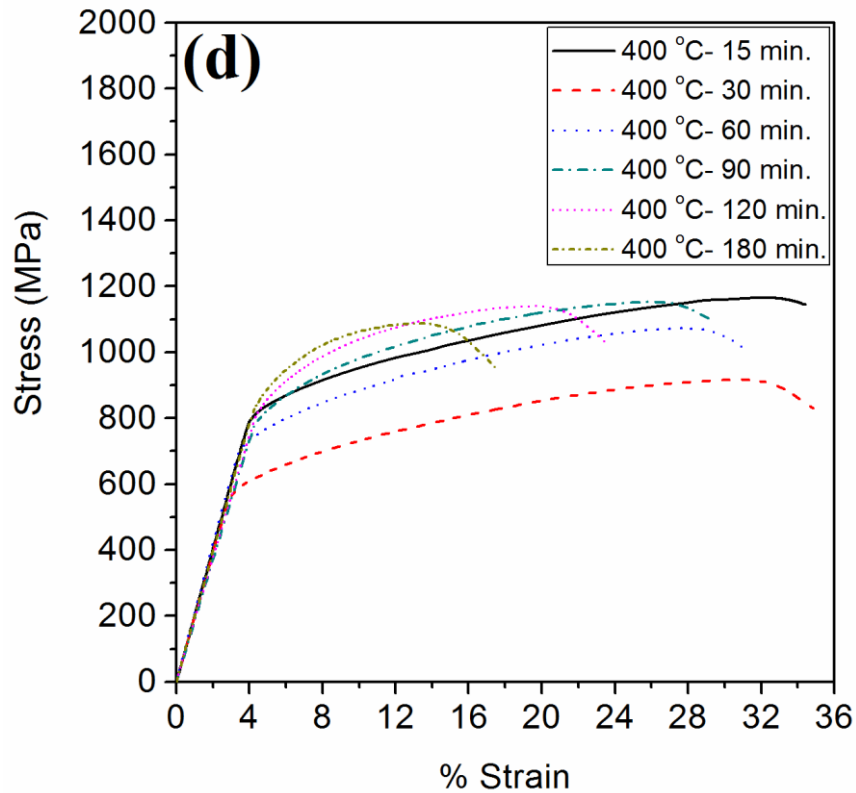
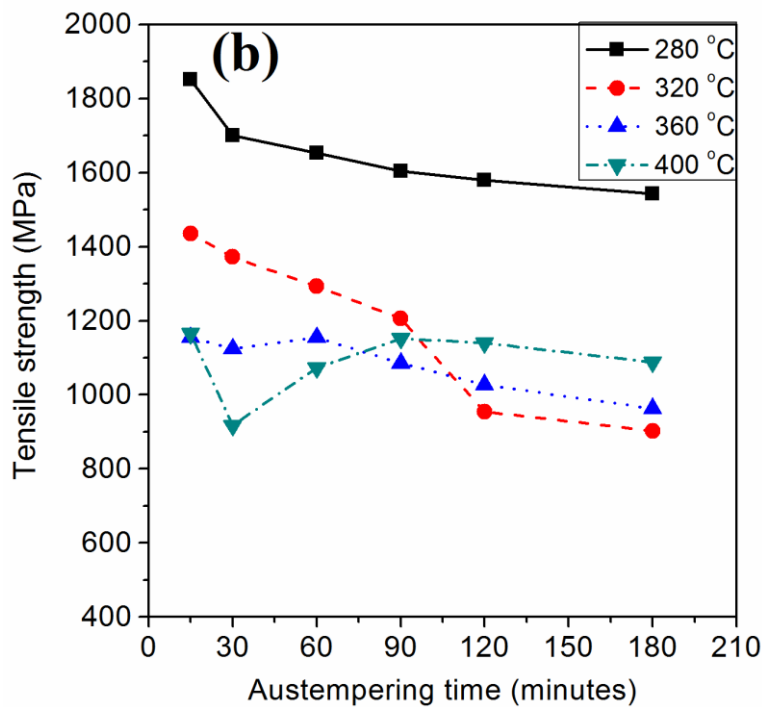
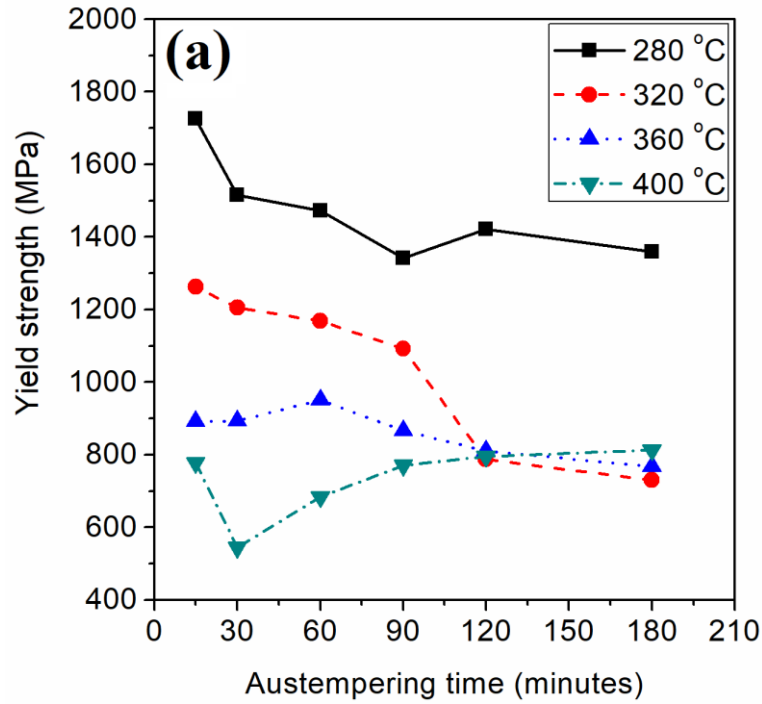


Figure 4.11 Engineering stress-strain curves for various austempering conditions (a) 280 °C (b) 320 °C (c) 360 °C (d) 400 °C.

From the above stress-strain plots, it can be observed that varying austempering parameters (temperature and time) resulted in remarkable improvement in their tensile properties viz. yield strength, ultimate tensile strength, ductility and modulus of toughness, when compared to that of as-received high silicon steel [Fig. 4.11 (a)]. Moreover specimens austempered at 360 and 400 °C showed superior strain hardening response compared to that of lower austempering temperatures (280 and 320 °C).

The variation of yield strength (YS), ultimate tensile strength (UTS), % elongation (% EL) and modulus of toughness (MT) with varying austempering heat treatment parameters are shown in figure 4.12 (a-d).



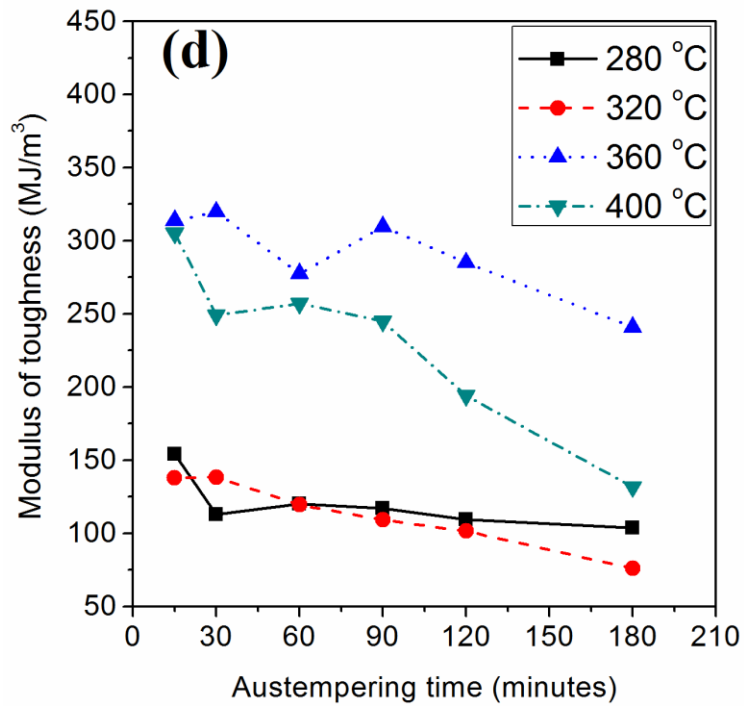
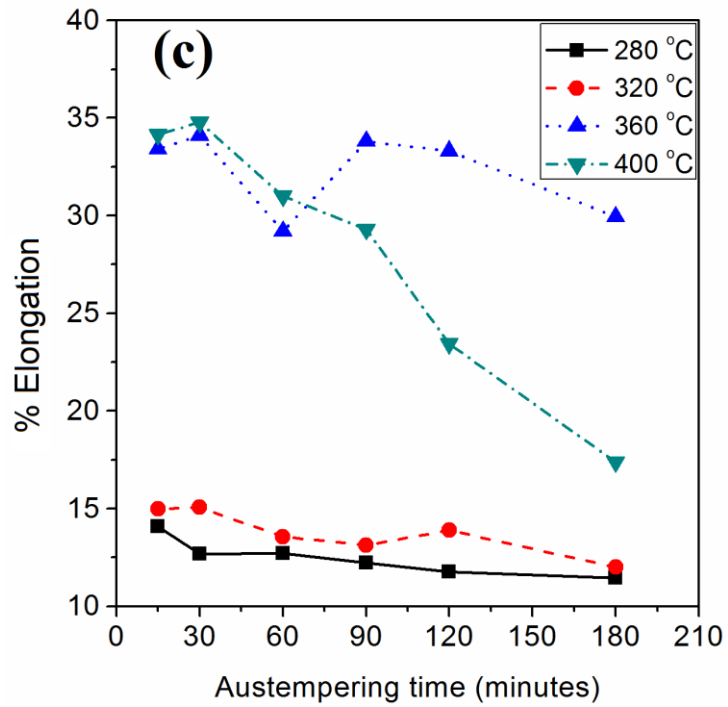


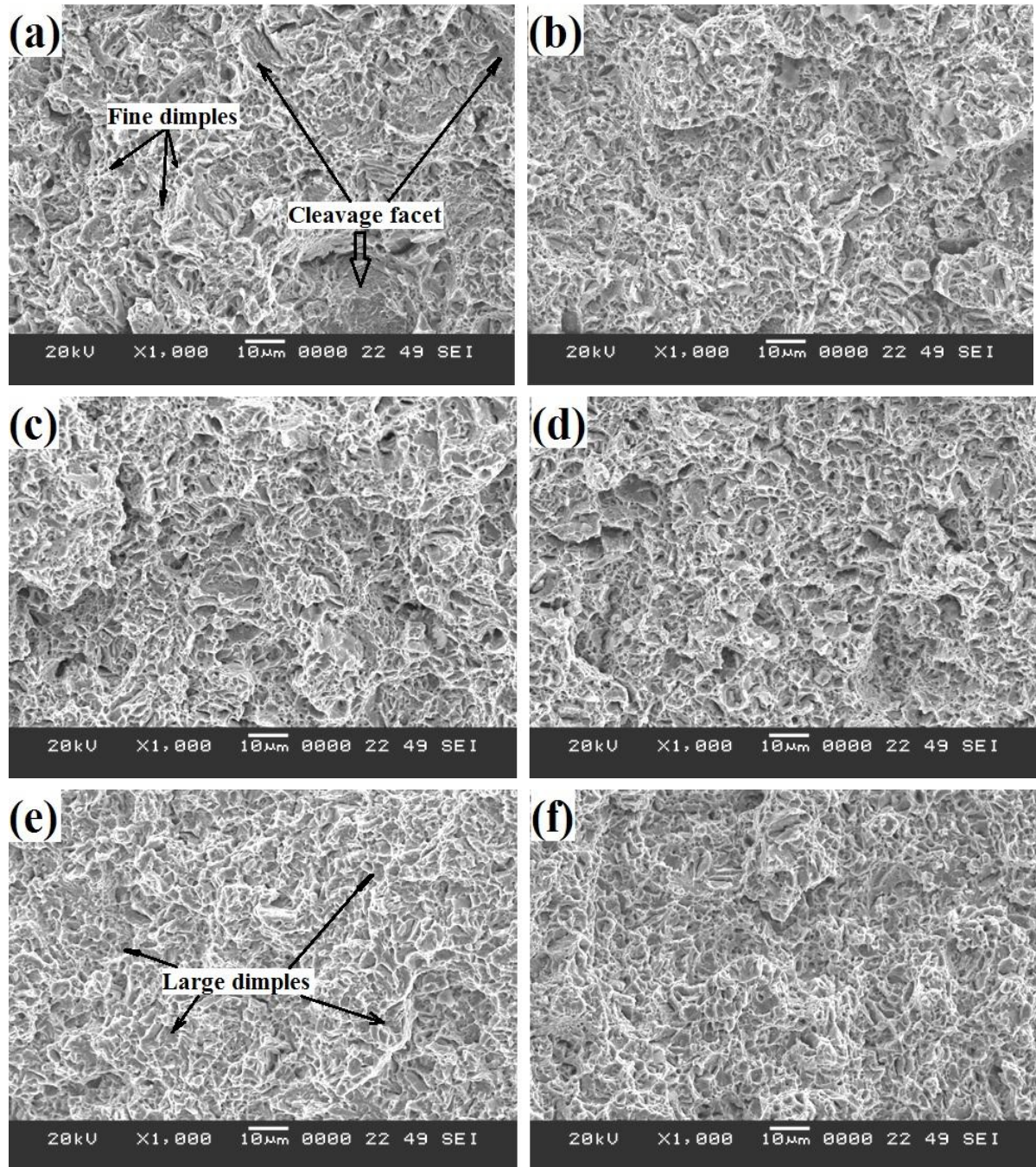
Figure 4.12 Influence of austempering temperature and time on the tensile properties of the specimens (a) Yield strength (b) Ultimate tensile strength (c) % Elongation (d) Modulus of toughness.

The profiles presented in figure 4.12 reveal the significant improvement in the tensile properties after subjecting this steel to austempering heat treatment. With an increase in austempering time, a decrease in the tensile properties was observed for almost all temperatures. The as-received steel showed UTS of 800 MPa along with % EL of 14.1% and MT of 89 MJm⁻³.

The same steel austempered at the lowest temperature, i.e. at 280 °C, for 15 minutes exhibits high UTS and comparable % EL, i.e. 1852 MPa and 14% respectively; the fine acicular bainitic ferrite resulting in high hardness contributes to the high UTS and also sufficient amount of retained austenite results in % EL. At an austempering temperature of 320 °C, the UTS of 1435 MPa and % EL of 15% was obtained at an austempering time of 15 min. Among the set of heat-treated steels the worst combination of strength and % EL was observed for those austempered at 320 °C beyond 90 min, which could be due to the precipitation of carbides and also due to poor strain hardening response at this temperature. Higher austempering temperatures, i.e. 360 and 400 °C, showed a reduction in the tensile strength of 1165 MPa, simultaneously registering remarkable improvement in the % EL and MT upto 35% and 325 MJm⁻³, respectively. Toughness of the steel is decided by the morphology of ferrite and quantity of carbon-rich retained austenite residing in between the coarsened bainitic ferrite laths. However, specimens austempered at 400 °C for a longer duration suffered a drastic reduction in toughness, due to the formation of blocky austenite that is less stable; hence the scope for martensite formation is more on cooling to room temperature (Liu et al. 2006). This inhomogeneous distribution of carbon in blocky austenite makes it mechanically unstable (Rao and Putatunda 1998); hence under moderate stress conditions it gets converted to martensite (strain induced martensite) (Putatunda 2001) and moreover the precipitation of carbides between ferrite and retained austenite results in a sharp reduction in elongation and toughness.

4.3.1.1 Fractography

The fractured surfaces of the austempered tensile specimens at various temperatures and durations were observed under SEM and are shown in Figure 4.13(a–h).



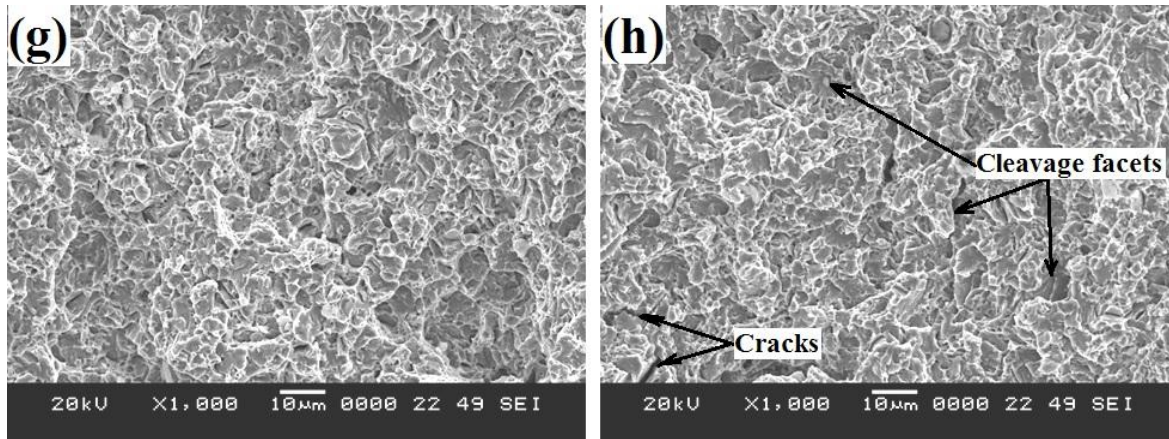


Figure 4.13. Fractographs of the austempered samples (a) 280 °C–15 min. (b) 280 °C–180 min. (c) 320 °C–15 min. (d) 320 °C–180 min. (e) 360 °C–15 min. (f) 360 °C–180 min. (g) 400 °C–15 min. and (h) 400 °C–180 min.

The fracture surfaces of almost all specimens showed a ductile mode of failure. However, at lower austempering temperatures, 280 and 320 °C (Figure 4.13(a–d)), a quasi-cleavage (mixed mode) type of fracture with incidental voids was revealed, due to the presence of a fine acicular bainitic ferrite (hard phase) structure that results in formation of cleavage and the presence of retained austenite (soft phase) leads to the formation of dimples. At higher austempering temperatures, 360 and 400 °C, for 15min duration (Figure 4.13(e & g)), an increase in dimple size was observed with a simultaneous decrease in the number of dimples per unit area due to the increased amount of retained austenite and also coarsening of bainitic ferrite, which reduces the hardness of the structure. A sample austempered at 400 °C for duration of 180 minutes showed the worst combination of strength and elongation, due to the fine carbide precipitation i.e. indicated in the micrographs in fig 4.8d & 4.15f resulting in brittle fracture which is justified by the presence of cleavage facets and cracks (Figure 4.13h).

4.3.1.2 Strain hardening behavior

Superior strain hardening response was recorded at higher austempering temperatures mainly 360 and 400 °C with reference to the engineering stress (σ_e)-strain (ϵ_e) curves i.e. wide range of strain from yield stress to ultimate tensile strength [Fig. 4.11(c&d)]. To analyze the strain hardening behavior, the engineering stress-strain datas were converted

to true stress–strain datas (equations 2 & 3), considering the points from yield stress up to the ultimate tensile stress- Engg. strain values were taken parallel to the elastic limit line from the engineering stress–strain curve to generate the true stress–strain diagram on a logarithmic scale. These data points followed a linear relationship, in each case confirming a Holloman relationship: $\sigma = K \varepsilon^n$ (1)

True stress, $\sigma_t = \sigma_e(1 + \varepsilon_e)$ (2), True strain, $\varepsilon_t = \ln(1 + \varepsilon_e)$ (3)

The true stress-strain curve for austempering temperature of 400 °C for durations ranging from 15 to 180 minutes is shown in figure 4.14.

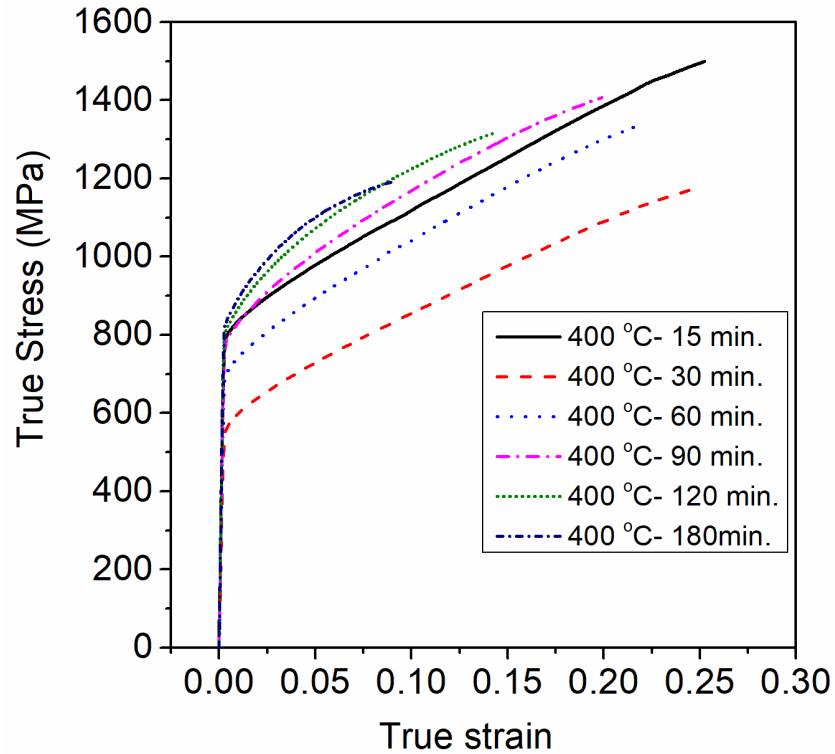


Figure 4.14 True stress-strain curves for austempering at 400 °C for various durations

The highest level of true strain (0.2524) was observed at austempering condition of 400 °C for 15 minutes and further increase in austempering time showed decrease in true strain to 0.0898 at 180 minutes. The reason for the decrease in true strain is same as that of engineering stress-strain plots reported in section 4.3.1., page no. 61.

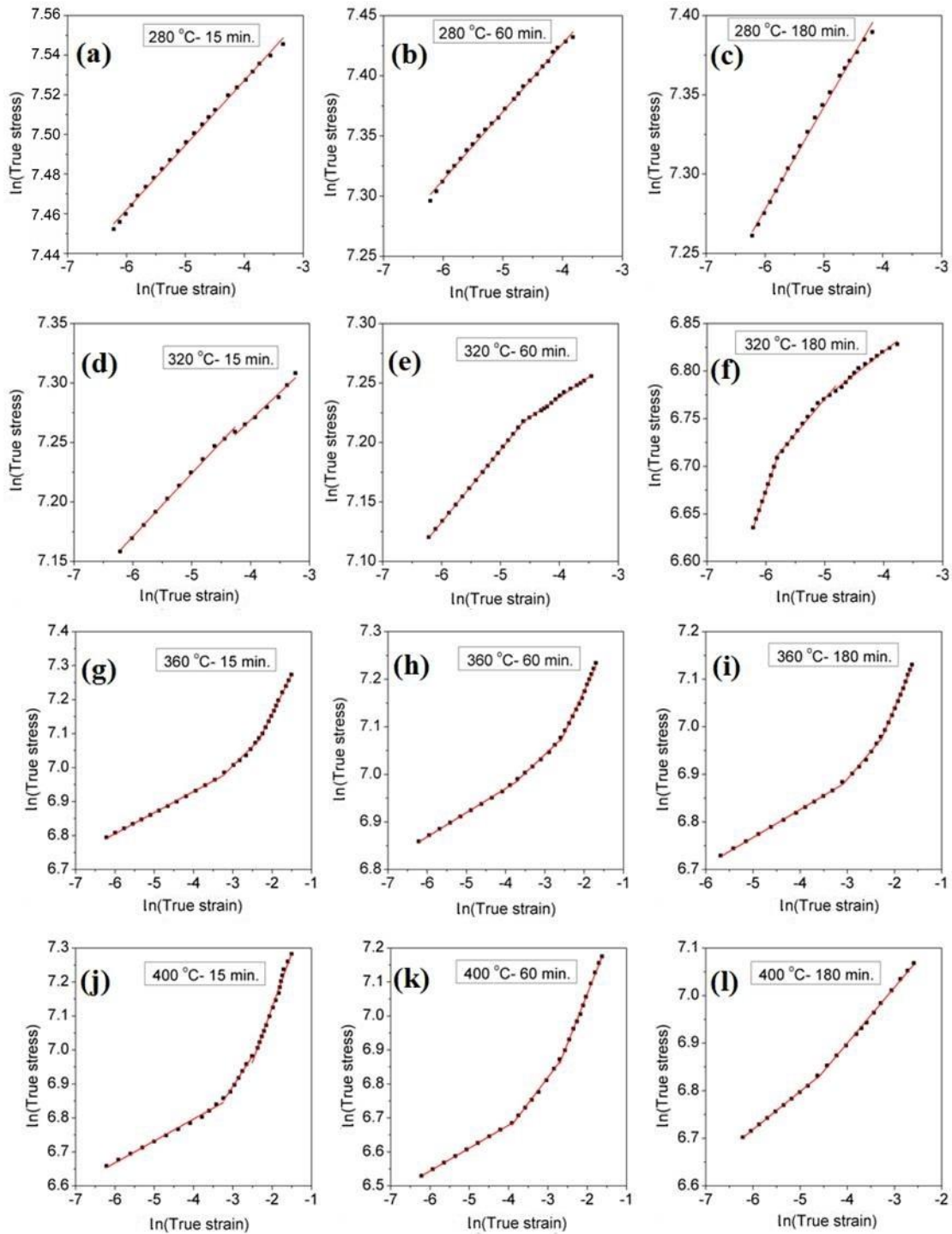


Figure 4.15. Strain-hardening behavior of the specimens austempered at (a) 280 °C–15 min. (b) 280 °C–60 min. (c) 280 °C–180 min. (d) 320 °C–15 min. (e) 320 °C–60 min. (f) 320 °C–180 min. (g) 360 °C–15 min. (h) 360 °C–60 min. (i) 360 °C–180 min. (j) 400 °C–15 min. (k) 400 °C–60 min. and (l) 400 °C–180 min.

Table 4.1 Variation of strain hardening exponent values with respect to varying austempering conditions.

Austempering temperature (°C)	Austempering time (minutes)	Strain hardening exponent		
		n ₁	n ₂	n ₃
280	15	0.0815	-	-
	30	0.0669	-	-
	60	0.0565	-	-
	90	0.0787	-	-
	120	0.0625	-	-
	180	0.0713	-	-
320	15	0.05305	0.0466	-
	30	0.0607	0.0339	-
	60	0.0592	0.0304	-
	90	0.0591	0.0314	-
	120	0.1070	0.0425	-
	180	0.1804	0.0736	0.0485
360	15	0.0664	0.1211	0.2402
	30	0.0583	0.0974	0.2169
	60	0.0508	0.0777	0.1766
	90	0.0548	0.1183	0.2158
	120	0.0584	0.1192	0.1936
	180	0.0569	0.1106	0.2262
400	15	0.0645	0.1777	0.3206
	30	0.0829	0.1632	0.3218
	60	0.0675	0.1527	0.2909
	90	0.0762	0.1426	0.2593
	120	0.0804	0.1318	0.1752
	180	0.0801	0.1173	-

Variation in the slope implies a change in the strain-hardening mechanism under loading conditions. Figure 4.15(a-l) shows the plot of \ln (true stress) vs. \ln (true strain) at four different austempering temperatures of 280, 320, 360 and 400 °C. At an austempering temperature of 280 °C, a single linear trend was observed with an ' n ' value of 0.08 for a holding duration of 15 min. Therefore, the specimens austempered at 280 °C showed no variation in the strain hardening behavior. However, the samples austempered at 320, 360 and 400 °C showed a change of slope (Figure 4.15(f-k)), with triple n values of the three stages, respectively. At 320 °C, nonlinearity in the strain hardening plots was observed (Figure 4.15(e and f)), where the soft ferrite phase undergoes plastic deformation in the initial stage due to the slide of mobile dislocations present near the hard bainite and retained austenite regions; the final stage involves plastic deformation of both ferrite and bainite. The encompassing hard bainitic ferrite laths induce severe stresses on the retained austenite, thereby substantially reducing the possibility of strain-induced martensitic transformation (Varshney et al. 2017). The specimens austempered at 360 and 400 °C do indicate articulated increment in strain-hardening exponent as they are progressively strained. This demonstrates certain progressions are occurring in the microstructure during the deformation stage. At 360 °C for 15 minutes holding time ' n ' values were found to be 0.06, 0.12 and 0.24 and at 400 °C for 15 min ' n ' values were found to be 0.06, 0.18 and 0.32. Hence it was observed that strain hardening exponent values increase with an increase in austempering temperature, which implies a continuous variation in the strain hardening nature as the samples undergo strain at an early stage.

For further clarity, the fractured surface was polished and etched metallographically to disclose the microstructure; notable development of martensite was observed (Figure 4.16(a-f)).

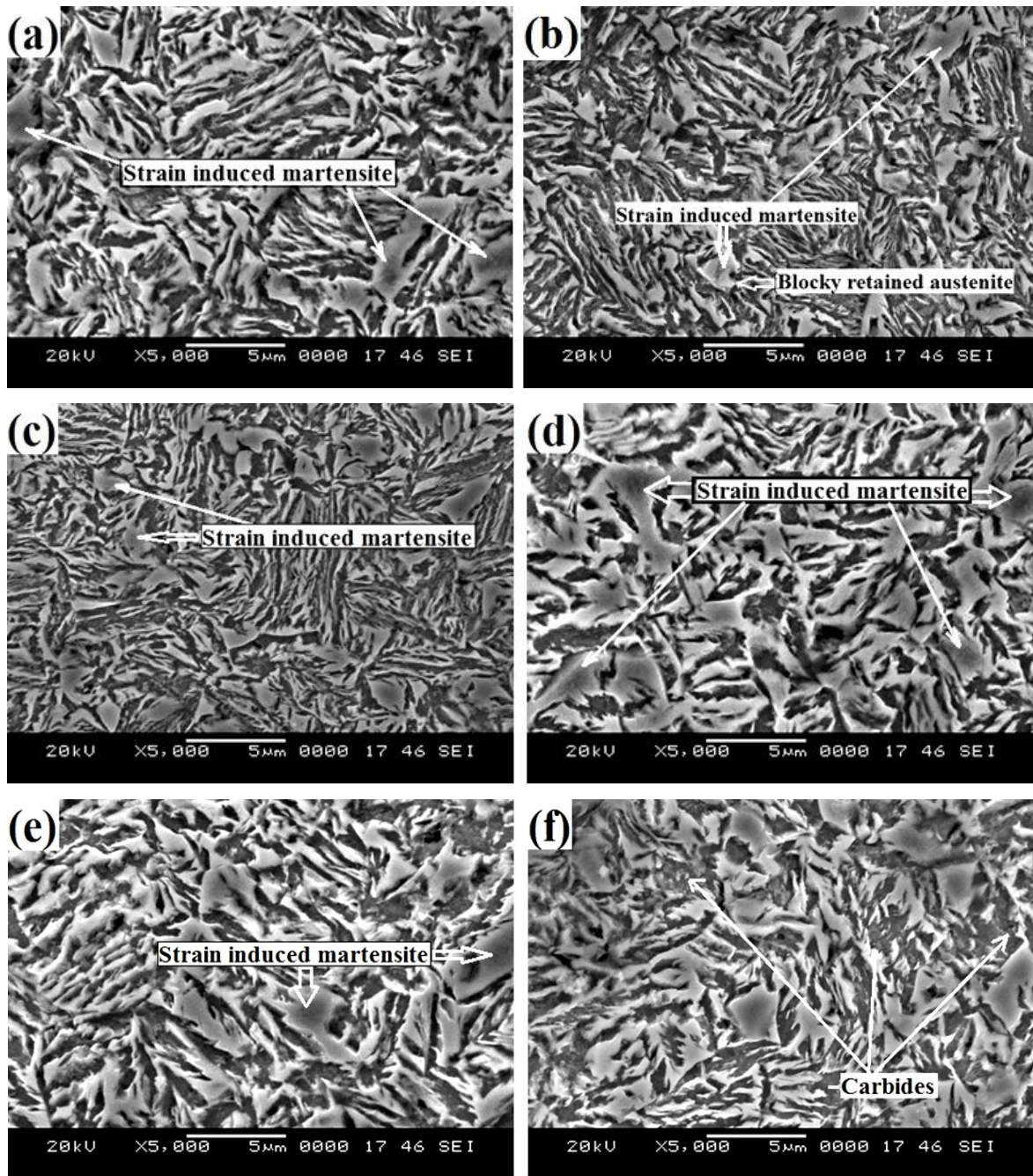


Figure 4.16. Microstructures of fracture surfaces of the specimens austempered at (a) 360 °C-15min. (b) 360 °C-60min. (c) 360 °C-180 min. (d) 400 °C-15min. (e) 400 °C-60min. (f) 400 °C-180 min.

In addition to this, the Vickers micro-hardness test (load = 20 g and dwell time = 30s) was also carried out on those regions indicated as martensite in the microstructure, which was found to have a maximum value of 870 HV. These are alluded to as strain-induced martensite formed from the blocky austenite (Figure 4.16(a–f)) and XRD studies carried out before and after tensile test confirm the presence of strain-induced martensite, i.e. by the absence of a retained austenite peak after tensile testing shown in Figure 4.17. Specimens austempered at 360–400 °C indicate blocky retained austenite is being supplanted by martensite which provides more prominent imperviousness to the moving dislocations. This is the basis for the increased strain hardening in these austempered specimens (Daber and Rao 2008). Strain induced martensite arrangement was observed in the specimens austempered at higher austempering temperatures, and very less in samples austempered at 280 °C.

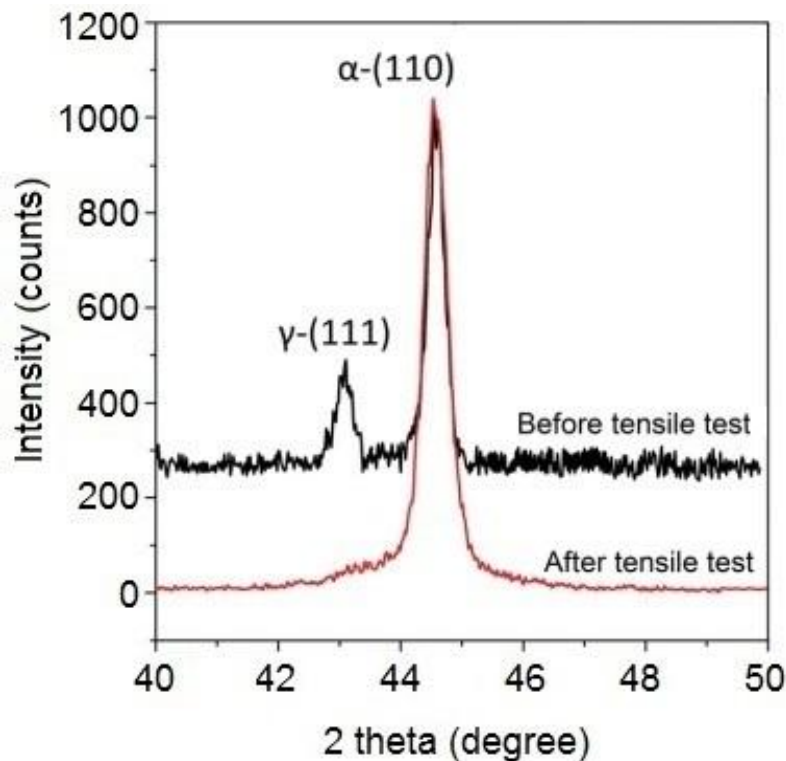


Figure 4.17 XRD profiles of the specimens austempered at 360°C for 60 min.

4.3.2 Microhardness measurement

Figure 4.18 indicates the influence of varying austempering parameters on Vickers microhardness, where the acicular bainitic structure possessed higher hardness compared to lath-structured bainite (from 280 to 400 °C). The as-received steel has a hardness of 334 HV.

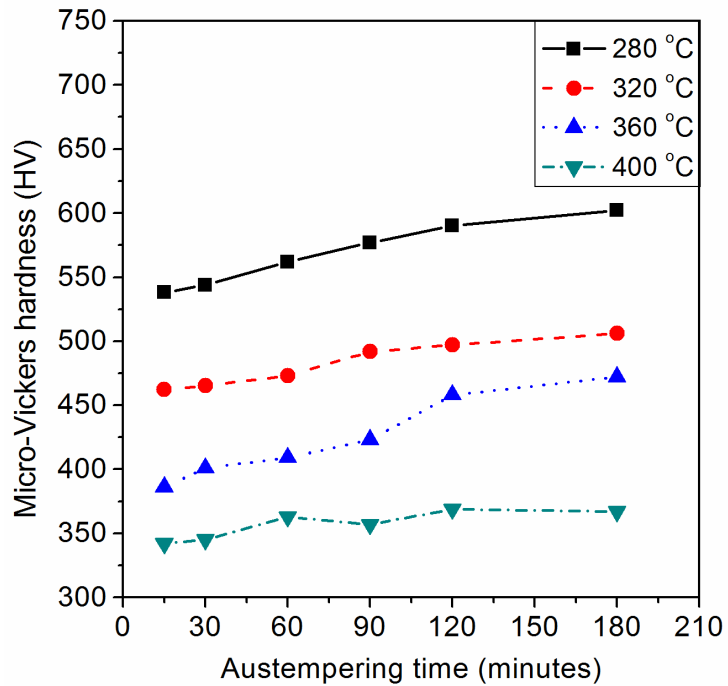


Figure 4.18. Variation of micro-Vickers hardness with austempering conditions

The highest hardness value of 600 HV was observed for the sample austempered at the lowest temperature (280 °C). At this low austempering temperature, the microstructure contains acicular bainitic ferrite and retained austenite. The fine-structured acicular bainitic ferrite and reduction in the retained austenite content result in an increased hardness at a lower austempering temperature. For a particular austempering time, the material hardness decreases with an increase in austempering temperature (360– 400 °C) due to the increased coarseness of bainitic ferrite and retained austenite. A slight increase in hardness was observed with respect to increasing austempering time for all austempering temperatures, due to the fineness of the bainite structure and decrease in retained austenite content.

4.4 Influence of Austempering Temperature and Time on the Wear Property

The wear behavior of AISI 9255 high silicon steel samples austempered at different temperatures was studied and their results are tabulated (table 4.2 & 4.3). The wear rate is given by the slope of cumulative weight loss against wear time graph. It can be seen from fig. 4.19 that the cumulative weight loss increases in approximate linearity with the wear time. It was observed that wear rate shows increasing trend with increase in austempering temperature and austempering time.

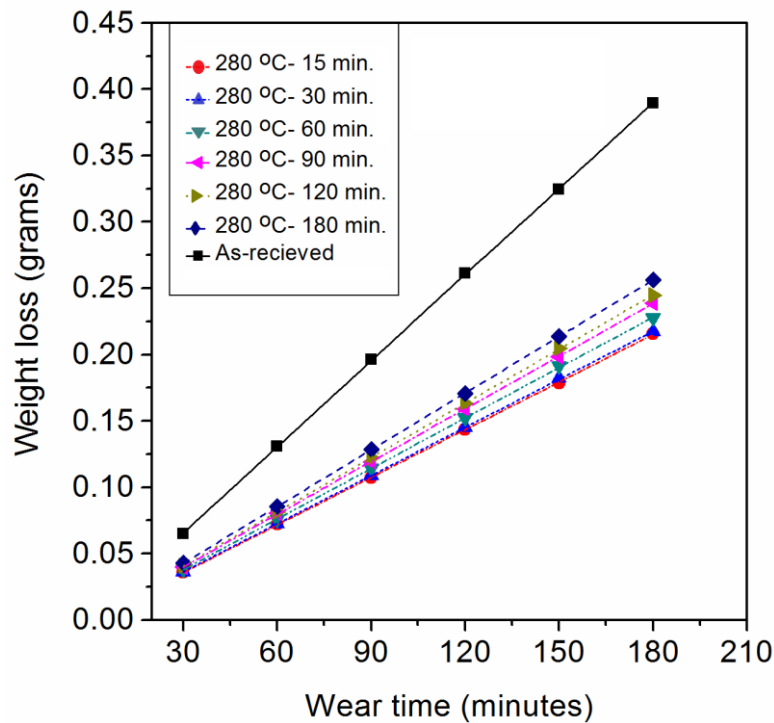


Figure 4.19 Cumulative weight loss against wear time plot for as-received and samples austempered at 280 °C for various durations.

Table 4.2 Wear property of the as-received steel

Wear rate $\times 10^{-4}$ (gram/minute)	Specific wear rate $\times 10^{-5}$ ($\text{mm}^3/\text{N}\cdot\text{m}$)
21.600	4.076

Table 4.3 Wear property of the austempered samples

Austempering temperature (°C)	Austempering time (minutes)	Wear rate $\times 10^{-4}$ (gram/minute)	Specific wear rate $\times 10^{-5}$ (mm ³ /N-m)
280	15	12.000	2.063
	30	12.100	2.076
	60	12.700	2.176
	90	13.200	2.286
	120	13.600	2.341
	180	14.200	2.450
320	15	13.700	2.355
	30	14.400	2.478
	60	14.900	2.554
	90	15.100	2.605
	120	15.500	2.681
	180	15.800	2.720
360	15	14.200	2.444
	30	14.800	2.547
	60	14.900	2.573
	90	16.200	2.780
	120	16.600	2.868
	180	17.900	3.075
400	15	14.600	2.522
	30	15.100	2.595
	60	16.200	2.780
	90	17.200	2.951
	120	17.400	2.982
	180	17.900	3.074

Specific wear rate (SWR) reveals slight increasing trend with extending austempering temperature and time (Fig. 4.20).

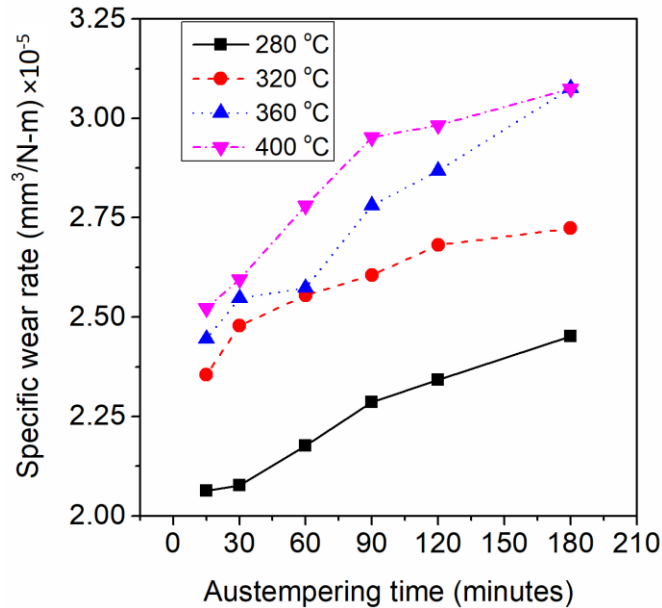


Figure 4.20 Variation in specific wear rate for different austempering conditions

This was ascribed to the way that while extending the austempering time, retained austenite content decreases and the amount of bainitic ferrite is increases, accordingly SWR shows marginal increase, which implies higher retained austenite content favours to enhance wear resistance.

The sample austempered at 280 °C for 15 minutes showed the lowest specific wear rate of $2.063 \times 10^{-5} \text{ mm}^3/\text{N-m}$, mainly due to the presence of fine acicular ferrite along with stabilized retained austenite contributes to the lower specific wear rate of the material, similar observation made by Bedolla-Jacuinde et al. (2015).

Superior blend of hardness and toughness of the materials decides its extent of improved wear resistance. As far as sliding friction is concerned, hardness plays a major role in increasing wear resistance, due to the slight impact during sliding friction. The austempered samples indicate respective decrease and increase in the hardness and toughness with increasing austempering temperature. Hence the austempered samples having higher wear resistance at lower temperature is ascribed to the improved hardness

and toughness, which is caused by the diminished lath thickness of bainite-ferrite and increase in retained austenite content (Yang et al. 2012).

4.4.1 Wear mechanism

Figure 4.21 shows the SEM images of worn out surfaces for different austempered samples.

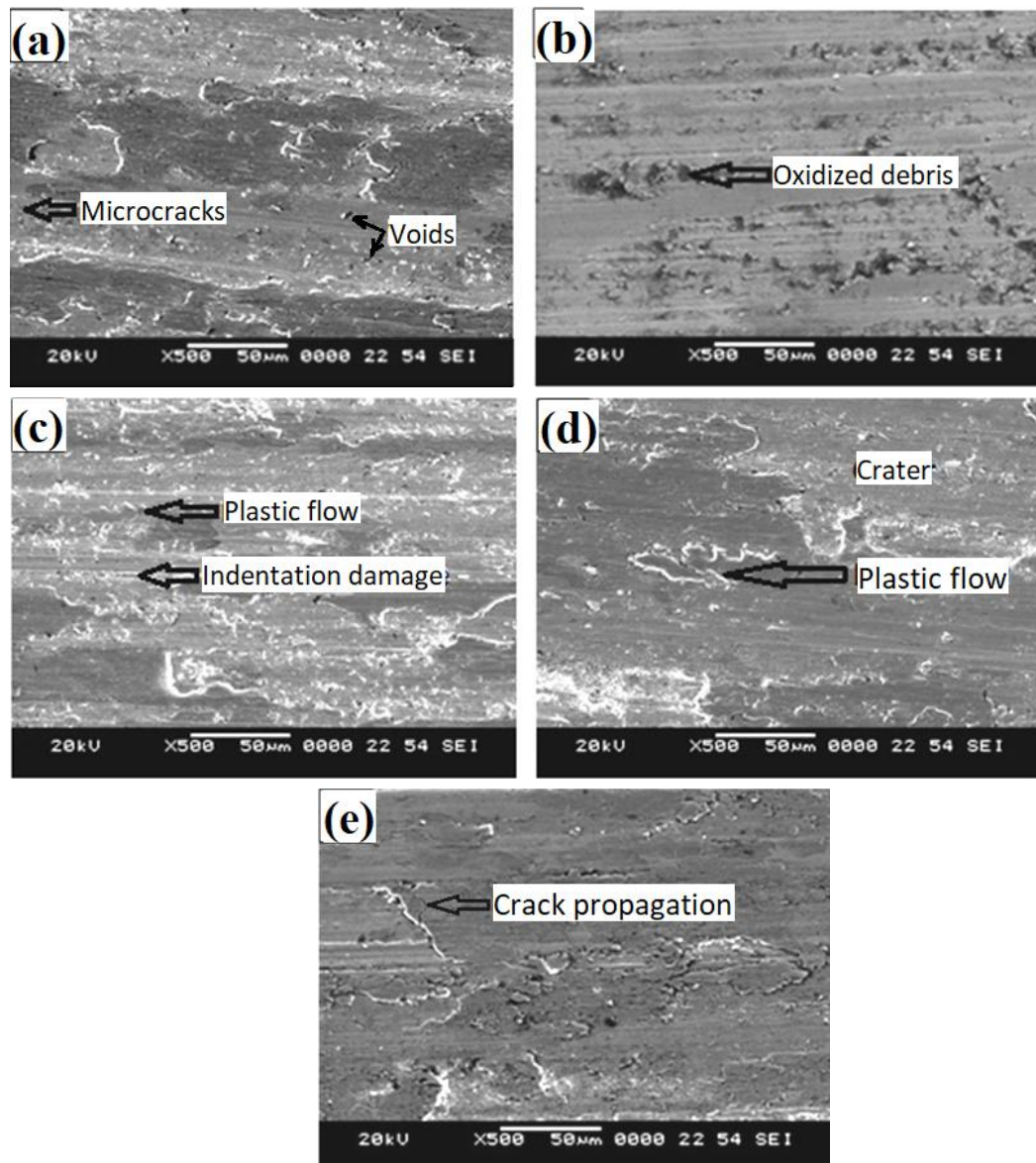


Figure 4.21 SEM of worn out samples austempered at (a) 280 °C- 15 min. (b) 280 °C- 120 min. (c) 320 °C- 60 min. (d) 360 °C- 120 min. (e) 400 °C- 180min.

Initially sliding wear is the main mechanism of material removal. The wear debris is pushed into the contact and is smeared by the acting forces. The main damage mechanisms observed in different austempered high silicon steels due to sliding contact were adhesion, indentation and surface fatigue. The examination of worn out surfaces of high silicon steel samples through SEM helped to understand the mechanism of wear. During the wear process formation of micro cracks, voids, crater, oxides, plastic flow of material and delamination takes place. The voids are the initiator of the crack formation; therefore crack will form near to voids. The coalescence of the voids enhances delamination of the worn surface. The oxidized wear debris accumulated in the surface is adequately hard causing indentation damage.

The observation of smeared debris indicates the occurrence of adhesive wear. During the running-in time, adhesion occurs by the plastic deformation of the surface asperities, that results in the formation of crack nucleation sites in the surface as the oriented microstructures and also the true contact area leading to development of residual stresses which could cause the work hardening of the material. In addition, the material transfer due to adhesion of the wear debris will occur. Further running-in time i.e., in steady state period, the hard wear debris causes plastic shearing on the surface and indentation damage.

PART B: Quenching and Partitioning (Q&P) Heat Treatment

Experiments were carried out to assess the microstructural characterization, mechanical properties and wear behavior of AISI 9255 high silicon steel subjected to quenching and partitioning heat treatment, their results and discussions are presented here.

4.5 Influence of Partitioning Temperature and Time on the Microstructure

4.5.1 Optical microscopy

Figures 4.22 and 4.23 shows the representative optical micrographs of Q&P heat treated steel samples quenched at 190 °C and partitioned at various temperatures i.e. 280, 320, 360 and 400 °C and times ranging from 15 to 90 minutes.

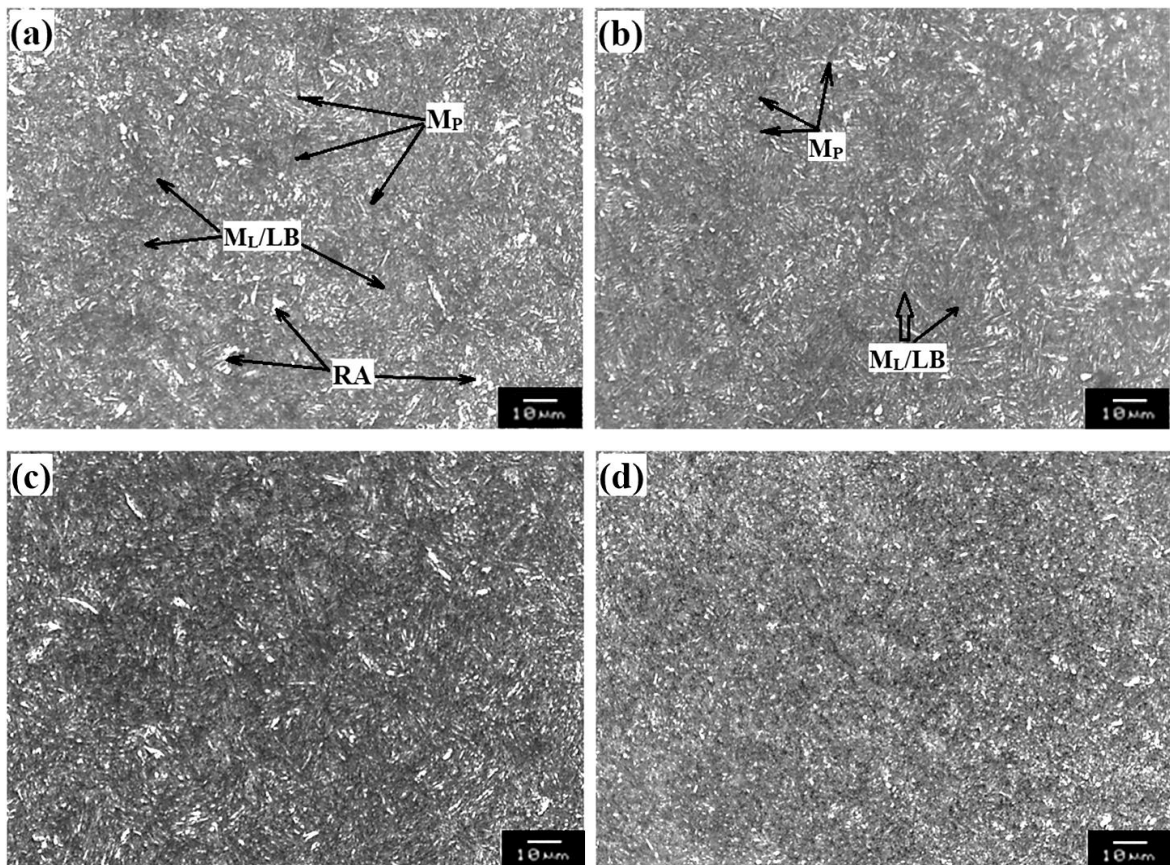


Figure 4.22 Optical micrographs of samples quenched at 190 °C and partitioned at 280 °C for (a) 15 minutes (b) 30 minutes (c) 60 minutes (d) 90 minutes.

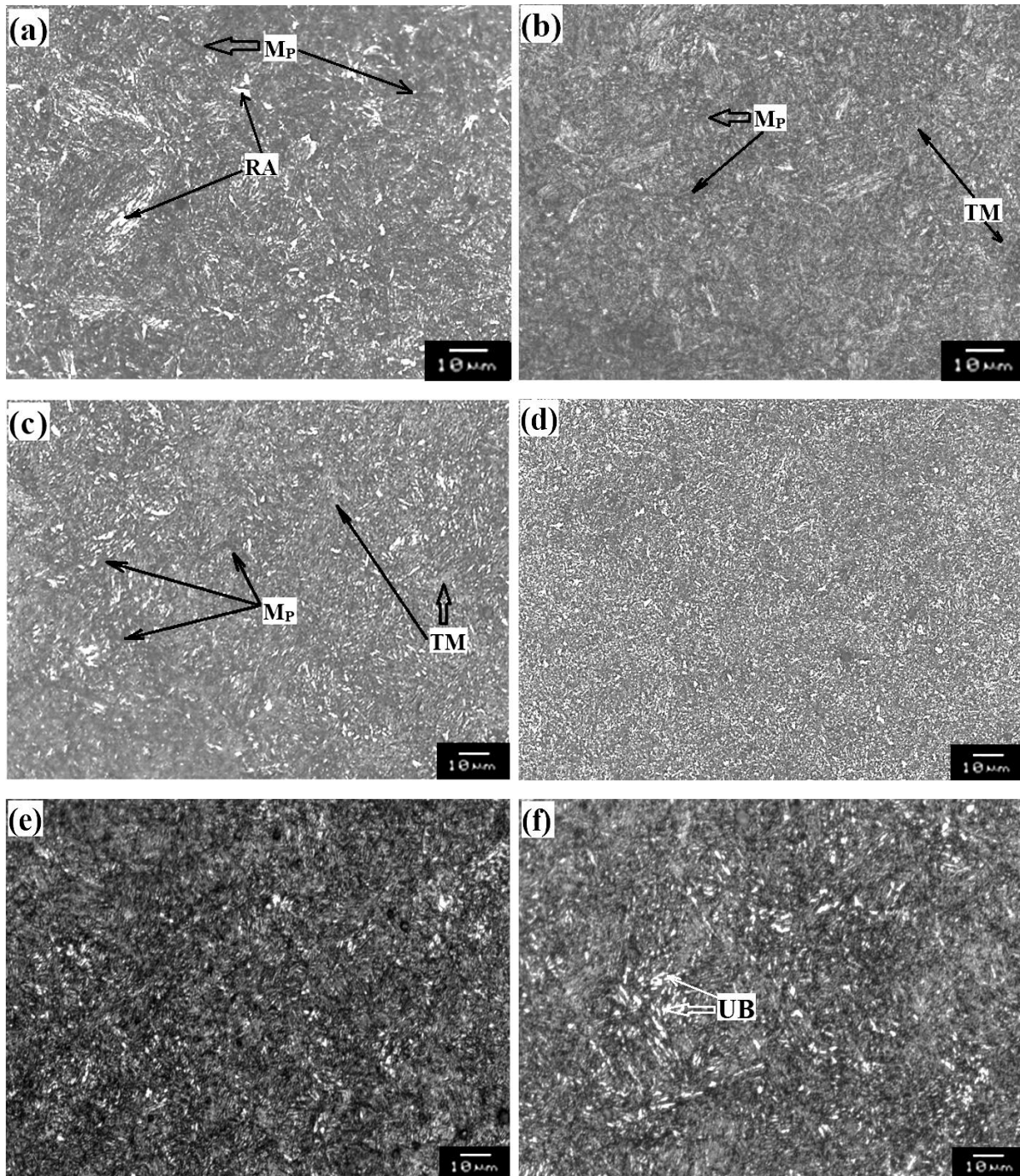


Figure 4.23 Optical micrographs of samples quenched at 190 °C and partitioned at (a) 320 °C for 15 minutes (b) 320 °C for 90 minutes (c) 360 °C for 15 minutes (d) 360 °C for 90 minutes (e) 400 °C for 15 minutes (f) 400 °C for 90 minutes.

Microstructures of specimens partitioned at 280, 320, 360 and 400 °C (figures 4.22 and 4.23) reveals martensite [i.e. M_L and M_P], TM, LB & UB and RA (White areas) for all heat treatment conditions.

Retained austenite is evidently seen in the specimens partitioned at shorter time i.e. 15 minutes at temperatures 280 and 320 °C (Fig. 4.22a & 4.23a) and retained austenite islands are comparatively less in high temperature partitioned specimens i.e. 360 and 400 °C (Fig. 4.23 (c & e)) and also with increase in partitioning time for all temperatures.

These retained austenite islands are typically found at prior austenite grain boundaries (PAGs). Depending on the carbon content, M_L and LB etched distinctively in contrast to M_P (Fig. 4.22) i.e. variation in contrast, martensite phase formed in the initial quenching stage is light etched, were as the dark etched martensite plates (lower width) in Fig. 4.23 are either formed at T_Q or actually fresh martensite containing high % of carbon. This fresh martensite was generated on final quenching stage were the carbon depletion through partitioning did not occur to a considerable level. Another form of fresh martensite was formed from low carbon rich metastable retained austenite (Tariq and Baloch 2014). The martensite formed at T_Q and the fresh martensite was transformed from austenite at distinct stages have varying carbon contents. However it was tricky to distinguish between martensite formed during initial quench, fresh martensite on final quenching to room temperature and LB as well due to morphological similarities between these transformation products.

The microstructural characteristics observed at higher partitioning temperature i.e. 400 °C (Fig. 4.23f) indicates UB arrangement that likely adds to extra carbon advancement of austenite and consequently advances its thermal stabilization concerning partitioning close to bainite start (B_s) temperature.

4.5.2 Scanning electron microscopy

Figure 4.24 and 4.25 shows the scanning electron micrographs of Q&P heat treated steel samples quenched at 190 °C and partitioned at various temperatures i.e. 280, 320, 360 and 400 °C and times ranging from 15 to 90 minutes.

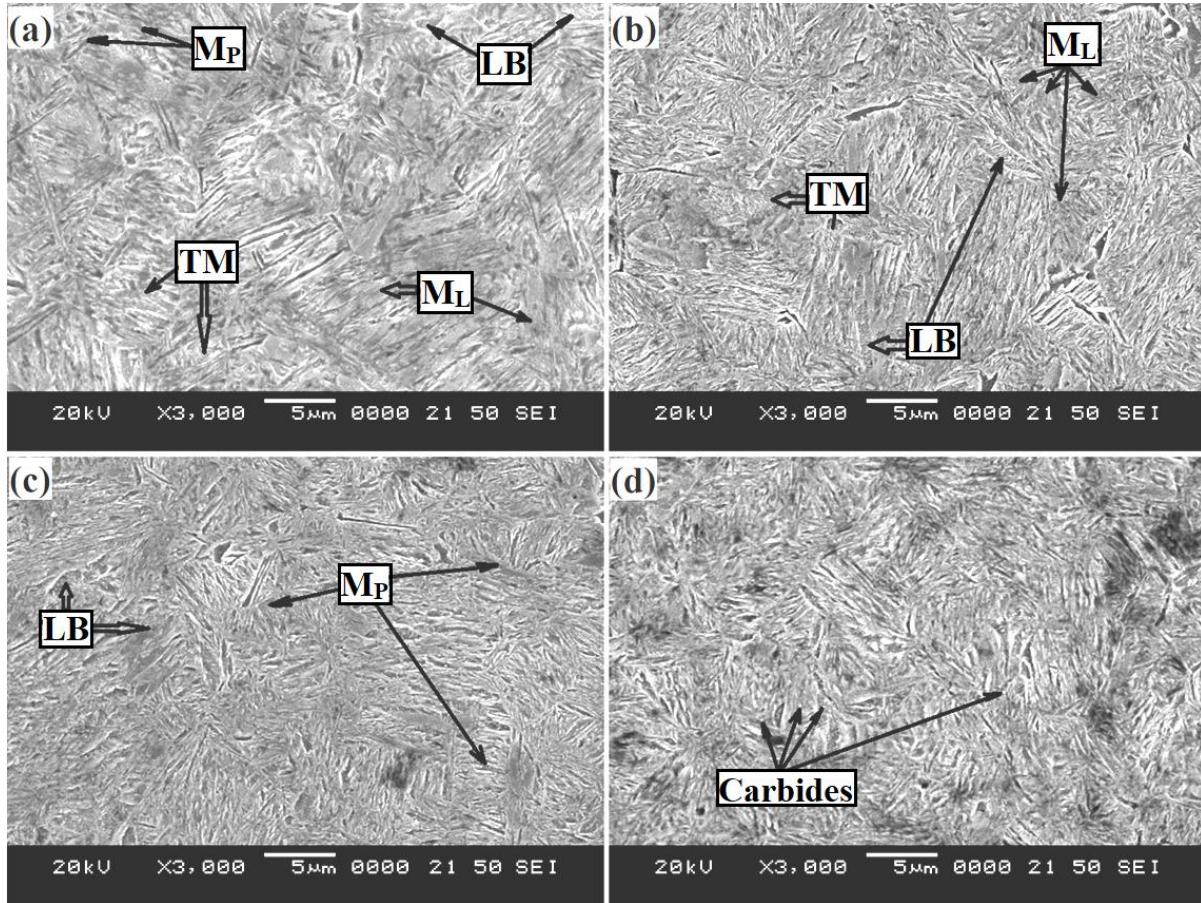


Figure 4.24 Scanning electron micrographs of samples quenched at 190 °C and partitioned at 280 °C for (a) 15 min. (b) 30 min. (c) 60 min. (d) 90 min.

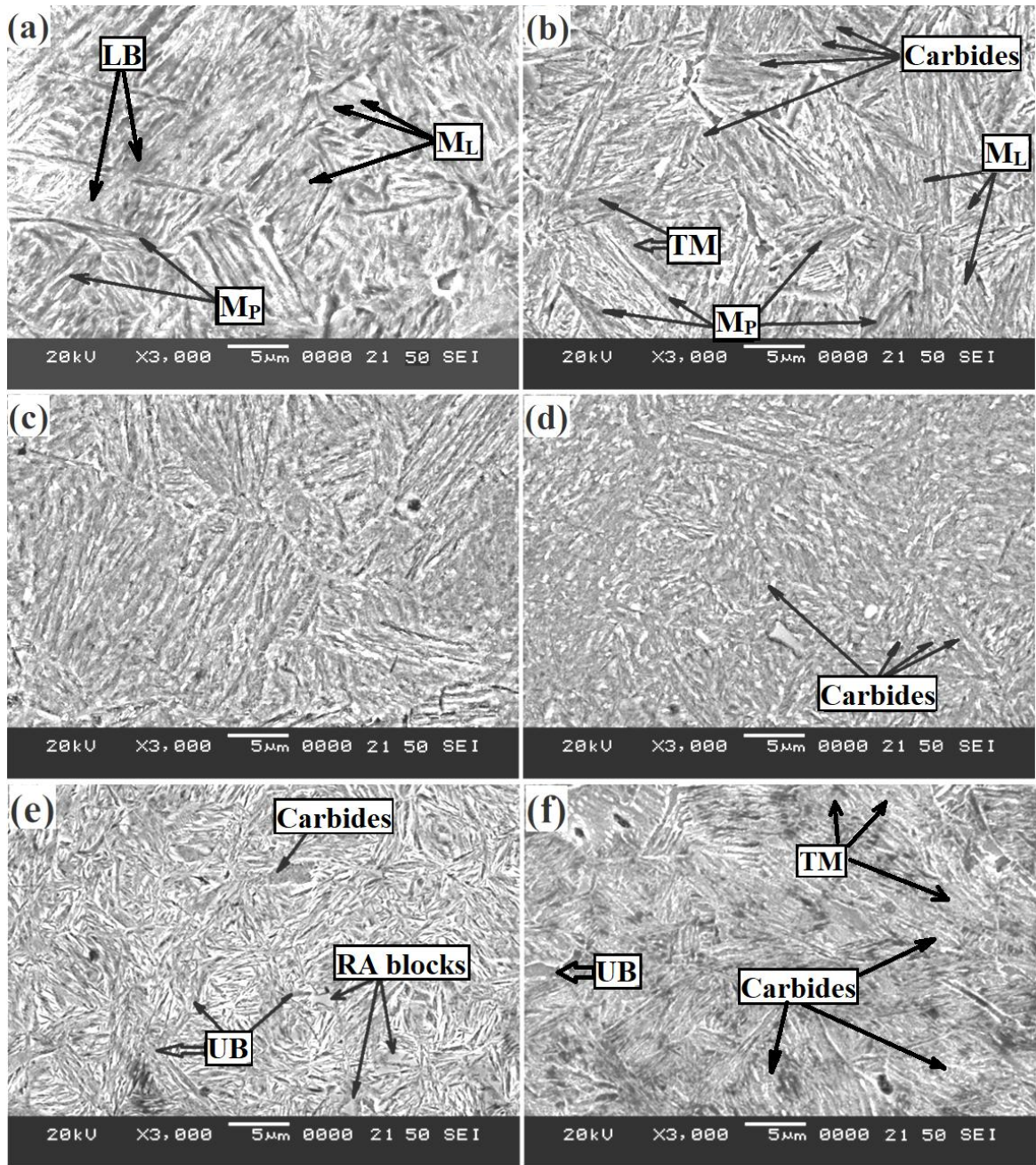


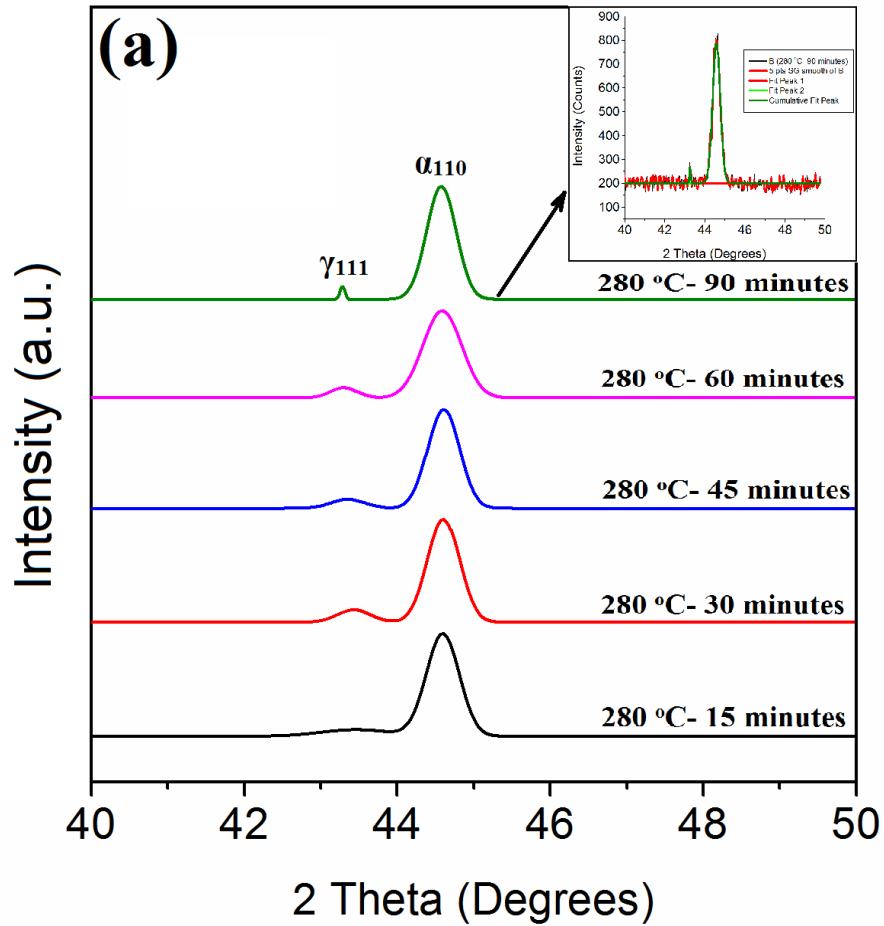
Figure 4.25 Scanning electron micrographs of samples quenched at 190 °C and partitioned at (a) 320 °C for 15 min. (b) 320 °C for 90 min. (c) 360 °C for 15 min. (d) 360 °C for 90 min. (e) 400 °C for 15 min. (f) 400 °C for 90 min.

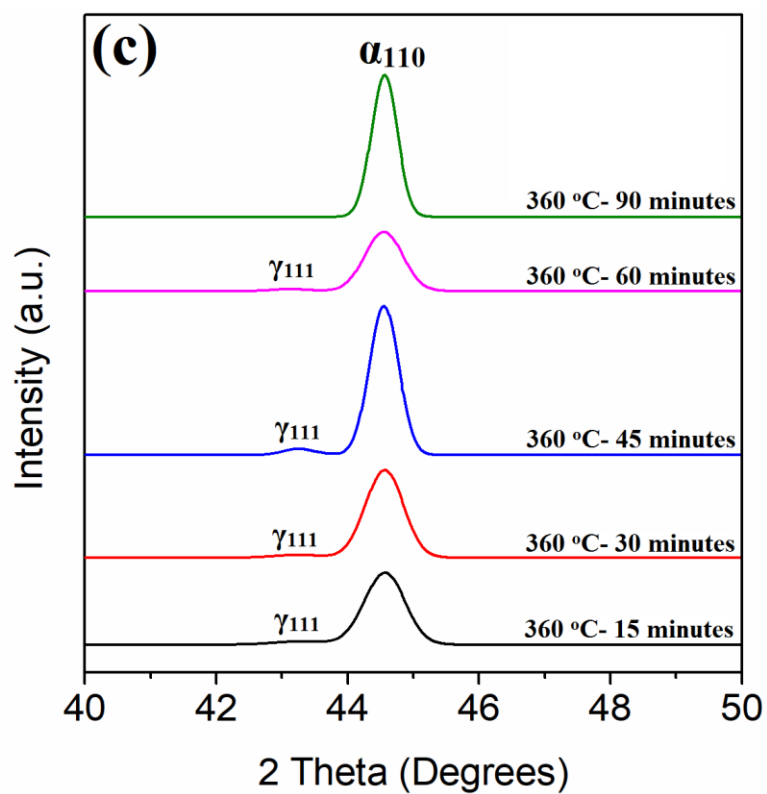
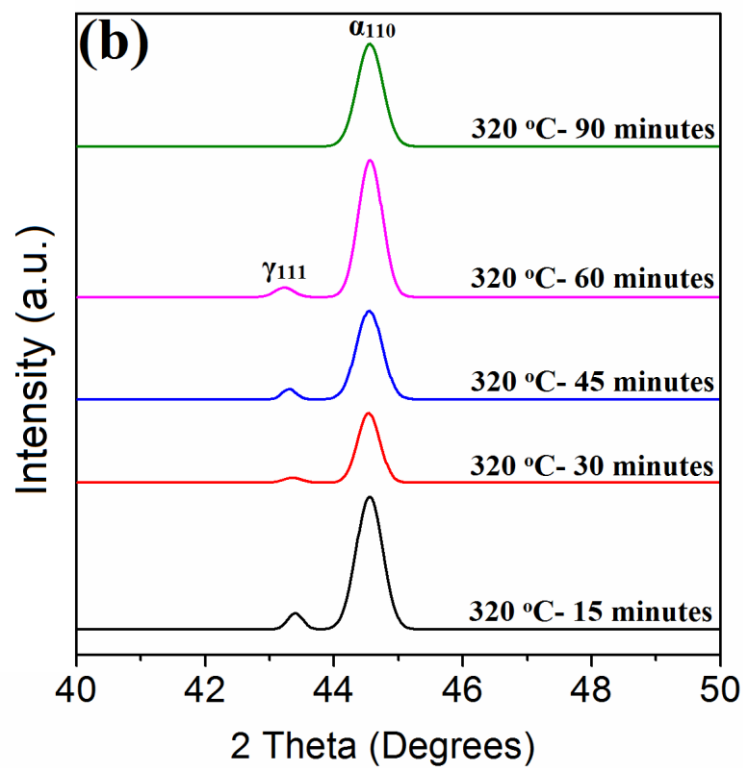
Above SE micrographs reveal the presence of various phases in the Q&P heat treated samples (Fig. 4.24 a-d). For partitioning condition of 280 °C for 15 minutes comprises of M_P , M_L , TM, LB and thin-film like RA, as shown in Fig. 4.24a. These M_L are assembled into packets (Fig. 4.24 a-d). RA is principally found inhomogeneously as films between these laths and sometimes on the packet boundaries. Microstructures shown in figures 4.24 and 4.25 reveals the entirely fine sized martensite blocks and packets with inherently high dislocation density. During partitioning stage, excess carbon relocates from martensite to retained austenite (acting as a potential sink for carbon) assuming constrained-carbon paraequilibrium (CCE) condition i.e. complete carbon partitioning from martensite to austenite. This prompts increment in carbon concentration and also lattice parameter of austenite along these lines making it chemically stable and retainable on final quenching. Conversely, low carbon enriched austenite is unstable and undergoes transformation to fresh martensite.

An additional perception is the existence of fine metastable carbides within tempered martensite (regions of M_L) at 360 and 400 °C (Fig. 4.25 (d, e and f)). The scope of carbide precipitation is less in carbon lean martensite. Tempering of martensite occurs that was formed in the initial quench stage i.e. auto tempering and conventional tempering process also occurs during partitioning stage i.e. a portion of the carbon leaving from martensite was used to form metastable transition carbides i. e. ϵ -carbides that are infrequently found in some martensitic plates. These ϵ -carbides appear in medium carbon steels containing silicon (Edmonds et al. 2011). Actually, higher Si content advances the ϵ -carbide arrangement at lower temperatures and furthermore prompts stabilization of transitional epsilon carbide which could be in turn due to the higher silicon solubility in this transitional carbide, which therefore holds on for longer partitioning times and to elevated temperatures (Fig. 4.25 (d, e & f)) (Edmonds et al. 2006). The microstructural characteristics observed at higher partitioning temperature i.e. 400 °C (Fig. 4.25 (e & f)) gives an indication of bainite arrangement that likely adds to extra carbon advancement of austenite and consequently advances its thermal stabilization concerning partitioning close to bainite start (B_s) temperature.

4.6 X-ray Diffractometry

X-ray diffraction analysis was performed to quantitatively determine retained austenite. Figure 4.26 (a-d) illustrates the XRD patterns fitted to the line profiles by Gaussian function for the specimens quenched at 190 °C and partitioned at various temperatures i.e. 280, 320, 360 and 400 °C for different times ranging from 15 to 90 minutes.





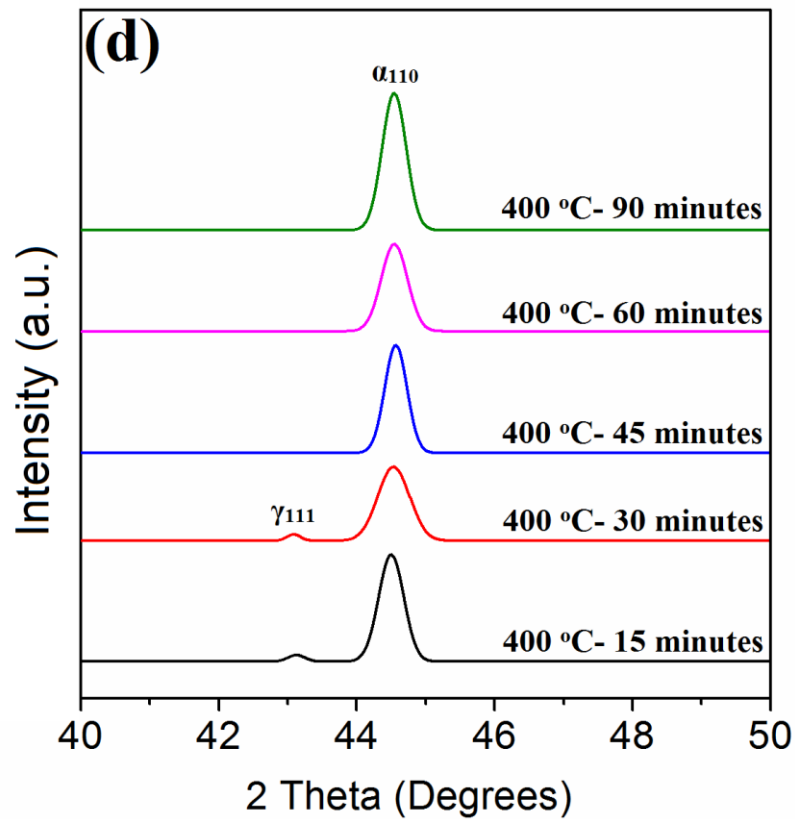


Figure 4.26 XRD patterns fitted to the line profiles by Gaussian function for samples quenched at 190 °C and partitioned at (a) 280 °C (b) 320 °C (c) 360 °C (d) 400 °C.

The above XRD line profiles display two peaks in the 2θ angle range of 40 to 50°. The first peak from (111) plane of austenite gives the information about the amount of retained austenite similarly the second peak from (110) plane indicates martensite/bainitic ferrite and its content in matrix. The XRD line profiles show a shift in austenite peak towards lower 2θ for varying partitioning times, especially at higher partitioning temperature of 400 °C (Fig. 4.26d) which indicates the increase in carbon content in retained austenite.

Figure 4.27 (a & b) shows the profiles depicting the variation of retained austenite (RA) content and carbon content in retained austenite respectively with varying partitioning times and temperatures.

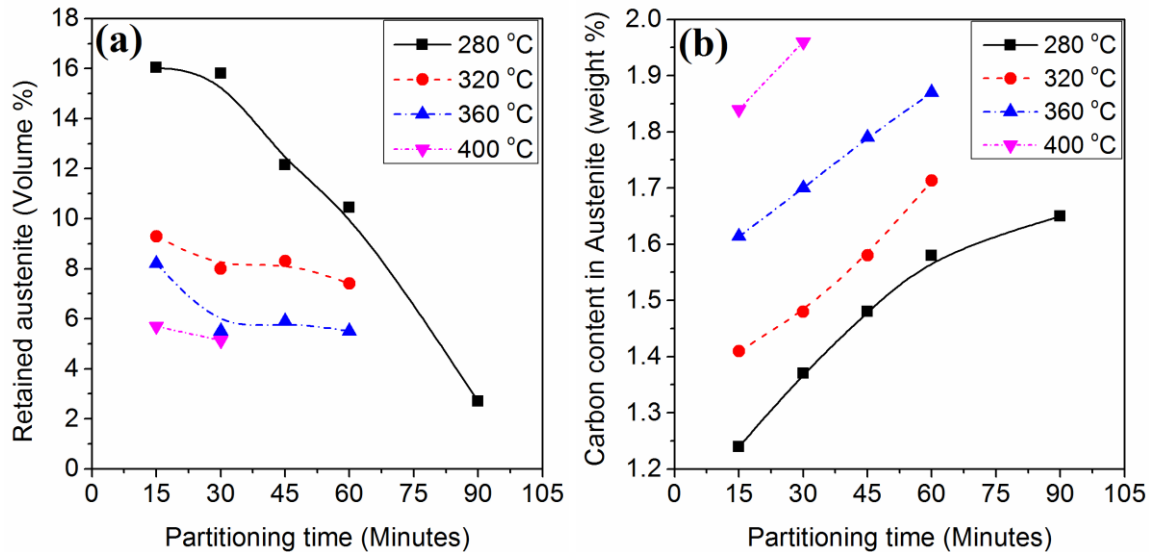


Figure 4.27 Effect of varying partitioning temperature and time on (a) Retained austenite content (b) Carbon content in retained austenite.

In figure 4.27a it is observed that the retained austenite content decreases with increasing partitioning time at 280 °C, and remains more or less constant for other partitioning temperatures i.e. 320, 360 and 400 °C. Maximum amount of RA i.e. 16% was attained at a partitioning temperature of 280 °C for time of 15 minutes. RA content was non-measurable for partitioning time of 90 minutes at temperatures 320, 360 °C and at 400 °C RA could be measured only up to 30 minutes partitioning time, which implies RA content to be very small at these intervals. The purpose behind this reduction in RA content is because of the carbide precipitation that happens most likely at austenite/martensite interface, the prevailing carbide at lower temperature is transitional epsilon carbide and that at higher temperature is cementite. However the steel used in the present work contains high silicon (nearly 2%) which successfully inhibits cementite precipitation during partitioning at higher temperature this can delay the 3rd stage martensite tempering (primarily, the cementite formation at the outlay of transition ϵ -carbide), all the while transition ϵ -carbide seems to get stabilized by silicon mainly due to the superior silicon

dissolvability in this transition ϵ -carbide, which therefore holds on for prolonged partitioning and to elevated temperatures (Owen W.S. 1954). Competition with bainitic transformation may likewise add to diminishing retained austenite content with extending partitioning times, since for partitioning, the austenite/martensite phase blend is reheated to the bainite transformation region.

Figure 4.27b shows the influence of partitioning temperature and time on the carbon content in retained austenite. It is observed that carbon content in retained austenite increases with increase in partitioning temperature and time. Carbon content in RA for all samples increases starting from 1.25% for 280 °C for 15 minutes partitioning and reaches to a maximum of 1.64% at 90 minutes and similar observations were made at 320 and 360 °C. Partitioning at 280 °C is slower than at 400 °C due to the lower carbon diffusion rates and therefore has a different influence on the austenite carbon content, accordingly the sample partitioned at 400 °C for 15 and 30 minutes showed carbon content of 1.83 and 1.96% respectively in austenite and retained austenite content was non quantifiable for partitioning beyond 30 minutes at 400 °C. This extent of carbon enrichment is necessarily influenced by transitional carbides that was formed in the quenching stage (autotempering) and presence of silicon in steel stabilizes these carbides at elevated partitioning temperatures and moreover bainite formation occurs through consecutive nucleation and diffusionless growth of bainitic ferrite plates that soon a while later partition the overabundance carbon to the encompassing austenite, that prompts the extra enhancement of carbon in retained austenite (Santofimia et al. 2009). Thus it is additionally vital to note that increase of carbon content in austenite does not really suggest increase in retained austenite content.

4.7 Electron Back Scattered Diffraction (EBSD) Analysis

The microstructural morphology and phase contents present in this Q&P heat treated specimens were further studied by EBSD and are discussed below.

Figure 4.28 to 4.33 shows the color coded phase distribution [PD] map (a), adjacently provided with orientation image by inverse pole figure [IPF] map (b) and misorientation angle distribution profile [Figure (c) in 4.28, 4.29, 4.30 & 4.33] for the selected conditions of specimens quenched at 190 °C and partitioning at different temperatures from 280 to 400 °C. In the PD map, green color indicates martensite and red indicates retained austenite (RA).

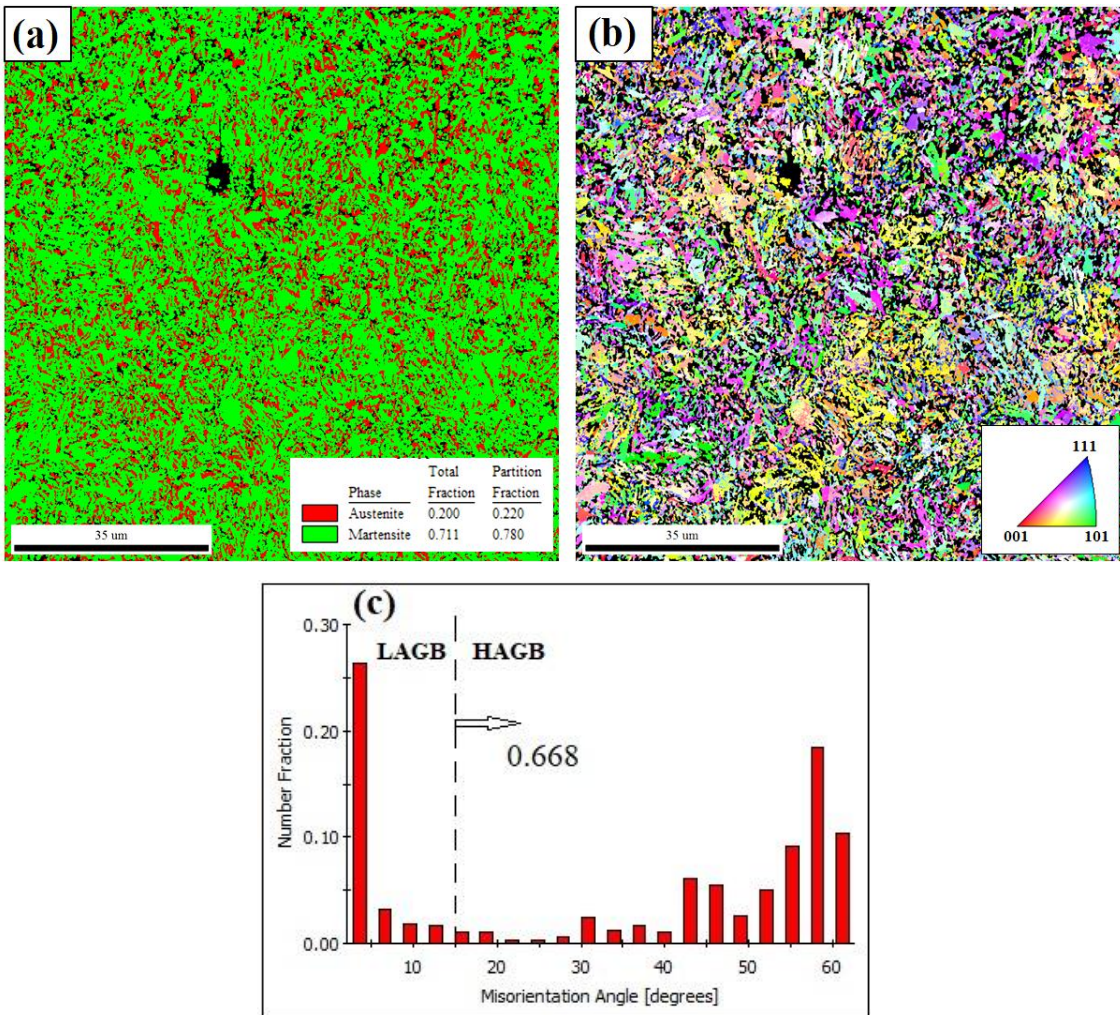


Figure 4.28 EBSD maps of the steel samples quenched at 190 °C and partitioned at 280 °C- 15 minutes (a) PD map (b) IPF map (c) Misorientation distribution profile

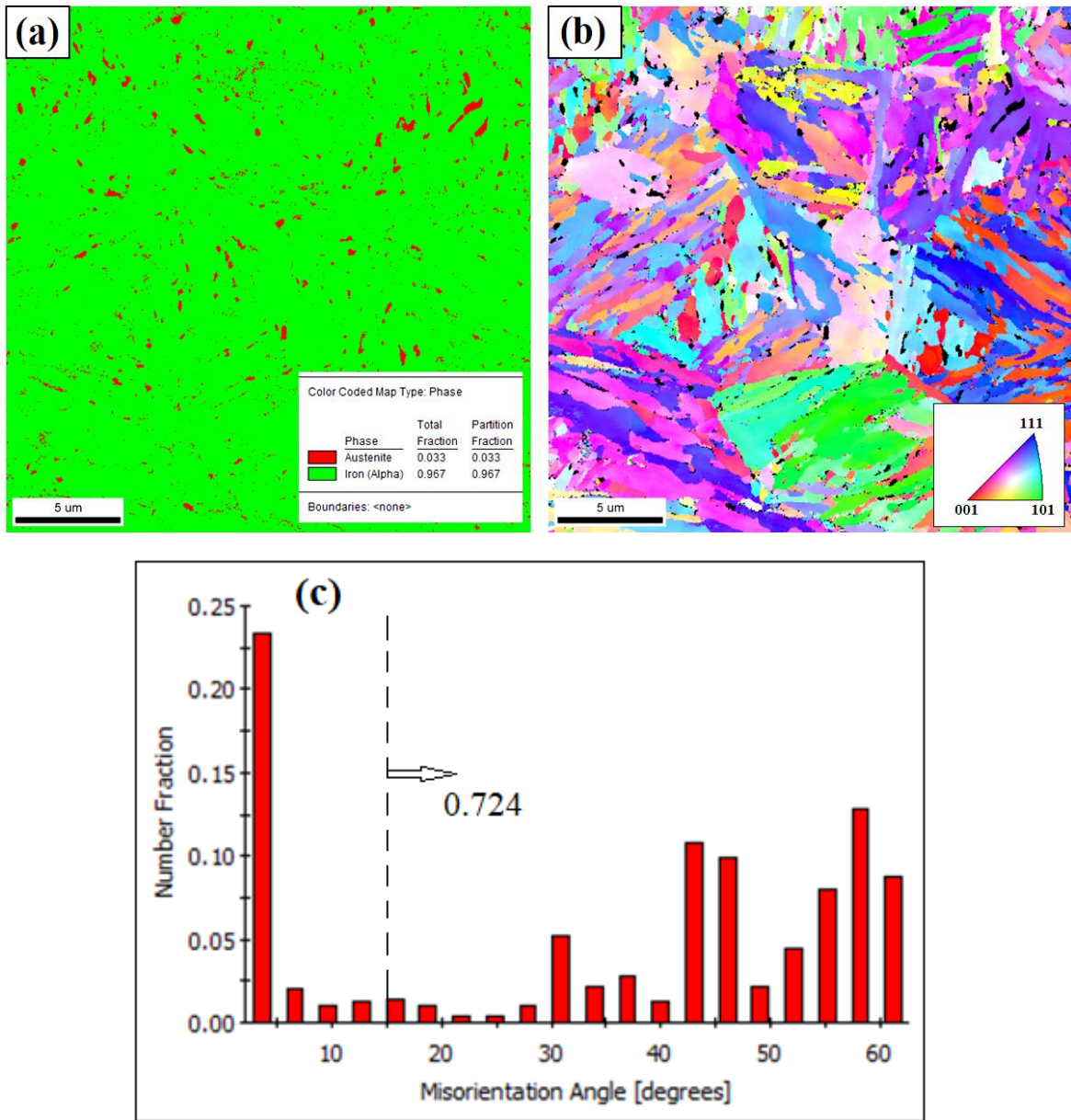


Figure 4.29 EBSD maps of the steel samples quenched at 190 °C and partitioned at 280 °C- 90 minutes (a) PD map (b) IPF map (c) Misorientation distribution profile

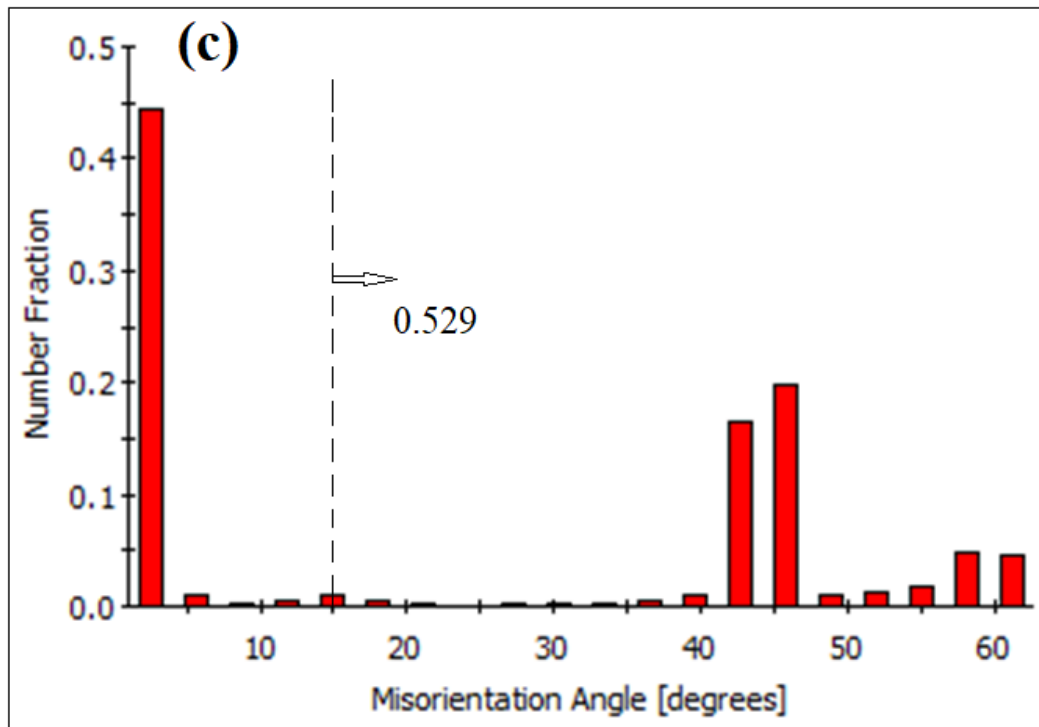
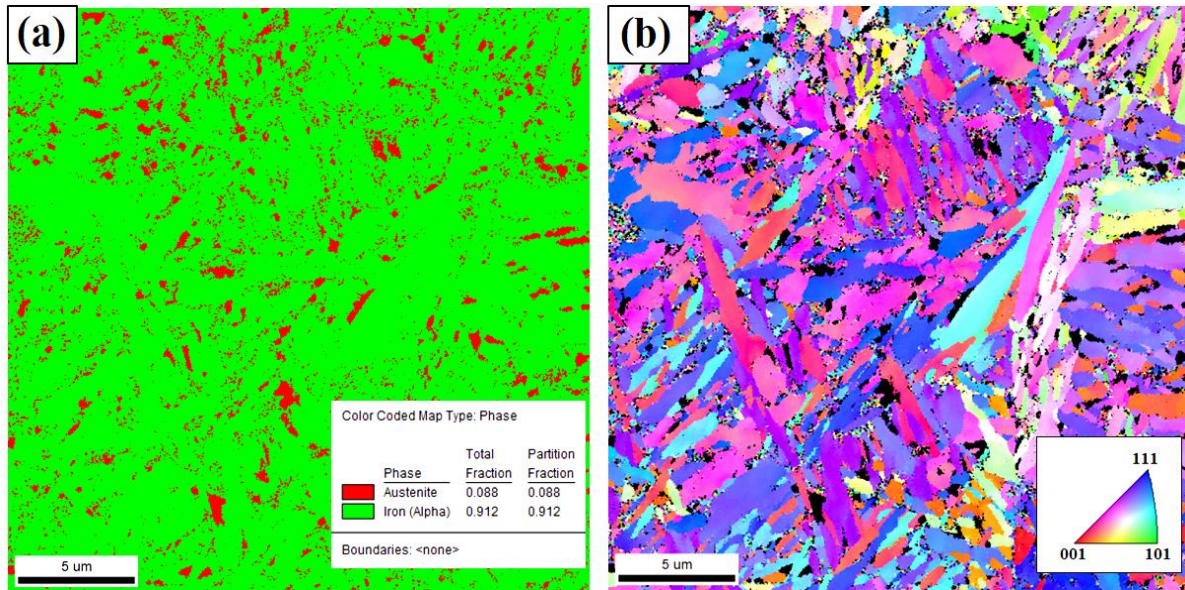


Figure 4.30 EBSD maps of the steel samples quenched at 190 °C and partitioned at 320 °C- 15 minutes (a) PD map (b) IPF map (c) Misorientation distribution profile

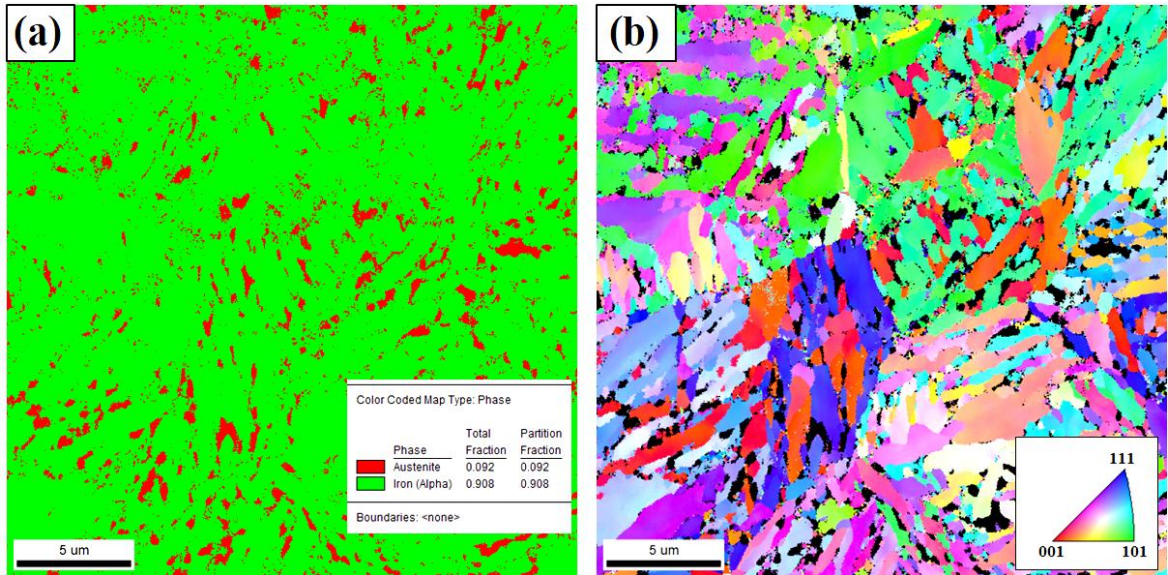


Figure 4.31 EBSD maps of the steel samples quenched at 190 °C and partitioned at 360 °C- 15 minutes (a) PD map (b) IPF map

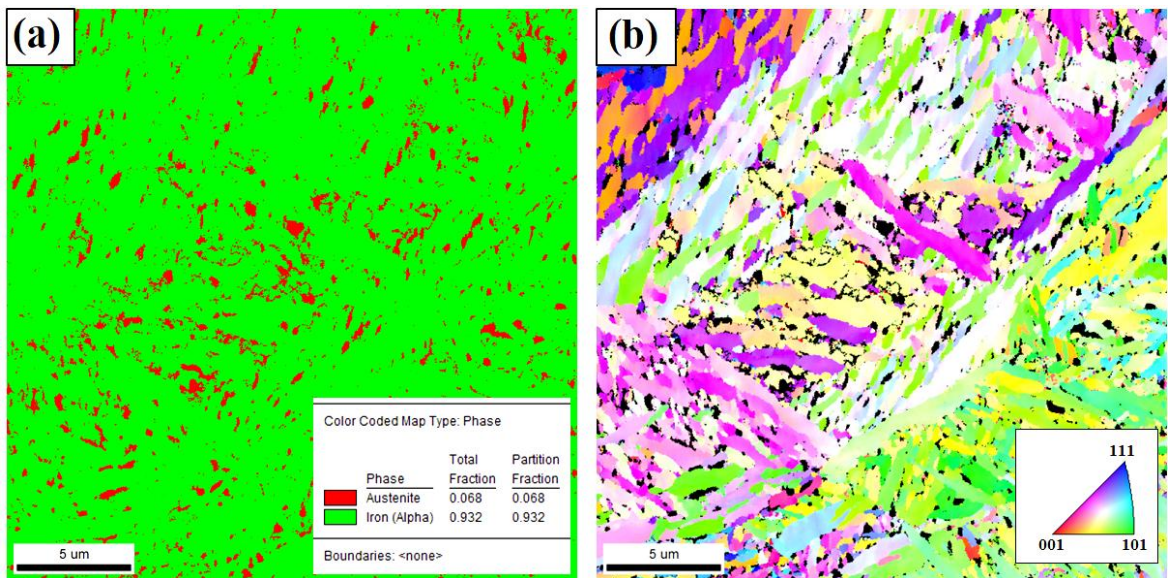


Figure 4.32 EBSD maps of the steel samples quenched at 190 °C and partitioned at 360 °C- 60 minutes (a) PD map (b) IPF map

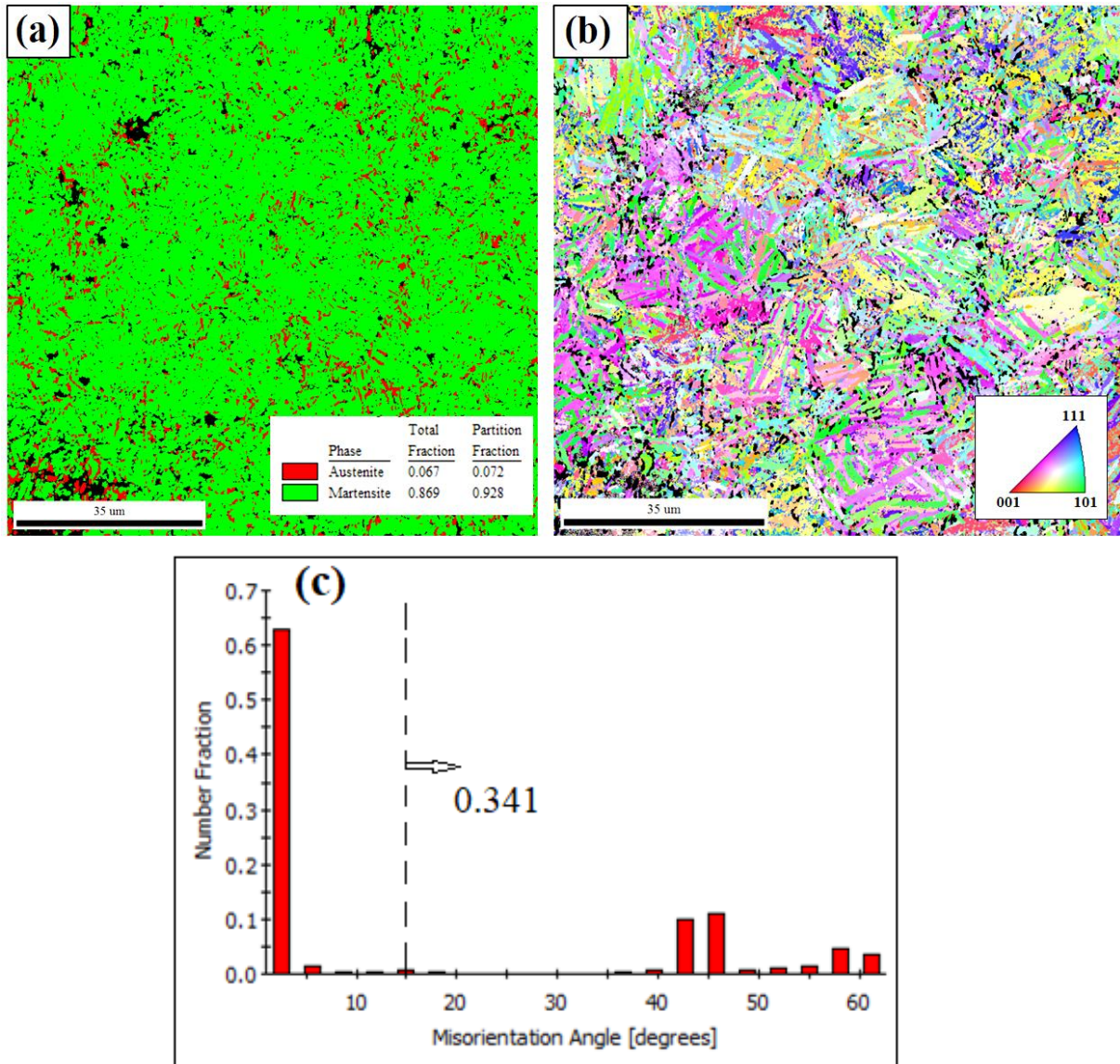


Figure 4.33 EBSD maps of the steel samples quenched at 190 °C and partitioned at **400 °C- 30 minutes** (a) PD map (b) IPF map (c) Misorientation distribution profile.

Localized EBSD scans defer quite closer values of retained austenite content when compared with the same obtained through XRD analysis shown in the previous section. For partitioning condition of 280 °C for 15 minutes RA content measured by EBSD was found to be 20% (Fig. 4.28a) and by XRD it was found to be 16%. At 280 °C for 90 minutes (Fig. 4.29a), the RA content obtained was 3.3% by EBSD and 2.7% by XRD. At 320 °C for 15 minutes RA content was 8.8% by EBSD and 9.3% by XRD (Fig. 4.30a).

At 360 °C for 15 minutes and 60 minutes was found to be 9.2% and 6.8% respectively by EBSD and by XRD 8.2% and 5.9% respectively (Fig. 4.31a & 4.32a) due to slightly coarser and easily noticeable interlath lamellar austenite grains. At 400 °C for 30 minutes 6.7% by EBSD and 5.7% by XRD (Figure 4.33a), which implies that subsequent to partitioning treatment, further the interlath austenite, blocky austenite grains were also stabilised.

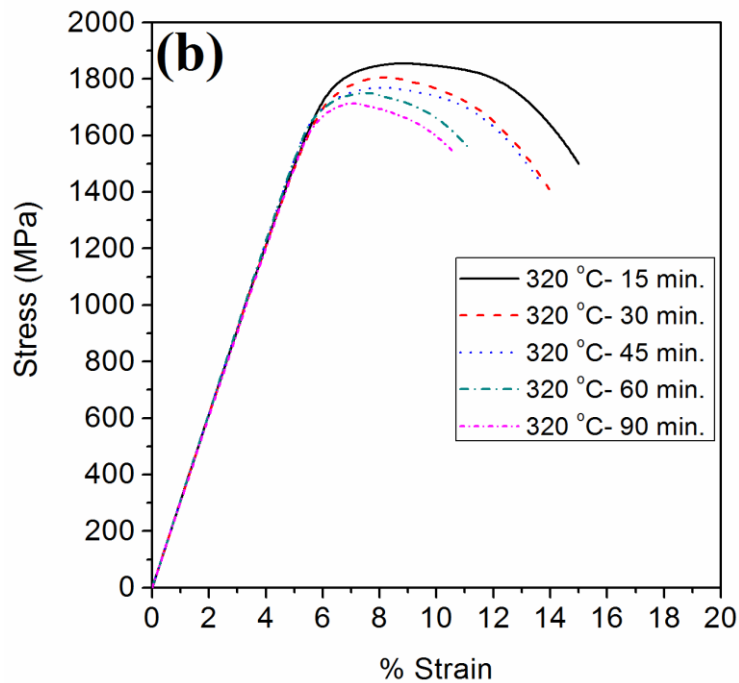
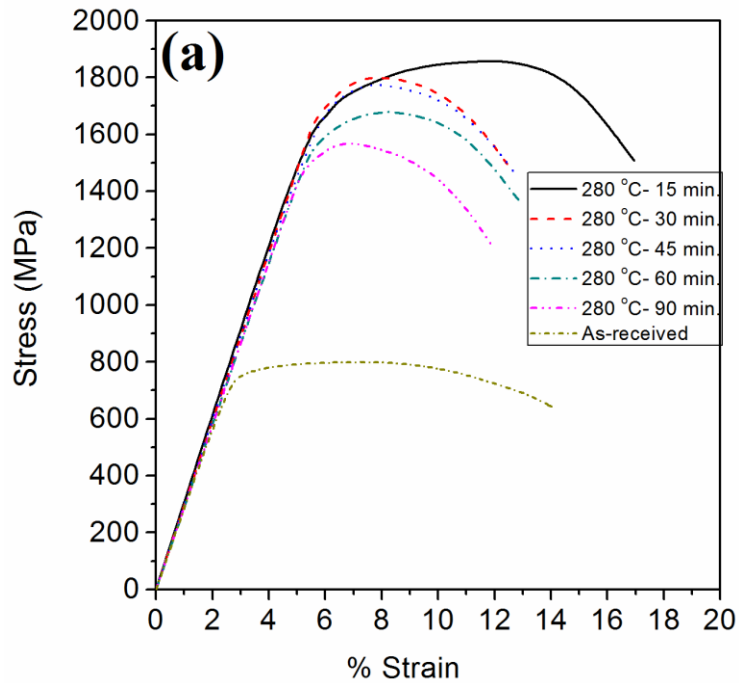
Figure [(4.28 to 4.33) (b)] shows the orientation image by IPF map of martensite phase for various partitioning conditions, variation in color indicates different crystallographic orientation of the martensite crystal (retained austenite appears black). In the IPF maps, the colored martensite phase shows majority of plate-like morphology along with some twin orientations. Despite the fact that the resolution by EBSD method is sensibly high since it works on a localized measurements, film like austenite grains between the martensite/bainitic ferrite laths are not consistently resolved (Thomas and Speer 2014), (Da Silva et al. 2015).

[Figure (c) in 4.28, 4.29, 4.30 & 4.33] shows the misorientation angle distribution profile for various partitioning conditions. The specimen partitioned at 280 °C for 15 min (Fig. 4.28c) and 280 °C for 90 min. (Fig. 4.29c), both conditions shows lower misorientation fraction up to 15° and large misorientation fraction beyond 15° indicating more of high angle grain boundaries (HAGB) than low angle grain boundary (LAGB), which indicates the multiphase structure (lower bainite, martensite of various morphologies and RA) generally comprise of prior austenite grain, packet and block boundaries (Long et al. 2014), (Li et al. 2017). At slightly higher partitioning condition of 320 °C for 15 min (Fig. 4.30c) shows the misorientation fraction of LAGB (0.471) slightly closer to HAGB (0.529), which still indicates the presence of LB and also scope for formation of some upper bainite (UB), due to the increased misorientation fraction of LAGB. Finally at highest partitioning condition of 400 °C for 30 min. (Fig. 4.33c), shows large misorientation fraction of LAGB (0.659) and misorientation fraction of HAGB (0.341), this indicates the formation of UB in the microstructure along with martensite of various morphologies, transition carbides and RA.

4.8 Influence of Partitioning Temperature and Time on the Mechanical Properties

4.8.1 Tensile properties

Figure 4.34 (a-d) shows the engineering stress-strain curves for the as-received specimen and all quenched and partitioned heat treated specimens.



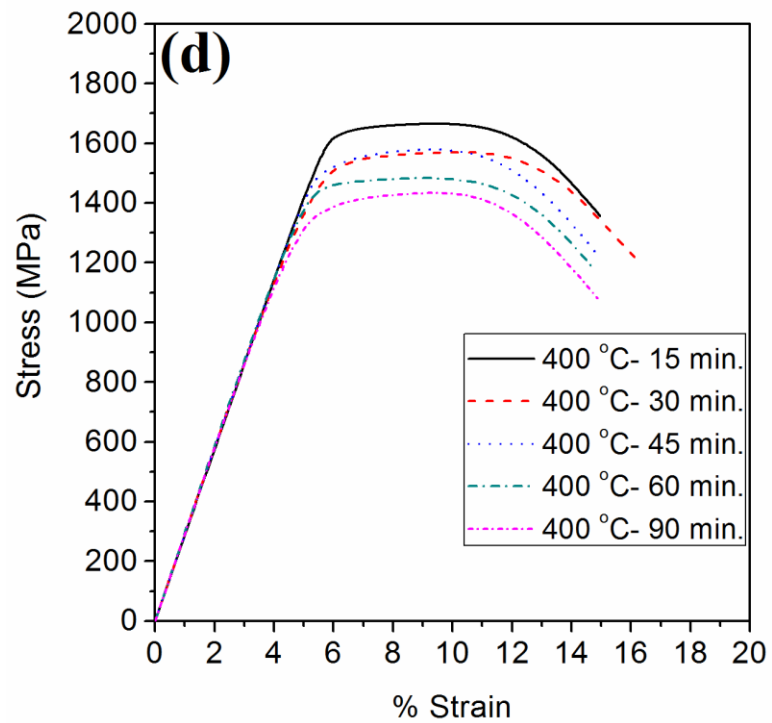
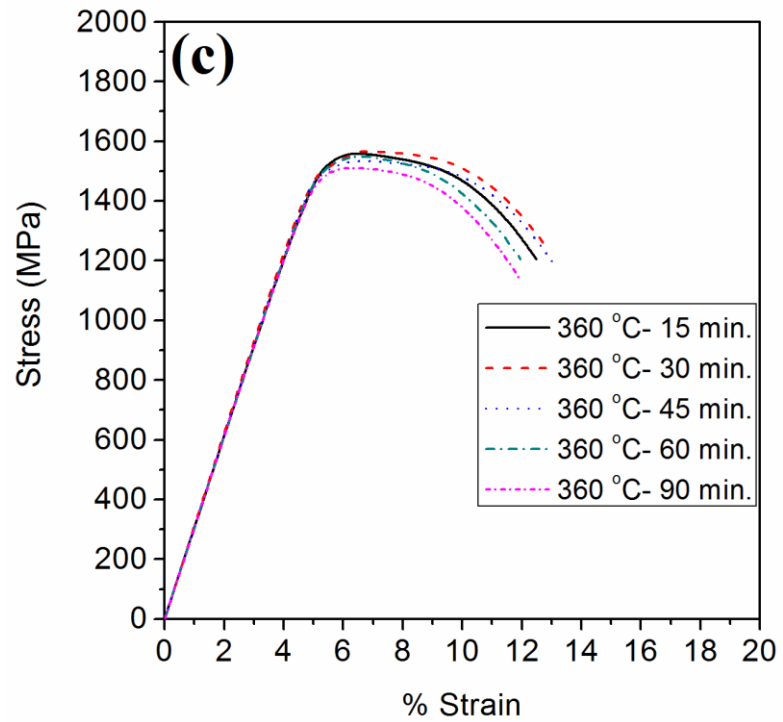
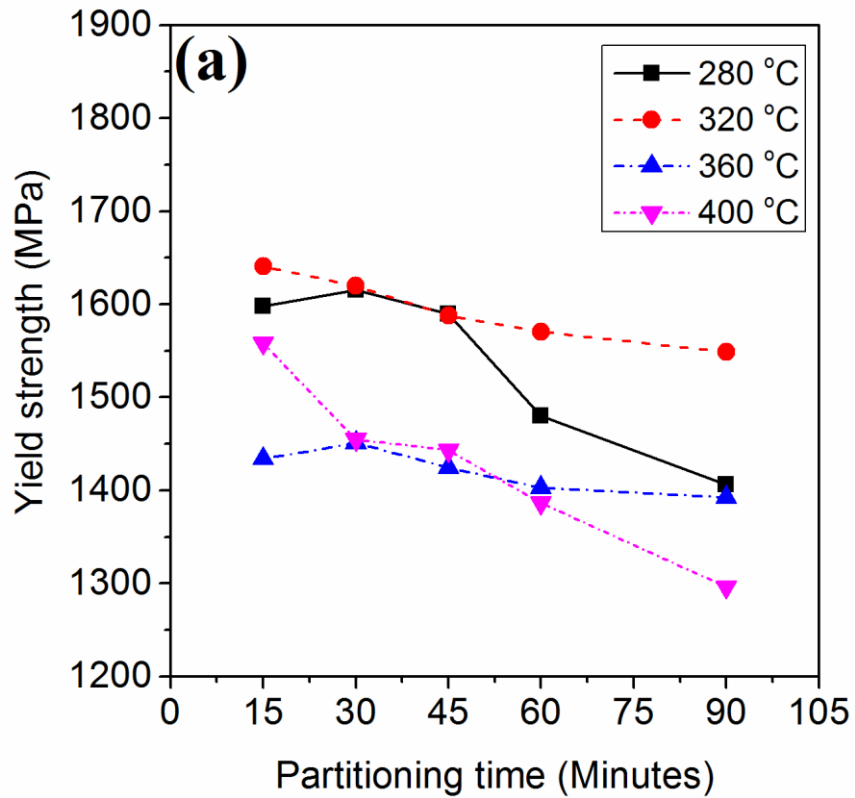
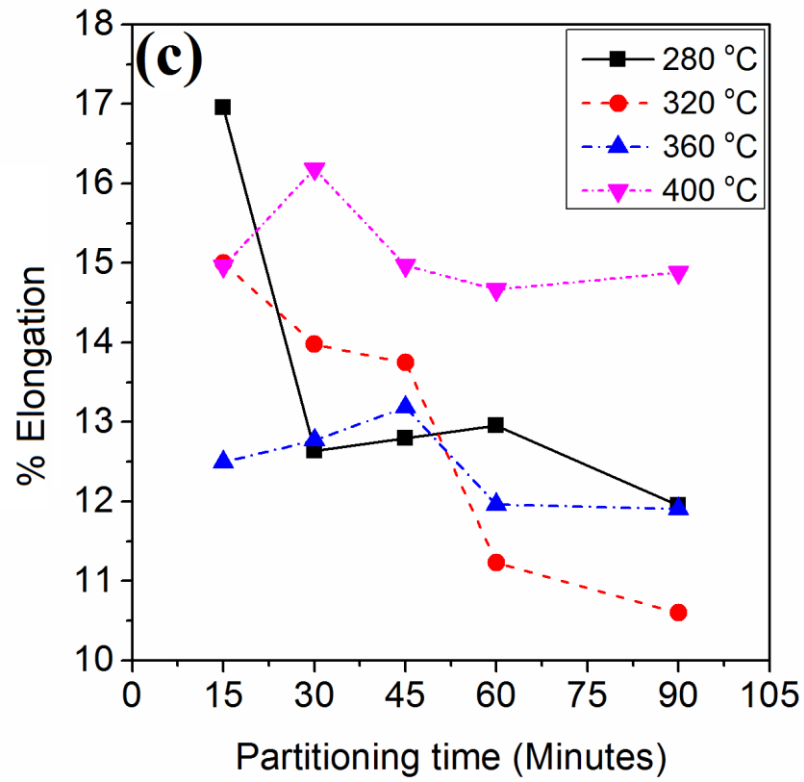
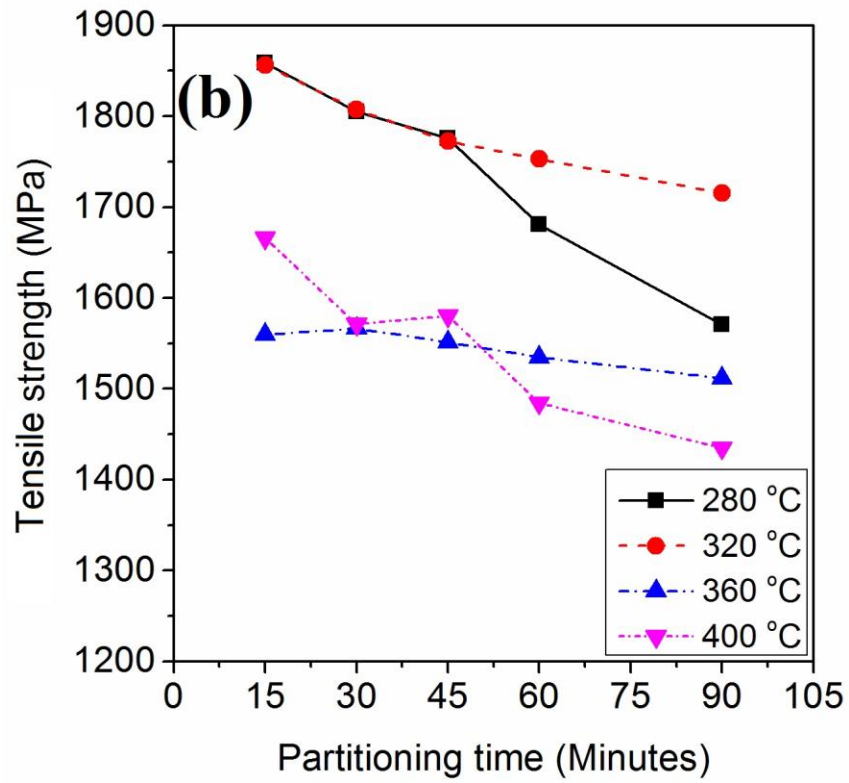


Figure 4.34 Engineering stress-strain curves for samples quenched at 190 °C and partitioned at (a) 280 °C (b) 320 °C (c) 360 °C (d) 400 °C.

From the above stress-strain plots, it can be observed that varying partitioning parameters (temperature and time) resulted in exceptional improvement in tensile strength along with rational ductility and modulus of toughness, when compared to that of as-received high silicon steel (Fig. 4.34a).

Figure 4.35(a-d) shows the variation of yield strength, ultimate tensile strength, % elongation and modulus of toughness with varying duration of partitioning heat treatment.





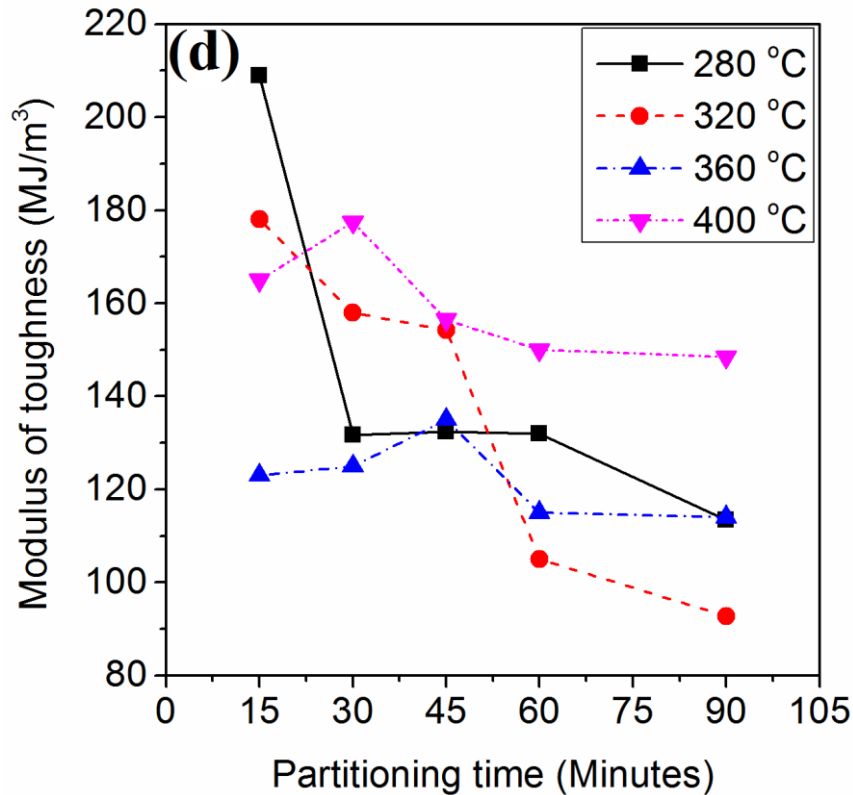


Figure 4.35 Influence of partitioning temperature and time on the tensile properties of the specimens (a) Yield strength (b) Ultimate tensile strength (c) % Elongation (d) Modulus of toughness.

As the partitioning time increases, yield strength (YS) and ultimate tensile strength (UTS) decreases for all partitioning temperatures (Figure 4.35(a & b)) and reduction in % elongation (% EL) and modulus of toughness (MT) was observed for long partitioning time for all temperatures (Figure 4.35(c & d)). Superior combination of strength and toughness was obtained at partitioning temperature of 280 °C and for partitioning time of 15 minutes i.e. YS of 1600 MPa, UTS of 1860 MPa, % EL of 17 and MT of 207 MJm⁻³, which is due to the presence tempered martensite M_L, M_P, lower bainite (LB) along with increased retained austenite content (16%). UTS attained at 320 °C for 15 to 45 minutes partitioning time was also found same as that of 280 °C, but simultaneously leading to reduction in % EL at higher partitioning times which is due to the reduction in the retained austenite content and also precipitation of transition carbides in the tempered martensite matrix. Partitioning at 360 °C shows a gradual decrease in UTS with increase

in partitioning time (Fig. 4.35(a & b)) while % EL and MT increased until 45 minutes due to stabilization of carbon rich austenite but decreased again for prolonged partitioning. Although the maximum RA fractions were attained at partitioning time of 15 minutes, carbon diffusion at this temperature was not adequate to mechanically stabilize the austenite. Partitioning beyond 45 minutes, the C_γ increased upto 1.87% with a simultaneous decrease in RA content due to its decomposition to bainite (Santofimia et al. 2009) & (De Knijf et al. 2015) which in turn caused reduction in % EL.

At highest partitioning temperature i.e. at 400 °C, for prolonged partitioning there was drastic reduction in YS (1558 to 1296 MPa) and also UTS (1666 to 1435 MPa) (Fig. 4.35(a & b)), due to the softening of fresh martensite i.e. by migration of carbon from the interstitial sites of martensite to austenite during partitioning, progressive tempering of the martensite, presence of stabilized transitional carbides and also due to the presence of bainitic ferrite laths (UB), conversely lead to fairly better % EL varying from (15-16) and also MT 150-180 MJ/m³ (Fig. 4.35(c & d)).

4.8.1.1 Fractography

Figure 4.36(a–h) shows the SEM of the fracture surface morphology for selected tensile tested specimens after quenching and partitioning at different conditions.

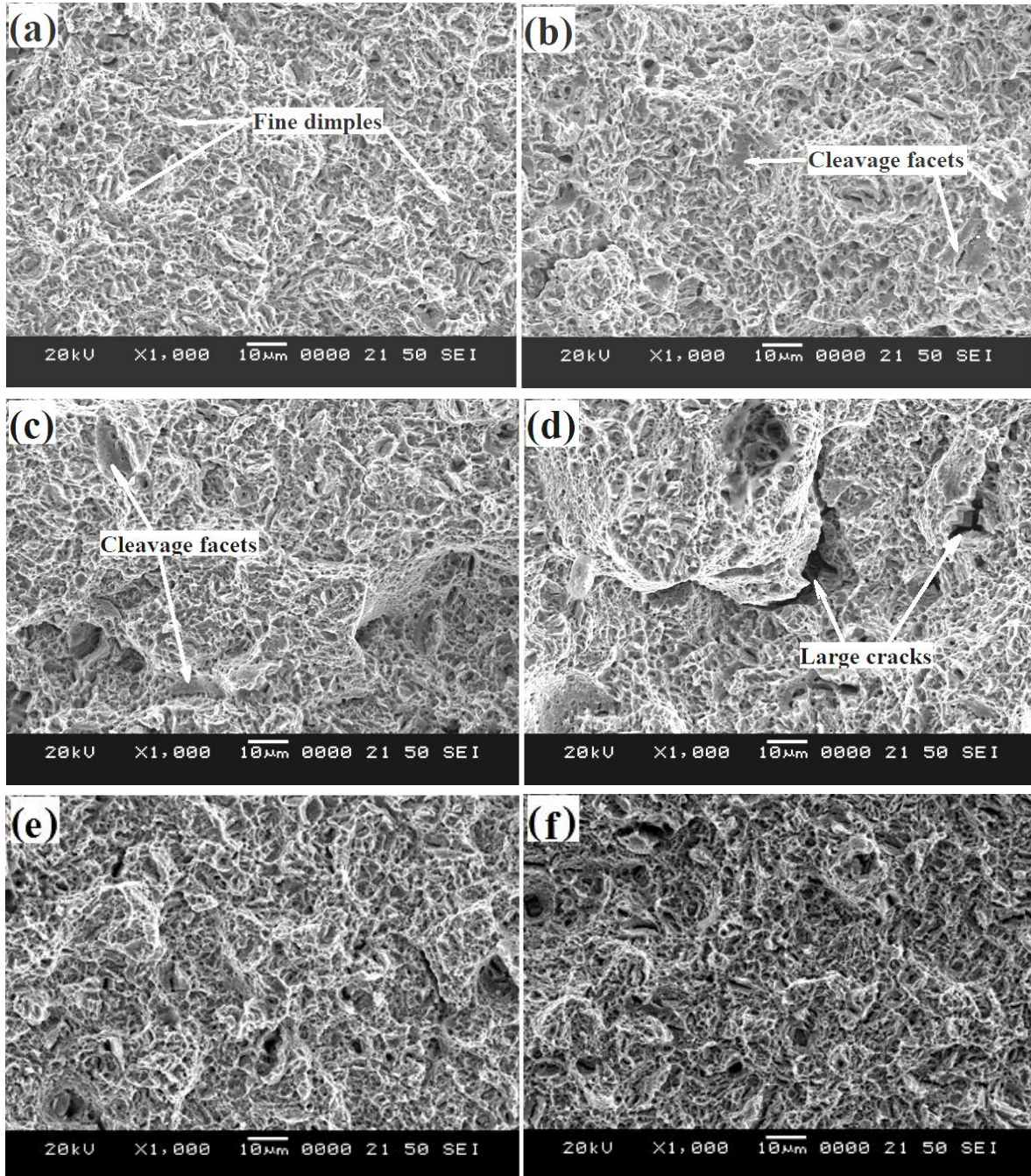


Figure 4.36 Fractographs of the Q&P samples (a) 280 °C- 15 min. (b) 280 °C- 90 min. (c) 320 °C- 15 min. (d) 320 °C- 90 min. (e) 400 °C- 15 min. (f) 400 °C- 90 min.

The fracture surface of specimen partitioned at 280 °C for 15 minutes (Fig. 4.36a) reveals very few cleavage facets and majority of fine equiaxed dimples representing superior amount of energy absorbed by nucleation and growth of micro-voids prior to fracture which can be supported by its maximum value of tensile strength and toughness when contrasted to those of other specimens. Fracture surfaces shown in fig. 4.36(b-h) reveals primarily flat cleavage facets with intergranular cracks and shallow dimples which are indicative of quasi cleavage mode of fracture. In the initial stage of partitioning at 320 °C (Fig. 4.36c), the fresh martensite blocks acted as stress concentrating points and the matrix therefore accommodated a significant measure of deformation, consequently fine dimples formed at these stress concentration points in the tempered matrix, whereas the neighbouring fresh martensite blocks failed in a brittle manner, which is supported by the high value of modulus of toughness 180 MJ/m³. Increment in partitioning time i.e. 90 minutes at 320 °C (Fig. 4.36d) demonstrates the formation of large cracks by micro void coalescence at the transformed retained austenite grains and unique fresh martensite blocks bringing about brittle failure (De Knijf 2015), which can be substantiated by exceptional decrease in toughness i.e. 92 MJ/m³ at this condition. At higher partitioning temperature i.e. at 400 °C (Fig 4.36(e and f)) demonstrates a fracture surface which is significantly coarser compared to those of partitioning temperatures (280 and 320 °C) i.e. slightly large sized dimples along with some fine dimples and cleavage facets, which is due to the tempered martensite situated between the voids and upper bainite that is plastically strained, in this manner making local instabilities and necking bringing about higher toughness.

4.8.2 Microhardness measurement

Fig. 4.37 shows the influence of varying partitioning parameters with respect to micro Vickers hardness. Hardness profile shows decreasing trend with increase in partitioning temperature and time.

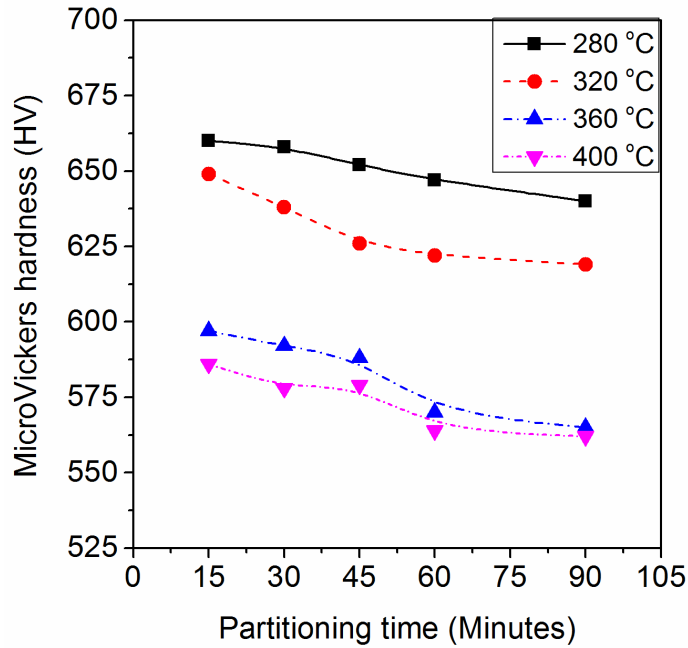


Figure 4.37 Variation of micro-Vickers hardness with partitioning times and temperatures

Maximum hardness value of 660 HV (57 HRC) was obtained in initial stage of partitioning at 15 minutes for 280 °C, similarly high hardness values were obtained for other partitioning temperatures as well in the initial stage and then decreases. After a partitioning time (PT) of about 45 minutes hardness tends to become more or less constant for all temperatures. Reduction in hardness beyond 15 minutes PT could be due to the loss of interstitial carbon from BCT martensite (α') that causes diminishment in α' tetragonality, as a result this carbon depleted martensite has less hardness compared to fresh martensite. As conventional tempering reactions additionally happen while partitioning, in this manner hardness decrease with PT is normal. This trend is in concurrence with different investigations (Li et al. 2010). However extending PT leads to precipitation of transition carbides in tempered martensite matrix which should have

resulted in higher hardness, still hardness decreases which is due to the enrichment of carbon in retained austenite and in the meantime carbon is likewise consumed in carbide formation (Tariq and Baloch 2014). Hence the carbon depleted martensite has lower hardness than fresh martensite with high carbon content and carbon escapes from martensite to austenite at higher rate at high temperatures (360 & 400 °C) and in addition to this formation of bainitic ferrite laths that further leads to the decreased hardness.

4.9 Influence of Partitioning Temperature and Time on the Wear Property

The wear behavior of AISI 9255 high silicon steel samples quenched at 190 °C and partitioned at different temperatures was evaluated and their results are tabulated (table 4.4 & 4.5). The chief constraints affecting the wear rate are the contact area, test cycles and pre hardness of the material. The wear rate is given by the slope of cumulative weight loss against wear time graph. It can be seen from fig. 4.38 that the cumulative weight loss increases in approximate linearity with the wear time. It was observed that wear rate shows marginal increase with increasing partitioning temperature and time.

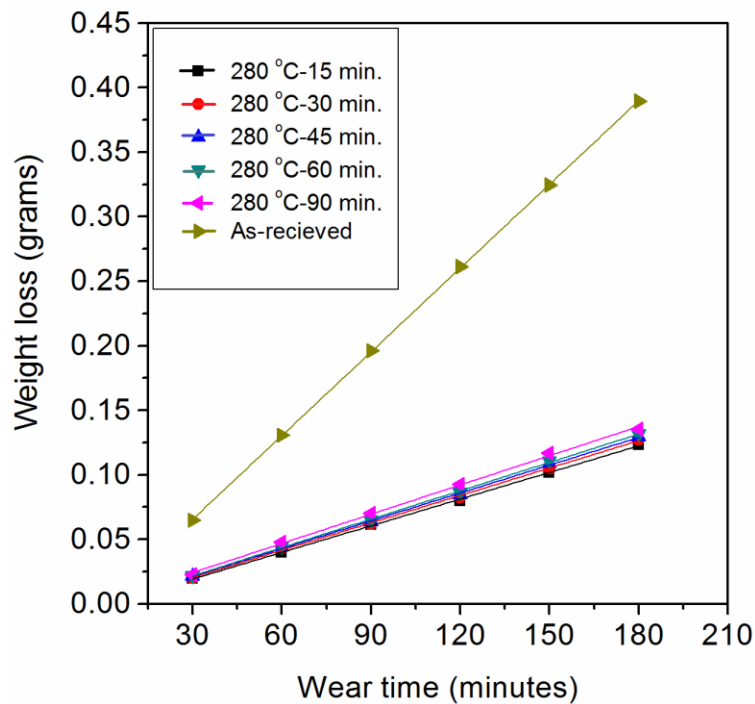


Figure 4.38 Cumulative weight loss against wear time plot for as-received and samples partitioned at 280 °C for various durations.

Table 4.4 Wear property of the Q&P heat treated samples

Partitioning temperature (°C)	Partitioning time (minutes)	Wear rate $\times 10^{-4}$ (gram/minute)	Specific wear rate $\times 10^{-5}$ (mm ³ /N-m)
280	15	6.877	1.179
	30	7.068	1.219
	45	7.177	1.237
	60	7.319	1.261
	90	7.550	1.334
320	15	7.390	1.255
	30	7.960	1.355
	45	8.433	1.425
	60	8.438	1.516
	90	8.869	1.539
360	15	11.100	1.900
	30	11.600	1.977
	45	11.800	2.023
	60	11.800	2.034
	90	12.100	2.103
400	15	11.600	2.012
	30	12.200	2.065
	45	12.300	2.118
	60	12.400	2.145
	90	12.500	2.165

Figure 4.39 shows the variation of specific wear rate (SWR) with respect to partitioning variables (temperatures and times). Q&P treated specimens revealed very lower specific wear rates when compared to the as received steel SWR of 4.076×10^{-5} ($\text{mm}^3/\text{N-m}$) [Part A- table 4.2]. SWR was found to be lowest for lower partitioning temperatures i.e. 280 & 320 °C and increased for higher temperatures i.e. 360 & 400 °C, SWR shows marginal increase with increasing partitioning time for all temperatures.

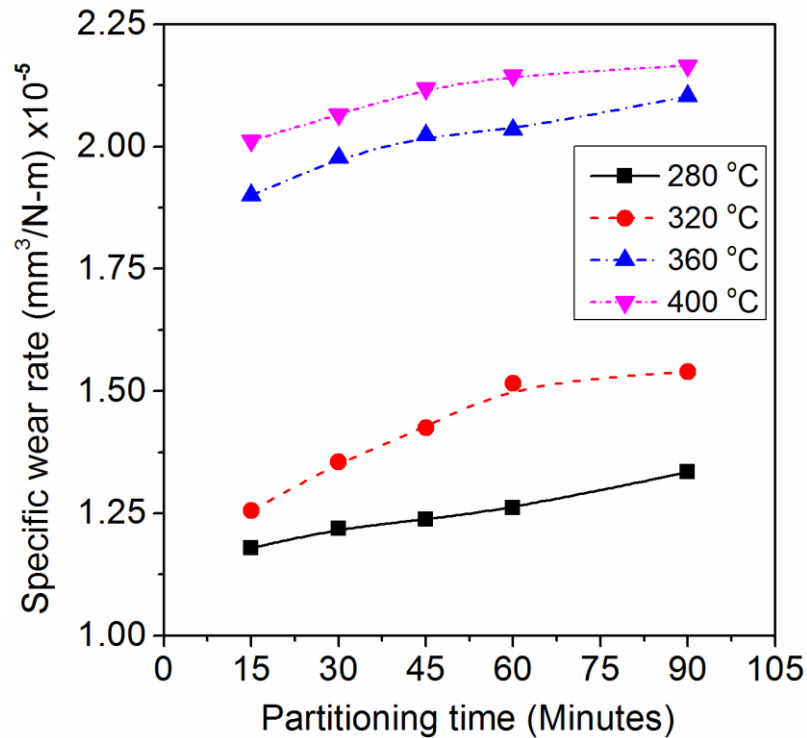


Figure 4.39 Variation in specific wear rate with partitioning times and temperatures

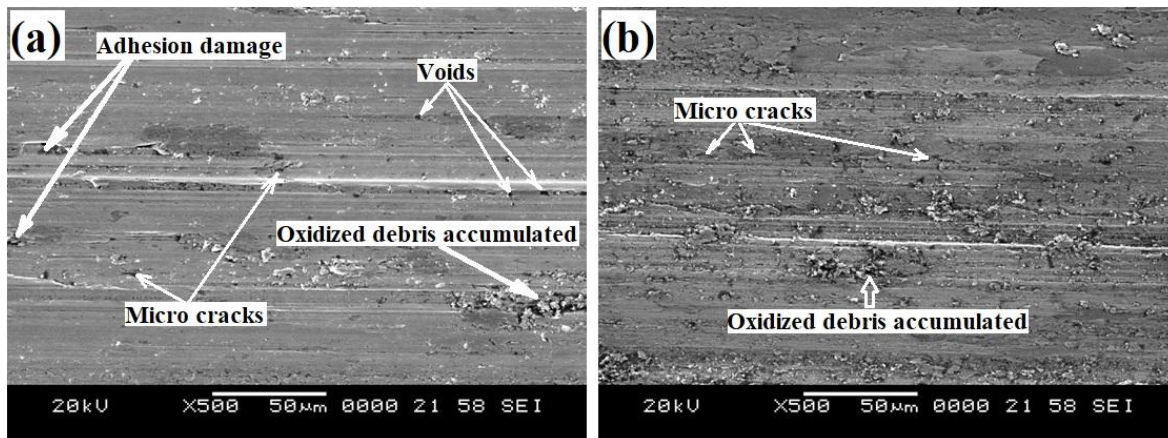
The sample partitioned at 280 °C for 15 minutes showed the least specific wear rate of 1.179×10^{-5} $\text{mm}^3/\text{N-m}$ which is mainly due to the presence of fine martensite packets that includes both lath (M_L) and plate (M_P), lower bainite along with stabilized retained austenite and it is also supported by the high initial hardness of 660 HV. Wear resistance is obtained by a blend of hardness and toughness of materials, by temperance of sliding contact, hardness assumes an imperative part in wear resistance, inferable from the slight impact in the midst of sliding friction (Yang et al. 2012). SWR was found to increase marginally with increase in partitioning time for all temperatures which is due to the

precipitation of transition carbides in tempered martensite matrix and moreover the enrichment of carbon in retained austenite and in the meantime carbon is likewise consumed in carbide formation (Tariq and Baloch 2014) which drastically reduces the hardness resulting in high SWR.

Increase in SWR was observed at higher partitioning temperatures i.e. at 360 and 400 °C, mainly due to progressive tempering of the martensite along with the presence of stabilized transitional carbides and additionally the formation of bainitic ferrite laths that causes further reduction in hardness. Hence the blend of high hardness along with adequate retained austenite content (contributes for toughness) is thought to be of conceivable attentiveness for bearing and gear appliances, where "damage tolerance" under pitting/contact fatigue conditions is improved by the presence of retained austenite in the microstructure (Speer et al. 2005).

4.9.1 Wear mechanism

The examination of worn out surfaces of Q&P heat treated high silicon steel samples through scanning electron microscope helped to understand the mechanism of wear (Fig. 4.40(a-h)).



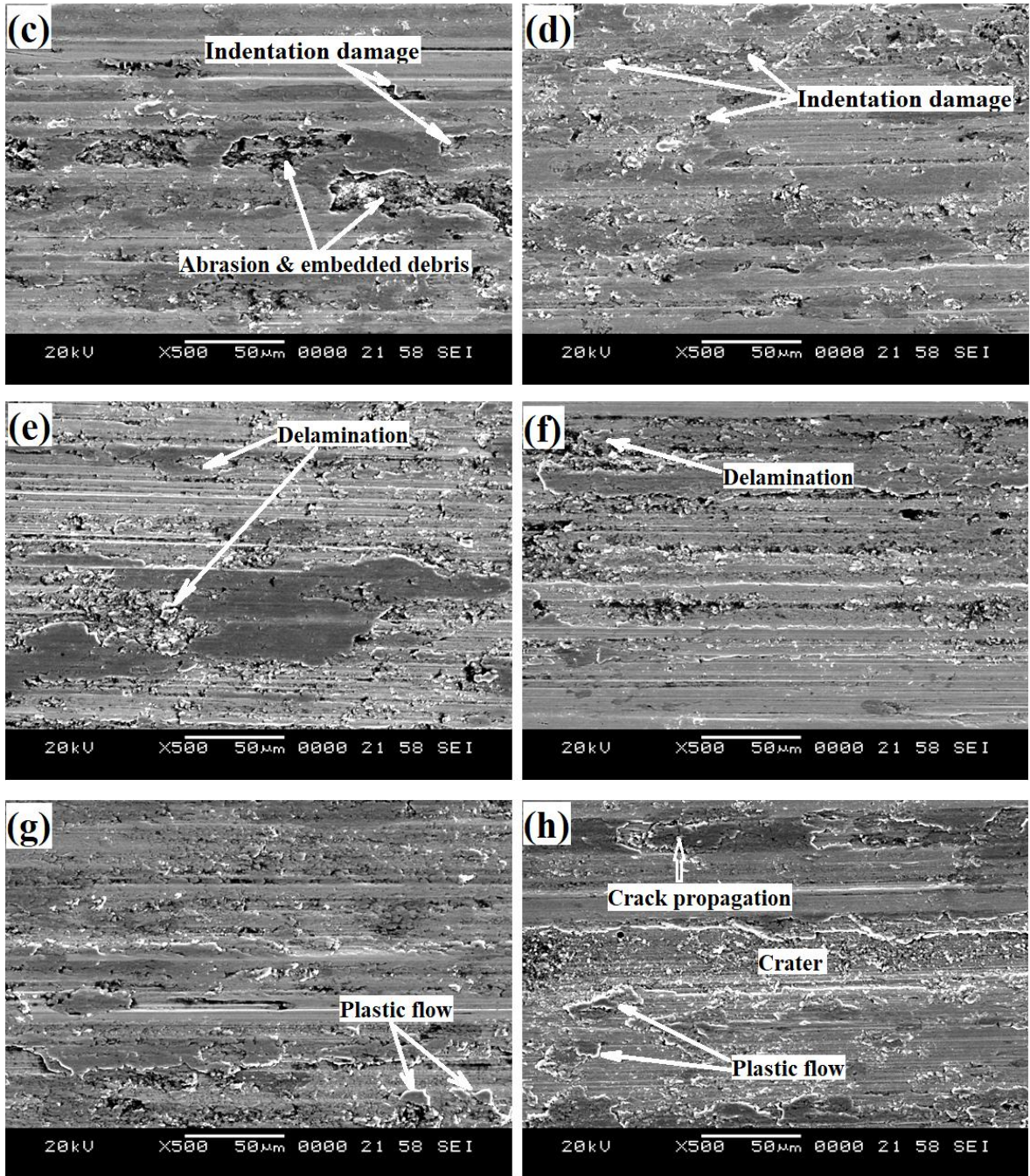


Figure 4.40 SEM of worn out samples partitioned at (a) 280 °C- 15 min. (b) 280 °C- 90 min. (c) 320 °C- 15 min. (d) 320 °C- 90 min. (e) 360 °C- 15 min. (f) 360 °C- 90 min. (g) 400 °C- 15 min. (h) 400 °C- 90 min.

Initially sliding wear is the main mechanism of material removal. The wear debris is pushed into the contact and is smeared by the acting forces. The observation of smeared debris indicates the occurrence of adhesive wear (Fig. 4.40a). The damage mechanisms observed in the worn surface of the Q&P treated samples includes sliding contact were adhesion, indentation and surface fatigue. During the wear process there is formation of micro cracks, voids, crater, oxides, plastic flow of material and delamination.

As sliding proceeds with more debris getting entrapped between the sliding surfaces and gets compacted because of dreary sliding, these mass oxide debris on the wear pin surface is sufficiently hard causing indentation damage and likewise contributes for lower wear rates (Fig. 4.40(a-d)). The voids are the initiator of the crack formation; therefore crack will form near to voids. The linkaging of voids enhance plastic deformation, cracking and surface delamination of worn surface especially at higher partitioning temperatures 360 and 400 °C (Fig. 4.40(e-h)), that shows large extent of damage caused on the worn surface resulting in excess loss of material, crater formation is also observed in some areas where metallic particles have come into debris due to delamination which further results in high SWR.

CHAPTER 5

CONCLUSIONS AND FUTURE ASPECTS

5.1 Conclusions

The following conclusions were drawn from the present study on microstructural aspects, mechanical and wear behavior of **austempered** AISI 9255 high silicon steel.

- Austempering heat treatment of this steel over a temperature range of 280–400 °C generated a bainite structure that consists of bainitic ferrite, soft ferrite in some regions and retained austenite. An increase in austempering temperature resulted in progressive coarseness of the bainite structure.
- Reduction in the retained austenite content was observed with an increasing austempering time for all temperatures from 280 to 400 °C.
- Tensile properties like ultimate tensile strength, percentage elongation and modulus of toughness were found to decrease with an increase in austempering time for all austempering temperatures. A superior combination of strength and % elongation was attained at austempering time of 15 min, i.e. (1852 MPa & 14%) at 280 °C, (1155 MPa & 33.4%) at 360 °C and (1165 MPa & 34%) at 400 °C.
- A decrease in hardness was observed with an increase in austempering temperature, which is due to the coarse bainitic ferrite and blocky retained austenite. With an increase in austempering time, a slight increase in hardness was observed for all austempering temperatures, due to the fineness of the bainite structure and decrease in retained austenite content.
- The fracture surfaces of almost all the austempered samples showed a ductile mode of fracture. However, a quasicleavage type of fracture with infrequent voids was observed at lower austempering temperatures, i.e. 280 and 320 °C.
- Strain-induced martensite formation was predominantly observed at higher austempering temperatures along with an increased strain hardening exponent and total elongation.

- Specific wear rate slightly increased with increasing austempering time from 15 to 180 minutes for all austempering temperatures i.e. from 280-400 °C. The sample austempered at 280 °C for 15 minutes exhibited superior wear resistance.
- Plastic flow, cracking and surface delamination were predominantly observed in almost all worn out samples.

The following conclusions were drawn from the present study on microstructural aspects, mechanical and wear behavior of **quenching and partitioning (Q&P)** heat treated AISI 9255 high silicon steel.

- Microstructures of specimens quenched at 190 °C and partitioned over a temperature range 280 to 400 °C generates multiphase microstructures containing major fraction of martensite i.e. lath (M_L) and plate-type (M_P), transitional ϵ -carbides in tempered martensite matrix, lower bainite and retained austenite (RA) for all heat treatment conditions. The microstructural characteristics observed at higher partitioning temperature i.e. 360 and 400 °C reveals some bainite ferrite laths along with martensite and RA.
- Retained austenite content decreased with increasing partitioning time at 280 °C and remains more or less constant for other partitioning temperatures. Maximum amount of RA of 16% was obtained at 280 °C for 15 minutes. RA was non quantifiable at prolonged partitioning at higher temperatures.
- Carbon content in retained austenite increased with increase in both partitioning time and temperature. Partitioning at 400 °C for 30 minutes, the decomposition of austenite to upper bainite lead to obvious increase in carbon content in austenite i.e. 1.96 wt.% simultaneously decreasing retained austenite content (5.5%).
- Retained austenite content obtained through EBSD phase distribution maps measure quite closer values when compared to the same measured through XRD. Martensite crystals in IPF maps reveal more of plate like morphology along with some twin orientations. Misorientation profiles indicated that at lower partitioning conditions i.e. 280 °C for 15 & 90 minutes revealed more HAGB, which implies

the presence of LB in the matrix and similarly at high partitioning condition i.e. 400 °C for 30 minutes showed more LAGB indicating the presence of UB along with martensite of various morphologies, transition carbides and RA.

- Tensile properties like yield strength, ultimate tensile strength, % elongation and modulus of toughness decreases with increase in partitioning time for all partitioning temperature. Superior combination of strength and % elongation was attained at partitioning time of 15 minutes i.e. (1859 MPa and 17%) and also with high value of modulus of toughness 207 MJ/m^3 at 280 °C.
- Hardness gradually decreases in the initial stage and thereafter becomes constant with increase in partitioning time for all temperatures. Maximum hardness of 660 HV was attained while partitioning at 280 °C for 15 minutes.
- Fracture surfaces of Q&P treated samples reveals primarily flat cleavage facets with intergranular cracks and dimples indicating quasi cleavage mode of fracture.
- Specific wear rate showed marginal increase with the increasing partitioning time from 15 to 90 minutes, SWR was observed to be high with increasing temperature from 280-400 °C. Least specific wear rate of $1.18 \times 10^{-5} \text{ mm}^3/\text{N-m}$ was obtained at a partitioning condition of 280 °C for 15 minutes.
- The damage mechanisms observed in the worn surface of quenched and partitioned (Q&P) high silicon steels includes sliding contact were adhesion, indentation and surface fatigue. However voids, surface cracks, oxidized debris, plastic flow and surface delamination was predominantly observed.

5.2 Summary of conclusions

The conclusions drawn from this study support the potential for Austempering to replace Quenching & Partitioning or vice-versa. Since these heat treatments revealed their own advantages and limitations, on the basis of their results on mechanical properties and specific wear rate. However the best results (mechanical properties & specific wear rates) obtained for these two heat treatments is indicated in Table 5.1.

Table 5.1 Summary of the “exceptional” mechanical properties and specific wear rate obtained with their processing conditions.

Processing condition	YS (MPa)	UTS (MPa)	% EL	MT (MJ/m ³)	Hardness (HV)	Specific-wear rate ×10 ⁻⁵ (mm ³ /N-m)
Austempered at 280 °C for 15 minutes	1725	1852	14.10	154	538	2.063
Austempered at 360 °C for 15 minutes	891	1155	33.40	314	386	2.444
Austempered at 400 °C for 15 minutes	778	1165	34.15	305	342	2.522
Quenched at 190 °C & Partitioned at 280 °C for 15 minutes	1598	1859	17	207	660	1.179
Quenched at 190 °C & Partitioned at 320 °C for 15 minutes	1641	1856	15	178	649	1.255

In the case of Austempering heat treatment results revealed high strength and wear resistance at low temperature i.e. 280 °C. However at higher temperatures 360 & 400 °C indicated lower strength and wear resistance but high % EL along with high strain hardening effect. **Hence Austempering is preferred over Q&P** mainly in the applications where strain hardening effect is of importance i. e. metal forming; due to the superior strain hardening response received at austempering temperatures 360 & 400 °C.

Quenching & Partitioning heat treatment contributed mainly for high strength, hardness and wear resistance but without much improvement in % EL. **Hence Q&P is preferred over Austempering** mainly in the applications where high strength, hardness & wear resistance is desired (Tool & die making, Gears...), which is supported by the lowest specific wear rate values at partitioning temperatures 280 & 320 °C.

5.3 Scope for Further Research

Austempering and Quenching and Partitioning (Q&P) heat treated AISI 9255 steel generates bainitic and martensitic structure respectively, that exhibit superior combination of properties has a great potential for wide variety of applications in the field of automotive and tool & dies. In fact, there are some research areas which can be focused further to bring them as an undeniable material into the engineering applications.

- The present work can be extended by modifying the alloying elements in AISI 9255 steel and thereafter varying the heat treatment parameters (temperature and time) for both austempering as well as quenching and partitioning for better understanding regarding their kinetics and bring about improvement in mechanical properties.
- Tensile and wear tests for these heat treated samples can be carried out at elevated temperatures.
- Dry sliding wear behavior can be studied by further varying wear testing parameters. Emphasis on the wear debris can help to gain an in-depth knowledge of the wear process. Detailed characterization of the microstructure using TEM after the wear process would develop an excellent understanding on the hardening mechanisms during the wear process.
- Consecutively to have an better life span of the steel, corrosion studies of this grade of high Si steel would also be very interesting apart from the wear resistance property, since the corrosion would likewise decrease the wear resistance when they are subjected to various environments during service.

REFERENCES

- Acharya, P. P., Udupa, R., and Bhat, R. (2018). "Microstructure and mechanical properties of austempered AISI 9255 high-silicon steel." *Mater. Sci. Technol. (United Kingdom)*, 34(3), 355–365.
- Arlazarov, A., Ollat, M., Masse, J. P., and Bouzat, M. (2016). "Influence of partitioning on mechanical behavior of Q&P steels." *Mater. Sci. Eng. A*, 661, 79–86.
- Avishan, B., Yazdani, S., Caballero, F. G., Wang, T. S., and Garcia-Mateo, C. (2015). "Characterisation of microstructure and mechanical properties in two different nanostructured bainitic steels." *Mater. Sci. Technol.*, 31(12), 1508–1520.
- Avner, S. H. (1964). "Introduction to physical metallurgy". New Delhi: Tata McGraw Hill edition.
- Bakshi, S. Das, Leiro, A., Prakash, B., and Bhadeshia, H. K. D. H. (2014). "Dry rolling / sliding wear of nanostructured bainite." *Wear*, 316(1–2), 70–78.
- Baradari, S., and Boutorabi, S. M. A. (2015). "Effects of isothermal transformation conditions on the microstructure and hardness values of a high-carbon Al-Si alloyed steel." *Mater. Des.*, 86, 603–609.
- Bedolla-Jacuinde, A., Guerra, F. V., Rainforth, M., Mejia, I., and Maldonado, C. (2015). "Sliding wear behavior of austempered ductile iron microalloyed with boron." *Wear*, 330–331, 23–31.
- Bhadeshia, H. K. D. H. (2001). *Bainite in steels: Transformations, Microstructure and Properties*.
- Bhadeshia, H. K. D. H., and Edmonds, D. V. (1979). "The bainite transformation in a silicon steel." *Metall. Trans. A*, 10(7), 895–907.
- Bhadeshia, H. K. D. H., and Edmonds, D. V. (1983). "Bainite in silicon steels: new composition–property approach Part 2." *Met. Sci.*, 17(9), 420–425.
- Burwell, J. T., & Strang, C. D. (1952). On the empirical law of adhesive wear. *Journal of*

Applied Physics, 23(1), 18-28.

Burwell, J. T. (1957). "Survey of possible wear mechanisms." *Wear*, 1(April), 119–141.

Caballero, F. G., and Bhadeshia, H. K. D. H. (2004). "High-strength bainitic steels." *Int. J. ISSI*, 1(1), 15–23.

Caballero, F. G., and Garcia-Mateo, C. (2005). "The role of retained austenite on tensile properties of steels with bainitic microstructures." *Mater. Trans.*, 46(8), 1839–1846.

Caballero, F. G., Miller, M. K., and Garcia-Mateo, C. (2014). "Influence of transformation temperature on carbide precipitation sequence during lower bainite formation." *Mater. Chem. Phys.*, 146(1–2), 50–57.

Chang, L. C. (2005). "The rolling/sliding wear performance of high silicon carbide-free bainitic steels." *Wear*, 258(5–6), 730–743.

Chang, L. C., and Bhadeshia, H. K. D. H. (1994). "Carbon content of austenite in isothermally transformed 300M steel." *Mater. Sci. Eng. A*, 184(1), 19–21.

Clarke, A. J., Speer, J. G., Miller, M. K., Hackenberg, R. E., Edmonds, D. V., Matlock, D. K., Rizzo, F. C., Clarke, K. D., and Moor, E. De. (2008). "Carbon partitioning to austenite from martensite or bainite during the quench and partition (Q & P) process : A critical assessment." *Acta Mater.*, 56(1), 16–22.

Clayton, P., and Jin, N. (1996). "Unlubricated sliding and rolling/sliding wear behavior of continuously cooled, low/medium carbon bainitic steels." *Wear*, 200(1–2), 74–82.

Cullity, B. D. (1974). "Elements of X-ray diffraction Reading (MA)": Addison-Wisley.

Daber, S., and Rao, P. P. (2008). "Formation of strain-induced martensite in austempered ductile iron." *J. Mater. Sci.*, 43(1), 357–367.

Dyson, D. J. and Holmes, B. (1970). "Effect of alloying additions on the lattice parameter of austenite." *J. Iron Steel Inst.*, 208, 469–474.

Edmonds, D., Matlock, D., and Speer, J. (2011). "The recent development of steels with carbide-free acicular microstructures containing retained austenite." *Metall. Ital.*, 103(1),

41–49.

Edmonds, D. V., He, K., Rizzo, F. C., Cooman, B. C. De, Matlock, D. K., and Speer, J. G. (2006). “Quenching and partitioning martensite—A novel steel heat treatment.” *Mater. Sci. Eng. A*, 438–440, 25–34.

Erik Navara, N. M. and D. M. (1995). “Ausferrite- A New Structure in High-Strength Steels.” *Metallography*, 55–64.

Eyre, T. S. (1979). “Wear resistance of metals” *Treatise on Materials Science & Technology*, 13, 363-442.

Fridberg, J., Torndahl, L., and Hillert, M. (1969). “DIFFUSION IN IRON.” *Jernkont. Ann.*, 153(6), 263–276.

Garcia-Mateo, C., and Caballero, F. G. (2005). “Ultra-high – strength bainitic steels.” *ISIJ Int.*, 45(11), 1736–1740.

Gerdemann, F. L. H., Speer, J. G., and Matlock, D. K. (2004). “Microstructure and Hardness of Steel Grade 9260 Heat-Treated by the Quenching and Partitioning (Q&P) Process.” *Ms&T*, 439–449.

Gui, X., Gao, G., Guo, H., Zhao, F., Tan, Z., and Bai, B. (2017). “Effect of bainitic transformation during BQ&P process on the mechanical properties in an ultrahigh strength Mn-Si-Cr-C steel.” *Mater. Sci. Eng. A*, 684, 598–605.

Haiko, O., Somani, M., Porter, D., Kantanen, P., Kömi, J., Ojala, N., and Heino, V. (2018). “Comparison of impact-abrasive wear characteristics and performance of direct quenched (DQ) and direct quenched and partitioned (DQ&P) steels.” *Wear*, 400–401, 21–30.

Hillert, M., and Agren, J. (2004). “On the definitions of paraequilibrium and orthoequilibrium gren.” *Scr. Mater.*, 50(5), 697–699.

Hofer, C., Winkelhofer, F., Clemens, H., and Primig, S. (2016). “Morphology change of retained austenite during austempering of carbide-free bainitic steel.” *Mater. Sci. Eng. A*, 664, 236–246.

- Holloman, J. H. (1945). "Tensile deformation." *Trans AIME*; 162:268–277.
- Huyghe, P., Malet, L., Caruso, M., Georges, C., and Godet, S. (2017). "On the relationship between the multiphase microstructure and the mechanical properties of a 0.2C quenched and partitioned steel." *Mater. Sci. Eng. A*, 701, 254–263.
- Jagtar, S., Pal, S. L., and Ankur, K. (2013). "Enhancing Wear Resistance of En45 Spring Steel Using Cryogenic Treatment." *Frict. Wear Res.*, 1(2), 22–27.
- Junior da Cruz, J. A., Vilela, J. J., Gonzalez, B. M., and Santos, D. B. (2014). "Effect of retained austenite on impact toughness of the multi-phase bainitic-martensitic steel." *Adv. Mater. Res.*, 922, 298–303.
- Kankanala, A. (2010). "Unlubricated rolling / sliding wear behaviour of high silicon carbide-free steels." Master's thesis, Lulea University of Technology, Sweden.
- Knijf, D. De. (2015). "Influence of quenching and partitioning parameters on the microstructure and mechanical properties of advanced high strength steels." Doctoral dissertation, Ghent University, Belgium.
- Knijf, D. De, Silva, E. P. Da, Föjer, C., and Petrov, R. (2015). "Study of heat treatment parameters and kinetics of quenching and partitioning cycles." *Mater. Sci. Technol.*, 31(7), 817–828.
- Lee, K. M., and Polycarpou, A. A. (2005). "Wear of conventional pearlitic and improved bainitic rail steels." *Wear*, 259(1–6), 391–399.
- Leiro, A. (2014). "Microstructure analysis of wear and fatigue in austempered high-Si steels." Doctoral dissertation, Lulea University of Technology, Sweden.
- Leiro, A., Kankanala, A., Vuorinen, E., and Prakash, B. (2011). "Tribological behaviour of carbide-free bainitic steel under dry rolling / sliding conditions." *Wear*, 273(1), 2–8.
- Leiro, A., Vuorinen, E., Sundin, K. G., Prakash, B., Sourmail, T., Smanio, V., Caballero, F. G., Garcia-mateo, C., and Elvira, R. (2013). "Wear of nano-structured carbide-free bainitic steels under dry rolling – sliding conditions." *Wear*, 298–299, 42–47.

- Li, H. Y., Lu, X. W., Li, W. J., and Jin, X. J. (2010a). "Microstructure and mechanical properties of an Ultrahigh-Strength 40SiMnNiCr steel during the one-step quenching and partitioning process." *Metall. Mater. Trans. A*, 41(5), 1284–1300.
- Li, H. Y., Lu, X. W., Wu, X. C., Min, Y. A., and Jin, X. J. (2010b). "Bainitic transformation during the two-step quenching and partitioning process in a medium carbon steel containing silicon." *Mater. Sci. Eng. A*, 527(23), 6255–6259.
- Li, Q., Huang, X., and Huang, W. (2017). "EBSD Analysis of Relationship Between Microstructural Features and Toughness of a Medium-Carbon Quenching and Partitioning Bainitic Steel." *J. Mater. Eng. Perform.*, 26(12), 6149–6157.
- Li, Y., and Chen, X. (2001). "Microstructure and mechanical properties of austempered high silicon cast steel." *Mater. Sci. Eng. A*, 308(1–2), 277–282.
- Lindstrom, A. (2006). "Austempered High Silicon Steel - Investigation of wear resistance in a carbide free microstructure." Master's thesis, Lulea University of Technology, Sweden.
- Liu, C., Zhao, Z., and Bhole, S. D. (2006). "Lathlike upper bainite in a silicon steel." *Mater. Sci. Eng. A*, 434(1–2), 289–293.
- Liu, L., He, B. B., Cheng, G. J., Yen, H. W., and Huang, M. X. (2018). "Optimum properties of quenching and partitioning steels achieved by balancing fraction and stability of retained austenite." *Scr. Mater.*, 150, 1–6.
- Liu, L., He, B., and Huang, M. X. (2017). *The Role of Transformation-Induced Plasticity in the Development of Advanced High Strength Steels. Adv. Eng. Mater.*
- Liu Ping and Bahadur. (1990). "Friction and wear behavior of high silicon bainitic structures in austempered cast iron and steel." *Wear*, 138(1–2), 269–284.
- Long, X. Y., Kang, J., Lv, B., and Zhang, F. C. (2014). "Carbide-free bainite in medium carbon steel." *Mater. Des.*, 64, 237–245.
- Lu, J., Yu, H., Kang, P., Duan, X., and Song, C. (2018). "Study of microstructure, mechanical properties and impact-abrasive wear behavior of medium-carbon steel treated

by quenching and partitioning (Q&P) process.” *Wear*, 414–415(August), 21–30.

Luo, P., Gao, G., Zhang, H., Tan, Z., Misra, R. D. K., and Bai, B. (2016). “On structure-property relationship in nanostructured bainitic steel subjected to the quenching and partitioning process.” *Mater. Sci. Eng. A*, 661, 1–8.

Mandal, D., Ghosh, M., Pal, J., De, P. K., Ghosh Chowdhury, S., Das, S. K., Das, G., and Ghosh, S. (2009). “Effect of austempering treatment on microstructure and mechanical properties of high-Si steel.” *J. Mater. Sci.*, 44(4), 1069–1075.

Mandal, D., Ghosh, M., Pal, J., Ghosh Chowdhury, S., Das, G., Das, S. K., and Ghosh, S. (2014). “Evolution of microstructure and mechanical properties under different austempering holding time of cast Fe-1.5Si-1.5Mn-V steels.” *Mater. Des.*, 54, 831–837.

Miller, R. L. (1964). “A rapid X-ray method for the determination of retained austenite.” *Trans. ASM*, 57, 892-899.

Monia, S., Varshney, A., Sangal, S., Kundu, S., Samanta, S., and Mondal, K. (2015). “Development of highly ductile spheroidized steel from high C (0.61 wt .% C) low-alloy steel.” *J. Mater. Eng. Perform.*, 24(11), 4527–4542.

Nayak, S. S., Anumolu, R., Misra, R. D. K., Kim, K. H., and Lee, D. L. (2008). “Microstructure–hardness relationship in quenched and partitioned medium-carbon and high-carbon steels containing silicon.” *Mater. Sci. Eng. A*, 498(1–2), 442–456.

Nishikawa, A. S., Santo, M. J., and Sietsma, J. (2018). “Influence of bainite reaction on the kinetics of carbon redistribution during the Quenching and Partitioning process.” *Acta Mater.*, 142, 142–151.

Oak Ridge, National laboratory – Metals and ceramics division online calculation. Available from: <http://calculations.ewi.org/vjp/secure/TTTCCTPlots.asp>.

Owen, W. S. (1954).”The effect of silicon on the kinetics of tempering” Transactions of the American Society for Metals 46:812-829.

Paravicini Bagliani, E., Santofimia, M. J., Zhao, L., Sietsma, J., and Anelli, E. (2013). “Microstructure, tensile and toughness properties after quenching and partitioning

treatments of a medium-carbon steel.” *Mater. Sci. Eng. A*, 559, 486–495.

Pierce, D. T., Coughlin, D. R., Williamson, D. L., Kähkönen, J., Clarke, A. J., Clarke, K. D., Speer, J. G., and Moor, E. De. (2016). “Quantitative investigation into the influence of temperature on carbide and austenite evolution during partitioning of a quenched and partitioned steel.” *Scr. Mater.*, 121, 5–9.

Podder, A. S., Lonardelli, I., Molinari, A., and Bhadeshia, H. K. D. H. (2011). “Thermal stability of retained austenite in bainitic steel : an in situ study.” *Proc. R. Soc. A Math. Phys. Eng. Sci.*, 467(2135), 3141–3156.

Putatunda, S. K. (2001a). “Fracture toughness of a high carbon and high silicon steel.” *Mater. Sci. Eng. A*, 297(1–2), 31–43.

Putatunda, S. K. (2001b). “Austempering of a silicon manganese cast steel.” *Mater. Manuf. Process.*, 16(6), 743–762.

Putatunda, S. K. (2003). “Influence of austempering temperature on microstructure and fracture toughness of a high-carbon, high-silicon and high-manganese cast steel.” *Mater. Des.*, 24(6), 435–443.

Putatunda, S. K., Singar, A. V, Tackett, R., and Lawes, G. (2009). “Development of a high strength high toughness ausferritic steel.” *Mater. Sci. Eng. A*, 513, 329–339.

Radziszewski, P., and Tarasiewicz, S. (1993). “Modelling and simulation of ball mill wear.” *Wear*, 160, 309–316.

Rao, P. P., and Putatunda, S. K. (1998). “Dependence of fracture toughness of austempered ductile iron on austempering temperature.” *Metall. Mater. Trans. A*, 29A(12), 3005–3016.

Sajjadi, S. A., and Zebarjad, S. M. (2007). “Isothermal transformation of austenite to bainite in high carbon steels.” *J. Mater. Process. Technol.*, 189(1–3), 107–113.

Santofimia, M. J., Zhao, L., Petrov, R., Kwakernaak, C., Sloof, W. G., and Sietsma, J. (2011). “Microstructural development during the quenching and partitioning process in a newly designed low-carbon steel.” *Acta Mater.*, 59(15), 6059–6068.

- Santofimia, M. J., Zhao, L., and Sietsma, J. (2009). "Microstructural evolution of a low-carbon steel during application of quenching and partitioning heat treatments after partial austenitization." *Metall. Mater. Trans. A*, 40(1), 46–57.
- Santos, D. B., Ronaldo, B., Oliveria, P. P. de, and Pereloma, E. V. (2009). "Mechanical behavior and microstructure of high carbon Si–Mn–Cr steel with TRIP effect." *ISIJ Int.*, 49(10), 1592–1600.
- Seo, E. J., Cho, L., Estrin, Y., and Cooman, B. C. De. (2016). "Microstructure-mechanical properties relationships for quenching and partitioning (Q&P) processed steel." *Acta Mater.*, 113, 124–139.
- Shah, S. M., Bahadur, S., and Verhoeven, J. D. (1986). "The erosion behavior of two austempered high silicon (2.5 wt.% Si) steels, one." *Wear*, 113(2), 279–290.
- Sharma, S., Sangal, S., and Mondal, K. (2011). "Development of new high strength carbide-free bainitic steels." *Metall. Mater. Trans. A*, 42A(13), 3921–3933.
- Shipway, P. H., Wood, S. J., and Dent, A. H. (1997). "The hardness and sliding wear behaviour of a bainitic steel." *Wear*, 203, 196–205.
- Silva, E. P. Da, Knijf, D. De, Xu, W., Föjer, C., Houbaert, Y., Sietsma, J., and Petrov, R. (2015). "Isothermal transformations in advanced high strength steels below martensite start temperature." *Mater. Sci. Technol.*, 31(7), 808–816.
- Son, J.-Y., Kim, J.-H., Kim, W.-B., and Ye, B.-J. (2010). "Effects of austempering conditions on the microstructures and mechanical properties in Fe-0.9%C-2.3%Si-0.3%Mn steel." *Met. Mater. Int.*, 16(3), 357–361.
- Speer, J. G., Assunção, F. C. R., Matlock, D. K., and Edmonds, D. V. (2005). "The 'quenching and partitioning' process: background and recent progress." *Mater. Res.*, 8(4), 417–423.
- Speer, J., Matlock, D. K., Cooman, B. C. De, and Schroth, J. G. (2003). "Carbon partitioning into austenite after martensite transformation." *Acta Mater.*, 51(9), 2611–2622.

Standard, A. S. T. M. (2001). A370-13: Standard test methods and definitions for mechanical testing of steel products. Annual Book of ASTM Standards, ASTM, West Conshohocken, PA, 17-24.

Standard, A. S. T. M. (2008). G99. Standard test method for wear testing with a pin-on-disk apparatus, ASTM International, West Conshohocken, PA.

Standard, A. S. T. M. (2009). E8/E8M. Standard test methods for tension testing of metallic materials. ASTM international, West Conshohocken PA; doi: 10.1520. E0008-E0008M-09, www.astm.org.

Sun, J., Yu, H., Wang, S., and Fan, Y. (2014). "Study of microstructural evolution, microstructure-mechanical properties correlation and collaborative deformation-transformation behavior of quenching and partitioning (Q&P) steel." *Mater. Sci. Eng. A*, 596, 89–97.

Tan, Z. L., Wang, K. K., Gao, G. H., Gui, X. L., Bai, B. Z., and Weng, Y. Q. (2014). "Mechanical properties of steels treated by Q-P-T process incorporating carbide-free-bainite/martensite multiphase microstructure." *J. Iron Steel Res. Int.*, 21(2), 191–196.

Tariq, F., and Baloch, R. A. (2014). "One-step quenching and partitioning heat treatment of medium carbon low alloy steel." *J. Mater. Eng. Perform.*, 23(5), 1726–1739.

Teer, D. G. and Arnell, R. D. (1975). Wear, in Principles of Tribology, (edited by Halling J.) Macmilan, Newyork.

Thomas, G. A., and Speer, J. G. (2014). "Interface migration during partitioning of Q&P steel." *Mater. Sci. Technol. (United Kingdom)*, 30(9), 998–1007.

Tomita, Y., and Okawa, T. (1993). "Effect of microstructure on mechanical properties of isothermally bainite-transformed 300M steel." *Mater. Sci. Eng. A*, 172(1–2), 145–151.

Varshney, A., Sangal, S., and Mondal, K. (2017). "Exceptional work-hardening behavior of medium-carbon high-silicon low-alloy steels." *Metall. Mater. Trans. A*, 48(2), 589–593.

Vuorinen, E. (2012). "Structure and Properties of Advanced Fine Grained Steels

Produced Using Novel Thermal Treatments.” Doctoral dissertation, Lulea University of Technology, Sweden.

Wang, C., Li, X., Chang, Y., Han, S., and Dong, H. (2016a). “Comparison of three-body impact abrasive wear behaviors for quenching-partitioning-tempering and quenching-tempering 20Si2Ni3 steels.” *Wear*, 362–363, 121–128.

Wang, K., Tan, Z., Gao, G., Gao, B., Gui, X., Misra, R. D. K., and Bai, B. (2016b). “Microstructure-property relationship in bainitic steel: The effect of austempering.” *Mater. Sci. Eng. A*, 675, 120–127.

Wang, M. M., Hell, J. C., and Tasan, C. C. (2017). “Martensite size effects on damage in quenching and partitioning steels.” *Scr. Mater.*, 138, 1–5.

Wang, X. L., Wu, K. M., Hu, F., Yu, L., and Wan, X. L. (2014). “Multi-step isothermal bainitic transformation in medium-carbon steel.” *Scr. Mater.*, 74, 56–59.

Wu, R., Jin, X., Wu, X., Li, W., Deng, J., Shen, Y., and Wang, L. (2016). “Enhancement of mechanical properties for quenched and partitioned steels via intragranular austenite.” *Ironmak. Steelmak.*, 43(8), 616–620.

Xiang, C., Esa, V., and Jonny, G. (2009). “In-situ SEM observation on fracture behavior of austempered silicon alloyed steel.” *China Foundry*, 6(3), 185–190.

Yang, J., Wang, T. S., Zhang, B., and Zhang, F. C. (2012a). “Microstructure and mechanical properties of high-carbon Si–Al-rich steel by low-temperature austempering.” *Mater. Des.*, 35, 170–174.

Yang, J., Wang, T. S., Zhang, B., and Zhang, F. C. (2012b). “Sliding wear resistance and worn surface microstructure of nanostructured bainitic steel.” *Wear*, 282–283, 81–84.

LIST OF PUBLICATIONS

Journals

Palaksha Pilar Acharya, Rajendra Udupa & Ravishankar Bhat (2018). “Microstructure and Mechanical Properties of Austempered AISI 9255 High-Silicon Steel.” *Materials Science and Technology, Taylor & Francis group*, 34(3), 355-365.

Palaksha Pilar Acharya & Ravishankar Bhat (2018) “Structure-Property Correlation of Quenching and Partitioning Heat Treated Silicon-Manganese Steel.” *Silicon, Springer publications*, 1-11, DOI: 10.1007/s12633-018-9973-2.

Conference Proceedings

Palaksha Acharya, Ajit Kumar & Ravishankar Bhat (2018). “Microstructure and Wear Behavior of Austempered High Carbon High Silicon Steel.” In *MATEC Web of Conferences*, EDP Sciences (Vol. 144, p. 02013).

Palaksha P. A. & Ravishankar K. S. (2017). “Influence of Austempering Heat Treatment on Microstructure and Mechanical Properties of Medium Carbon High Silicon Steel.” *IOP Conference Series: Materials Science & Engineering* (Vol. 225, No. 1, p. 012006).

Palaksha P. A., Syamkrishna P., & Ravishankar K. S. (2017). Effect of Austempering Heat Treatment Parameters on the Microstructure and Dry Sliding Wear Behavior of AISI 9255 High Silicon Steel. *Materials Today: Proceedings*, Elsevier, 4(10), 10757-10763.

BIO-DATA

Name : Palaksha P. A.
Date of Birth : 28-01-1989
Permanent address : Door # 17-62/4.
“DHARMASHREE”, Poonja road
Surathkal-Munchur
P.O. Srinivasnagar
Mangaluru - 575025
Email : palaksha.pa@gmail.com

Academic qualification

- Bachelor of Engineering (B.E.) in Mechanical Engineering; St. Joseph Engineering College; Vamanjoor, Mangaluru; 2010.
- Master of Technology (M.Tech.) in Process Metallurgy; National Institute of Technology Karnataka, Surathkal; 2013.
- Ph.D. in Metallurgical & Materials Engineering; National Institute of Technology Karnataka, Surathkal; 2019.